Beaufort Coast Wind Climatology and Case Study of a High Wind Event

David Small

Department of Atmospheric and Oceanic Science

McGill University

Montreal, Quebec, Canada

August, 2009

A thesis submitted to McGill University in partial fulfillment of the requirements of the degree of Master of Science

Abstract

Tuktoyaktuk, a community along the Beaufort coast in the western Canadian Arctic, experiences serious coastal erosion during periods of strong and persistent northwesterly winds during the late summer season when the sea ice coverage reaches its annual minimum. The prevalence of strong northwesterly winds along the Beaufort coast has often been linked to the passage of powerful storms. In this study, a climatology of late summer winds at Tuktoyaktuk is compiled that links the observed wind regime to the orography of the Brooks Range. The climatology and a detailed case study of an extreme wind event indicate that an anticyclone over the Chukchi or western Beaufort Seas is conducive for cold air damming events north of the Brooks Range that alter the pressure gradient in a direction favorable for strong northwesterly geostrophic winds over Tuktoyaktuk to be mixed to the surface in a neutrally stratified atmosphere.

Résumé

Tuktoyaktuk, une communauté sur la côte de Beaufort à l'ouest de l'arctique canadien, est aux prises à de graves épisodes d'érosion côtière à la fin de l'été, lorsque la couverture glacière est à son minimum et que soufflent de persistants et forts vents du nord-ouest. La prévalence de forts vents du nord-ouest le long de la côte de Beaufort a souvent été lié au passage de puissantes tempêtes. Dans cette étude, une climatologie des épisodes de vent de fin d'été est établie et mise en lien avec avec l'orographie de la chaîne de montagnes Brooks. La climatologie ainsi qu'une étude de cas détaillée d'un épisode de vents de force extrême indiquent qu'un anticyclone au dessus de la mer de Chukchi ou la mer de Beaufort conduit à un blocage d'air froid au nord de la chaîne Brooks qui modifie le gradient de pression dans une direction favorable à un mélange des forts vents géostrophiques nord-ouest au dessus de Tuktoyaktuk jusqu'à la surface dans une atmosphère stratifiée à stabilité neutre.

Acknowledgements

First and foremost, I would like to acknowledge my thesis advisor, Professor John Gyakum, for his advice and expert guidance. The interest and enthusiasm he showed towards my work helped to make this project the greatest learning experience of my life. Secondly, I would like to thank Dr. Eyad Atallah for sharing his insight and expertise so freely. I can't imagine how I would have finished this work without his input. In addition, I would like to thank Dr. Steve Solomon and Dr. Will Perrie at the Bedford Institute of Oceanography for their encouragement and interest in this study of the wind regime along the Beaufort coast. I would also like to acknowledge that an International Polar Year (IPY) grant from the National Sciences and Engineering Research Council made this research possible. I also need to thank the professors, students and staff of the Department of Atmospheric and Oceanic Sciences for their help and kindness. In particular, I would like to thank Vaughn Thomassin and Michael Havas for all of their assistance and Dominik Jacques for translating the abstract into French. Last, but certainly not least, I need to thank my wife Margaret. In addition to being my love and my best friend, she's also my biggest supporter. Her love and encouragement made this possible.

Table of Contents

Figure List

Chapter 1

Introduction

Anthropogenic global warming has led to dramatic changes in the environment of the Arctic, with the most rapid increases in temperature (Comiso, 2003) and decreases in sea ice (Barber and Hanesiak, 2004) occurring over the western Canadian arctic, Beaufort Sea and Mackenzie River basin. The latest Intergovernmental Panel on Climate Change report (Christensen et al., 2007) indicates that the increase in temperature and decline in sea ice coverage over the Arctic is "very likely" to continue over the course of the 21st century as temperatures rise. Yet, the complexity of the arctic climate system and the lack of consistent, long-term observations (Serreze and Barry, 2005) have limited our progress in understanding this critical and fast changing region of the earth. This study is motivated by the challenge of understanding the physical processes that contribute to the wind regime along the Beaufort coast, an important component of the complex and fast changing Arctic climate system.

Recent studies have reported that near surface atmospheric temperature across most of the Arctic have increased faster than the global average since 1960 (Jones and Moberg, 2003; Zhang 2005) with permafrost (Jorgenson et al., 2006) and sea surface (Steele et al., 2008) temperatures also significantly increasing over the period. Increasing temperatures and changes in circulation have also led to dramatic decreases in the sea ice extent, which eventually reached record minima in 2002 and again in 2007 (Cavalieri et al., 2003; Serreze et al., 2003; Serreze et al., 2007; Stroeve et al., 2007; 2008). Changes in sea ice alter the surface albedo and the exchange of heat, moisture, and momentum between the atmosphere and ocean, a major factor in the polar amplification of anthropogenic warming simulated by many climate models (Christensen et al., 2007; Serreze and Francis, 2006).

The increase in open water and degradation of the permafrost (Jorgenson et al., 2006) from the rapid warming have in turn led to large increases in the rate of coastal erosion in many regions of the Arctic, including the Beaufort coast, where the rates are already among the highest the world (Jones et al., 2009; Solomon, 2005). The coastal

community of Tuktoyaktuk along the Beaufort coast in the Canadian Arctic is especially vulnerable to coastal erosion during frequent periods of persistent northwesterly winds observed along the Beaufort coast in August and September (Manson and Solomon, 2007; Danard et al., 2003; Solomon, 2005) when the Beaufort Sea is generally ice-free (Jones et al., 2009).

The link between anticyclonic wind anomalies and the thickness and extent of sea ice in the Arctic (Rigor and Wallace, 2004; Ogi and Wallace, 2007; Ogi et al., 2008; Zhang et al., 2008; Comiso et al., 2008) and Beaufort Sea (Rogers, 1978; Tremblay and Mysak, 1998; Arfeuille et al., 2000; Drobot and Maslanik, 2003) is well established. For example, summer anticyclonic surface wind anomalies over the Arctic have been shown to explain as much as 60 percent of the variance of the year-to-year fluctuations in September sea ice extent since 1979 (Ogi et al., 2008). The expectation that the thickness and extent of sea ice will continue to decline has led some authors to suggest that polar amplification of temperature changes (Christensen et al., 2007) and coastal erosion will also increase in the Arctic (Simmonds et al., 2008), including along the Beaufort coast (Manson and Solomon, 2007; Jones et al., 2009). The IPCC models, however, are less certain about wind and circulation changes in the Arctic than about changes in temperature over the next century (Christensen et al., 2007). This uncertainty highlights the importance of understanding the wind regimes of the Arctic, especially those that affect the fastest changing regions such as the Beaufort coast and Mackenzie basin in western Canadian Arctic.

Previous studies have found that the wind regime along the Beaufort coast is bi-modal during the late summer with high frequencies of northwesterly and southeasterly winds (Solomon et al., 2005; Manson and Solomon, 2007; Atkinson, 2005; Hudak and Young, 2002). The prevalence of northwesterly winds along the Beaufort coast has often been linked to the passage of powerful storms (Manson and Solomon, 2007; Hudak and Young, 2002). Although cyclone activity in the arctic reaches its maximum in summer, the Beaufort Sea is a region with relatively few cyclones (Keegan, 1958; Serreze et al., 1993; Serreze 1995; Brummer et al., 2000; McCabe et al., 2001; Lynch et al., 2003; Zhang et al., 2004; Simmonds et al., 2008), thus motivating a further analysis of contributors to strong northwesterly winds.

Two objectives are addressed in this study. The first objective is to analyze the wind climatology of Tuktoyaktuk during the late summer.

Previous studies have found that the wind regime along the Beaufort coast is bi-modal during the late summer with high frequencies of northwesterly and southeasterly winds (Solomon et al., 2005). Most discussions of the hourly (or 6-hourly) wind regime in the Beaufort Sea have focused on the relationship between the passage of strong storm events and the high frequency of observed northwesterly winds. While severe storms certainly play an important role in producing strong winds, another mechanism, possibly related to the upstream topography, likely contributes to the strong bimodality of the hourly wind regime. The first objective of this study is to compile the climatology of the late summer hourly winds to identify the role, if any, of upstream topography on the bimodal wind regime reported along the Beaufort coast at Tuktoyaktuk.

Our second objective is to identify the physical processes contributing to the strength and persistence of the northwesterly winds during the September 1999 storm surge.

Between 24 and 28 September 1999, the hamlet of Tuktoyaktuk, a community along the Beaufort coast of Canada, experienced significant storm surge damage during a period of unusually strong and persistent northwesterly winds that began after a strong cyclone developed to the southwest and moved to the east along the Beaufort coast. The storm is notable not only because of the strength of the cyclone that passed along the Beaufort coast or the persistence of the northwesterly winds observed over Tuktoyaktuk, but also because of the unusual sequence of meteorological events that occurred over the previous five days. The goal of this component of the study is to identify the dynamic and thermodynamic processes that created conditions favorable for strong northwesterly winds to persist near Tuktoyaktuk for a period of several days.

Chapter 2

Beaufort Coast Wind Regimes

2.1 Introduction

This study focuses on the winds at Tuktoyaktuk, an Inuit community along the Beaufort coast in the Canadian Arctic. We have chosen to focus on Tuktoyaktuk because this community suffers extreme coastal erosion damage during storm surge events that occur during periods of persistent westerly to northwesterly winds (Solomon, 2005; Manson et al., 2005; Manson and Solomon, 2007; Danard et al., 2003). Tuktoyaktuk is also located at the conjunction of the Mackenzie River basin and the Beaufort Sea, the region of the Arctic experiencing the most rapidly increasing temperatures (Comiso, 2003) and rapidly decreasing sea ice (Barber and Hanesiak, 2004). Of all the coastal stations in the region, the hourly station data from Tuktoyaktuk has the longest continuous record of hourly winds (1971 – 2007) that is relatively complete. For most of the available record, observations are not reported when the airport is closed from 0500UTC to 1100UTC, but the record is otherwise 94 percent complete, yielding a longer record and more complete record than available at any other coastal station along the Beaufort coast of Canada. Tuktoyaktuk is also located approximately 50km from the upper air station at Inuvik, the only source of rawinsonde data for the region.

A map is presented in Figure 2.1 that shows the locations of Tuktoyaktuk, Inuvik and several geographic features that are mentioned this study, including the Barents, Chukchi and Beaufort Seas, the Brooks Range and the Gulf of Alaska. The map also shows that the topography of the Beaufort coast is dominated by the confluence of the east to west oriented Brooks Range and the northern extent of the Rocky Mountains. The Brooks Range turns north from the interior of Alaska and becomes oriented in the northwest to southeast direction parallel to the Beaufort coast near the Canadian border.

2.2 Circulation Features Impacting the Wind Regime

The importance of anticyclonic circulation and wind anomalies over the Arctic on the thickness and extent of sea ice in the Beaufort Sea (Rogers, 1978;Tremblay and Mysak, 1998; Arfeuille et al., 2000) is also well established. The sea ice pack of the Beaufort Sea normally rotates in a wind-driven anticyclonic gyre centered around 78°N and 150°W owing to the presence of a persistent anticyclone over the region (Rogers, 1978; Barber and Hanesiak, 2004; Drobot and Maslanik, 2003). During the summer, anticyclonic surface wind anomalies have been shown to explain as much as 60 percent of the variance of the year-to-year fluctuations in September sea ice extent since 1979 (Ogi and Wallace; 2007; Ogi et al., 2008).

Anticyclonic circulation anomalies over the Beaufort and Chukchi Seas are consistent with the negative phase of the Arctic Oscillation (AO), the leading pattern of winter circulation variability in the northern hemisphere (Thompson and Wallace, 1998). The arctic oscillation is characterized by sea level pressure anomalies of one sign in the Arctic and anomalies of the opposite sign centered between 37°N and 45°N. The negative phase is associated with anomalously high pressure over the Arctic and low pressure over the mid-latitudes with opposite SLP anomalies during the positive phase. During the negative phase of the AO, anticyclonic circulation anomalies are observed over the Arctic, leading many authors to suggest the importance of the Arctic Oscillation on the anticyclonic wind regime and sea ice transport over the region (Barber and Hanesiak, 2004; Drobot and Maslanik, 2003; Rigor et al., 2002). For example, Barber and Hanesiak (2004) found that circulation anomalies associated with the AO could explain more than 25 percent of the interanual variance in sea ice pack in the southern Beaufort Sea. The rapid decrease in sea ice coverage since the 1980's has also been linked to the positive phase of the Arctic Oscillation (Rigor et al., 2002; Zhang et al., 2005; Barber and Hanesiak, 2004), although the decrease in sea ice continued after the Arctic Oscillation index became negative, causing this hypothesis to be challenged (Overland and Wang, 2005; Zhang et al., 2008a,b).

It is well known that anticyclones appear frequently over the Beaufort-Chukchi region (Cassano et al., 2006; Reed and Kunkel, 1960). Lynch et al. (2004) suggest that

high wind events at Barrow are often caused by synoptic conditions other than strong cyclones, including a ridge over the Beaufort-Chukchi region. Colucci and Davenport (1987) and Serreze et al. (1993) identified the Beaufort and Chukchi Seas of Alaska and western Canada as the regions of the Arctic with the highest frequency of anticyclogenesis. This is likely due to a persistent ridge that is often located over the Siberia-Chukchi-Beaufort region during fall and winter (Serreze et al., 1993; Serreze and Barrett, 2008). In fact, anticyclones are more frequently observed over the region than cyclones (Serreze and Barry, 2005).

Cyclogenesis in the arctic tends to occur in preferred regions along the arctic front. In summer and early autumn, the season of open ice in the Beaufort Sea, one such region of preferred cyclogenesis is along the coast of Siberia (Serreze et al., 2001; Serreze and Barrett, 2008; Reed and Kunkel, 1960). The high frequency of cyclogenesis is related to the strong baroclinic zone that forms separately from the polar front in summer (Reed and Kunkel, 1960) that Serreze and Barrett (2008) and Lynch et al. (2001) suggest is due to the trapping of cold arctic air by the coastal topography. The enhancement of the baroclinicity by cold air is much less pronounced over Alaska than Siberia, possibly explaining why the Beaufort and Chukchi Seas are not areas of frequent cyclone activity. Cyclones forming along the Eurasian coast near Siberia are more likely to move into the central Arctic Ocean than farther east into the Chukchi and Beaufort seas (Keegan, 1958; Reed and Kunkel, 1960; Serreze et al., 1993; Lynch et al., 2003). Cyclones migrating into the Beaufort and Chukchi seas form primarily along the coast of Alaska (Serreze et al., 2001) where the frequency of cyclogenesis is much lower. Another possible reason for the low cyclone frequency in the region is because the presence of significant orography in Alaska blocks the passage of storms near the Aleutian Islands from moving into the arctic (Serreze and Barry; 2005, Serreze and Barrett, 2008).

Anticyclonic circulation anomalies over the Beaufort Sea have been linked to the transport of sea ice across the region. The role of anticyclonic circulation anomalies in the northwesterly wind regime near Tuktoyaktuk has not been addressed in the literature.

Barrier jets are another feature of the local wind regime that has not been linked to the climatology of winds downstream of the Brooks Range at Tuktoyaktuk.

2.3 Barrier winds and the wind regime north of the Brooks Range

Barrier jets are strong mesoscale winds oriented parallel to steep topography that form along the windward slopes of steep topography outside the tropics when stable low-level flow is blocked by topography (Loescher et al., 2006; Colle et al., 2006; Doyle, 1997). They also occur during cold air damming events, a cold season phenomenon frequently observed along the eastern edge of the Appalachian (Bell and Bosart, 1988) and Rocky (Colle and Mass, 1995) Mountains when cold air from the north is turned to the west by the Coriolis force and trapped by the topography.

The blocking occurs when the Froude number is less than one and the flow doesn't have enough kinetic energy to cross the topographic barrier (Bluestein, 1992; Barry, 2008). The Froude number is defined in Equation 2.1,

$$Fr = \frac{u}{h_m N} \tag{2.1}$$

where u is the component of the wind perpendicular to the barrier, h_m is the height of the topography and N is the Brunt-Väisällä frequency. The Brunt-Väisällä frequency indicates that the stability of the flow is crucial to the formation of a barrier jet because stable stratification opposes the upslope flow. The blocking of the flow further cools the atmosphere adiabatically through forced ascent (Mass and Ferber, 1990), producing higher pressure along the slope than at the same level over the adjacent plain and enhancing the component of the pressure gradient parallel to the topography. Within one Rossby radius of the topography, geostrophic balance cannot be established and the cold air is accelerated from high pressure to low pressure like a density current along the unbalanced pressure gradient (Barry, 2008; Bluestein, 1992). The Rossby radius of deformation, L_R, is defined in Equation 2.2 as,

$$L_R = \frac{NH}{f} \tag{2.2}$$

where N is the layer average Brunt-Väisällä frequency, H is the depth of the troposphere and f is the Coriolis parameter. The Rossby radius of deformation is a measure of the length scale of mid-latitude systems and indicates the scale at which buoyancy and Coriolis forces are equal (Barry, 2008). A mesoscale ridge develops parallel to the topography as a hydrostatic response to the trapping of cold air at low levels by the mountains. The characteristic U-shaped ridge of high pressure parallel to the topography can be used to identify the dome of cold air from synoptic sea level pressure charts.

Thermal wind reasoning has also been used to argue that the Brooks Range exerts a significant influence on the low-level flow along the Beaufort coast near Barter Island, Alaska (Dickey, 1961; Schwerdtfeger, 1974; Kozo and Robe, 1986). In this case, the cyclonic turning of the streamlines when northerly flow encounters the mountains is the primary ageostrophic circulation induced by the barrier in the presence of highly stable air (Schwerdtfeger, 1974). In winter, when potentially cold, stable air with a low Froude number flows southward from the Beaufort Sea and encounters the Brooks Range, the cyclonic turning of the flow builds up a mass of cold air near the surface north of the orography that results in a temperature inversion with warmer air on top of the cold. The temperature gradient in this layer is perpendicular to the Brooks Range, with cold air trapped by the topography and warmer air to the north, producing an easterly thermal wind parallel to the mountains in the layer below the top of the topography. The geostrophic wind at the surface can be estimated by subtracting the thermal wind in the layer from the upper level geostrophic wind. Schwerdtfeger (1974) showed that the surface winds depend on the slope of the topography, temperature inversion and static stability.

Dickey (1961) developed a simple model to explain the modification of the pressure field and flow around the "bulge" where the Brooks Range turns to be parallel to the coast. He observed that the strongest westerly winds at Barter Island occurred with cold air at all levels of the atmosphere and very stable air throughout the lowest 8,000 feet, consistent with findings of Schwerdtfeger (1974). Kozo and Robe (1986) extended the analysis of Dickey (1961) to summer to explain why buoys deployed along Beaufort Coast of Alaska during the summer and early fall of 1983 tended to drift to the southeast.

Their results also suggest that the high frequency of westerly winds along the Beaufort Coast in summer could also be explained by an orographic modification of the geostrophic winds by the Brooks Range.

The aforementioned studies focused on the wind regime directly north of the topography at Barter Island. Tuktoyaktuk is located 1000 km to the east of Barter Island and several hundred kilometers to the west of where the Brooks Range ends. Other physical processes might also be important for the wind regime at Tuktoyaktuk.

2.3 Valley flows

Other physical mechanisms have also been described to explain how the overlying geostrophic wind influences the surface winds within a mountain valley. One mechanism is downward momentum transfer (Whiteman and Doran, 1993). When the geostrophic wind aloft is in the same direction as the observed winds at the surface, this suggests that momentum is being mixed to the surface from aloft by turbulent eddies or gravity waves. For momentum to be efficiently mixed to the surface, the atmosphere must be neutrally to unstably stratified.

Another mechanism is pressure driven channeling (Gross and Wippermann, 1987; Whiteman and Doran, 1993; Roebber and Gyakum, 2003). During instances of pressure driven channeling, surface winds in the valley are determined by the component of the overlying geostrophic pressure gradient along the direction of the valley. The pressure gradient along the direction of the valley is zero only when the geostrophic wind is oriented along the direction of the valley. As long as the geostrophic wind has a component perpendicular to the topography, the pressure gradient along the direction of the topography is non-zero and the surface winds will be directed parallel to the mountains.

A third mechanism is forced channeling, which occurs when strong geostrophic winds above a narrow valley are channeled by the sides so that the winds are aligned along the axis of the topography (Whiteman and Doran, 1993).

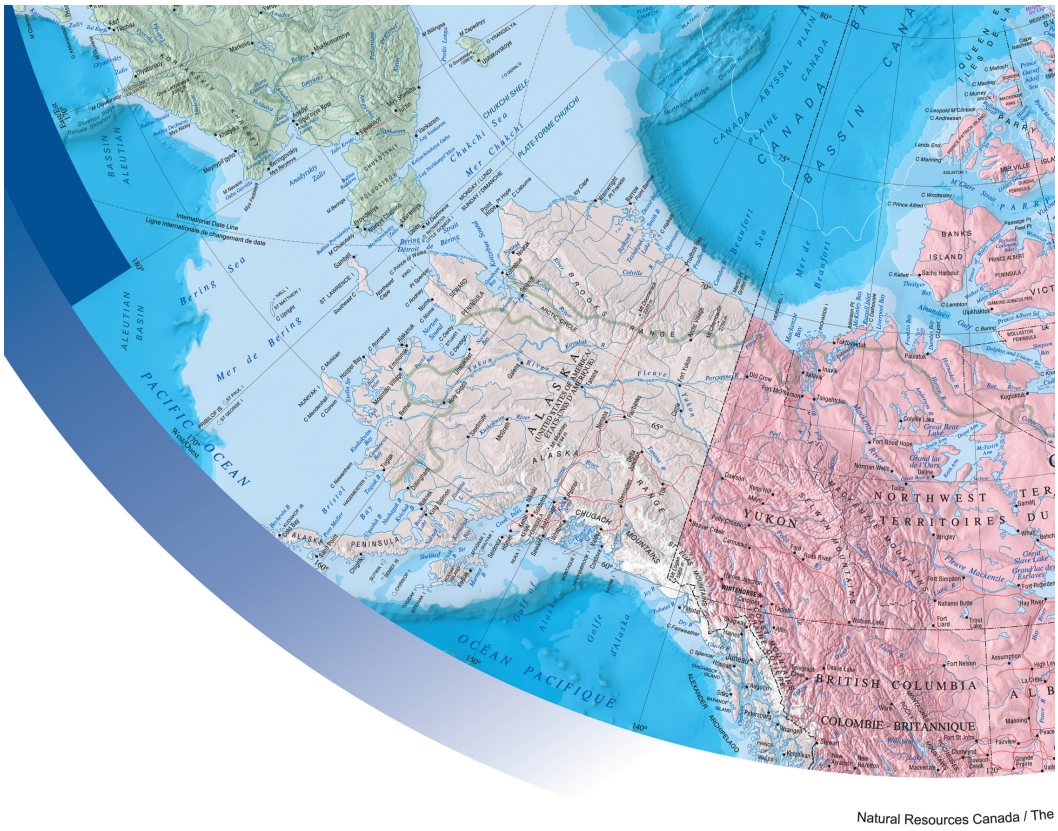

Figure 2.1. The geography of the study area. The map is courtesy of the International Polar Year program.

Chapter 3

Late Summer Wind Climatology for Tuktoyaktuk

3.1 Introduction

The town of Tuktoyaktuk along the Beaufort Coast in the Canadian Arctic has experienced significant coastal erosion damage from storm surge events over the last several decades (Solomon and Covil, 1995). Although storm surges can occur any time of the year, the most dramatic impacts are observed during storm surge events that occur in the late summer and early fall (July through September) when the sea ice coverage reaches its minimum (Manson and Solomon, 2007).

Tuktoyaktuk is located on a narrow peninsula that reaches out into the Kugmalit Bay that is protected on three sides such that only a northwesterly wind produces a long fetch over the Beaufort Sea. Strong northwesterly winds have often been linked to the passage of powerful storms across the Beaufort Sea (Manson and Solomon, 2007; Hudak and Young, 2002). The relatively low frequency of cyclones in the Beaufort Sea (Keegan, 1958; Serreze et al., 1993; Serreze 1995; Brummer et al., 2000; McCabe et al., 2001; Lynch et al., 2003; Zhang et al., 2004; Simmonds et al., 2008) suggests, however, that other physical processes contribute to the high frequency of northwesterly winds at Tuktoyaktuk. One possible contributing factor is the presence of the northwest to southeast oriented Brooks Range upstream from Tuktoyaktuk. Several studies have linked the Brooks Range to strong northwesterly winds at Barter Island, an island directly to the north of the topography (Dickey, 1961; Schwerdtfeger 1974; Kozo, 1980; Kozo and Robe, 1986).

In this study, the late summer wind climatology is compiled for Tuktoyaktuk. The distribution of the observed surface winds is compared to the overlying geostrophic winds to identify the mechanism by which the Brooks Range interacts with the local circulation to produce the high frequency of northwesterly winds at Tuktoyaktuk during

the ice-free months. The role of the topography shaping the distribution of winds at Tuktoyaktuk is examined by addressing the following objectives:

1. Document the surface wind climatology at Tuktoyaktuk for the months of July, August and September

2. Discuss the possible role of topography in this climatology, and document the meteorological conditions associated with a preferred wind regime along the Beaufort coast.

3.2 Data

Environment Canada hourly surface wind observations for Tuktoyaktuk are utilized from 1971 to 2007. For most of the available record, observations from 0500UTC to 1100UTC are not reported, but the wind data is otherwise over 94 percent complete. The observed wind data are used instead of wind fields from the several reanalysis data products because there are more samples per day and because the observations are believed to be more reliable in the arctic where the data assimilation model is less constrained by observations (owing to the sparseness of observations).

Geopotential height data used to estimate the geostrophic wind at Tuktoyaktuk are from the National Center for Environmental Prediction/National Center for Atmospheric Research (NCAR/NCEP) global Reanalysis at a 2.5-degree horizontal resolution (Kalnay et al., 1996). The geostrophic wind at 925hPa was estimated from the geopotential height and then linearly interpolated to the Tuktoyaktuk station (69.4°N, 133.0° W). Temperature data are from the North American Regional Reanalysis (NARR) data (Mesinger et al., 2006) on a 32-km Lambert conformal grid for the period 1979 to 2006. The NARR temperature data are used to estimate the low-level static stability because upper air observations are not available at Tuktoyaktuk and because the NARR model assimilates IR surface brightness temperature and precipitation and uses a much finer 25 hPa level spacing in the boundary layer. The NARR temperature data was also linearly interpolated to the location of the Tuktoyaktuk station before the stability was estimated.

3.3 Seasonality of the wind speed at Tuktoyaktuk

The seasonal cycle of hourly wind speed at the Tuktoyaktuk station is depicted in Figure 1.1. Box and whisker plots (box plots) of the hourly wind speeds from each month are used to depict the seasonal cycle instead of the monthly mean to compensate for the non-Gaussian distribution of the hourly wind speeds. Box and whisker plots allow the shape and location (i.e. central tendency) of the distribution to be visualized without making any assumptions about the statistical distribution of the data. On a box and whisker plot of observed data, the top and bottom of the box indicate the 75^{th} and 25^{th} percentile values respectively. The location of the box therefore indicates where the middle 50 percent of the data lies with the width of box representing the spread in the data. The line inside the box marks the location of the median (50^{th} percentile) value and allows the skewness or asymmetry of the underlying distribution around the median to be visualized. Whiskers extend to the most extreme values within 1.5 times the inter-quartile range (IQR) from the ends of the box. The IQR is defined as the separation between the 25^{th} and 75^{th} percentile values and is often used as a measure of the spread in the distribution. Observations with values beyond the ends of the whiskers are assumed to be outliers and are indicated by crosses.

The box and whisker plots in Figure 3.1 indicate that the monthly distribution of hourly wind speeds is slightly asymmetric with the shape and location of the distribution depending on the season. The median wind speed is larger in the warm season (May through September) than in the cold season (October through April). The location of the median wind speed within the box also suggests that the distribution is more positively skewed (i.e. towards the right tail or the larger values) in the winter months than during the summer. The inter-quartile range (IQR; the width of the box) is smaller during the warm season months of March to July and is narrowest in June, suggesting that the wind speed is less variable in the summer than the winter. The widest spread of observed wind speed is observed in the cold months of December through February.

The box and whisker plots demonstrate that even though the median wind speed is larger in the warm season, the distribution of the wind speed during the cold season is wider (more variable) and more heavily skewed towards larger wind speeds. The

narrowness of the distribution in the summer months compared with winter demonstrates that larger surface wind speeds are observed more frequently at Tuktoyaktuk during the cold season than during the summer. To quantify the seasonality in the magnitude of extreme winds, the distribution of the hourly wind speeds at Tuktoyaktuk is estimated empirically from the data and again by fitting the observations to the Weibull distribution (Weibull, 1951). The two-parameter Weibull distribution is chosen because it has often been used to model hourly wind speed in the engineering and climate literature (Monahan, 2006) and was found to fit the observations quite well.

The empirical histogram and theoretical probability distribution function of the hourly winds at Tuktoyaktuk assuming a Weibull distribution are shown in Figure 3.2. The empirical histogram (black bars) is constructed from the Kaplan-Maier estimate (Cox and Oakes, 1984) of the cumulative distribution function (CDF) of the observations and is normalized so that the area (probability) under the bars is approximately one. The Kaplan-Maier is a non-parametric estimator that provides a robust, distribution-free estimate of the cumulative distribution function from the observed data. The red lines are the probability distribution function (PDF) of the Weibull distribution defined by the parameters estimated directly from the hourly wind speed observations using maximum likelihood estimators. The fitness of the Weibull distribution for representing the wind speed distribution was verified using a Chi-square test on the data from each month. Although the Weibull distribution tends to slightly underestimate the wind speeds for wind speeds exceeding the 99.5^{th} percentile value, the Chi-square test of the wind speeds assuming a Weibull distribution gives p-values less than 0.05.

The Weibull parameter estimates were used to determine the critical values (i.e. the median, 75^{th}, 90^{th}, 95^{th}, 99^{th}, 99.5^{th} percentile) of wind speed for each month (Figure 3.3). The median wind speed determined from the fitted distribution is largest during the months of May through September with values that agree with the box and whisker plots in Figure 3.1. Figure 3.3 indicates that the upper percentile classes of the wind speed distribution abruptly shift to the right (take on higher values) in August and remain larger throughout the winter with a peak in February. This is consistent with the box plots of Figure 3.1, which showed that the distribution of the wind speed is wider and more

positively skewed during the winter months. The winds in August and September, the peak months of the open ice season, appear to be unique because they have a larger median wind speed than observed in winter and larger extreme wind speeds than observed in summer. The fitted values of the percentile classes of wind speed are used later to define what constitutes an extreme wind event.

3.4 Dependence of wind speed on direction

The previous discussion has suggested that the magnitude of extreme wind speeds depends on the season, but has not considered the dependence of the wind speed on direction. The following analysis of the wind speed and direction focuses on July, August and September because these months represent the season of the sea ice minimum when the storm surge risk along the Beaufort Coast is greatest.

The hourly wind speeds for July, August and September were first separated into bins of 30 degrees of meteorological wind direction (measured in degrees from north) and a box and whisker plot constructed for the wind speeds in each bin. This allows the distribution of the wind speed in each direction to be visualized and directly compared with those in the other directions. The box plots of the wind speed by direction (Figure 3.4) indicate that the entire distribution of hourly wind speed is shifted towards higher wind speeds for meteorological wind directions between 270 and 330 degrees (westerly to northwesterly). The shift in the distribution towards higher wind speeds is also much larger in August and September than in July. A much smaller shift in the distribution towards higher wind speeds is also observed for observations with a meteorological wind direction between 90 and 120 degrees (easterly to southeasterly), with the largest difference also observed in August and September. The dependence of the wind speed distribution on the wind direction is quite striking. For wind observations with meteorological directions other than westerly to northwesterly or easterly to southeasterly, the distribution of the wind speed is very similar and displays little dependence on direction.

The strong dependence of the wind speed on direction is an important consideration for modeling of wind speeds at Tuktoyaktuk. Because the distribution of the wind speed depends so strongly on the wind direction, the wind speed observations

are clearly not independent identically distributed (I.I.D.) random variables. Any statistical modeling of the wind speed must therefore take into account the directional dependence. Stochastic modeling of the directional dependence of the wind speed is not one of the stated goals and is beyond the scope of the current study.

The entire distribution of the wind speed is preferentially shifted towards higher values for westerly and northwesterly winds (Figure 3.4), suggesting a physical mechanism that produces larger wind speeds for northwesterly winds all across the distribution and not just in the right tail (extreme values). Because small and median wind speeds are also enhanced, the passage of powerful storms, though certainly important for generating the most extreme winds, cannot alone explain the high frequency of northwesterly winds. The direction of the observed shift in the distribution of the wind speed is approximately parallel to the northwest to southeast orientation of the upstream Brooks Range and suggests a role for the upstream topography in the modification of the wind speed.

3.5 Possible Physical Mechanism for Bimodality of Winds

The results presented in the previous section documented a systematic modification of the wind speed distribution at Tuktoyaktuk for northwesterly winds. In this section, the wind speed and direction are linked to the upstream topography. The topography of Beaufort coast near Tuktoyaktuk (Figure 3.5) is dominated by the convergence of the Brooks Range and the Rocky Mountains. To the west of Tuktoyaktuk, the Brooks Range turns north from the interior of Alaska and becomes oriented in the northwest to southeast direction along the Beaufort coast. If the topography plays an important role in the production of strong westerly and northwesterly winds at Tuktoyaktuk, the distribution of the wind speed and direction should indicate a preference for strong northwesterly or southeasterly winds parallel to the Brooks Range.

3.5.1 Methods

Many studies have addressed the question of wind regimes in the presence of topography. Whiteman and Doran (1993) described several mechanisms by which mountain valleys influence the distribution of surface winds. One mechanism is

momentum mixing, which produces surface winds parallel to the mountain valley when the momentum of the synoptic scale flow over a mountain valley is vertically mixed to the surface by turbulent eddies in a neutral to unstably stratified atmosphere. When the geostrophic wind aloft and the observed surface wind are in the same direction, vertical momentum mixing is likely to be a significant factor. Another mechanism discussed by Whiteman and Doran (1993) is pressure driven channeling, which produces winds parallel to the topography during periods of high stability when the geostrophic wind is perpendicular to the topography. When the geostrophic wind is perpendicular to the topography, the pressure gradient has a component is parallel to the topography and produces an ageostrophic component of the wind down the pressure gradient. To determine whether either of these mechanisms is the primary mechanism favorable for frequent northwesterly winds, the observed winds at Tuktoyaktuk are directly compared to the geostrophic winds aloft.

The 925mb geostrophic winds from the global NCAR-NCEP Reanalysis were linearly interpolated to the Tuktoyaktuk station and used to construct geostrophic wind roses for each month. The 925mb level is chosen because it is below the top of the topography and above the surface. The NCAR-NCEP Reanalysis is used because it covers the entire period of observations and is less noisy than the much finer resolution NARR when estimating horizontal derivatives. Wind roses of the observed surface wind and the geostrophic wind were constructed for each month to compare the distribution of the observed and geostrophic wind directions. The observed surface wind direction is then directly compared to the 925hPa geostrophic wind at the corresponding 6-hour period in the NCAR Reanalysis data by constructing 2-dimensional histograms estimating the joint distribution of the geostrophic and surface wind directions. A joint distribution defines the probability of events in terms of two random variables. In the current study, the two random variables are observed and geostrophic wind direction (speed). We constructed the histogram by binning the surface wind and 925hPa geostrophic wind directions into the same 10-degree bins and counting the number of occurrences for each possible combination of wind directions. Two-dimensional histograms were also created to directly compare the speed of the 925hPa geostrophic to the speed of the observed surface winds.

To evaluate the mechanism favorable for the frequent northwesterly winds, the relationship between the static stability and the winds must also be estimated. We evaluated the stability by calculating θ_z at 975hPa with centered finite differences and estimating the empirical cumulative distribution function (CDF) for each month from the NARR data. Here, θ_z is the derivative of the potential temperature with height in units of K m^{-1}. The vertical derivative is estimated with finite differences calculated between the 950 hPa and 1000 hPa pressure surfaces. The NARR data is used because the fine resolution in the boundary layer is needed to reliably estimate the stability in the layer below the top of the topography. The cumulative distribution function (CDF) of the stability is evaluated for each month from the calculations of θ_z to quantify the seasonal differences in the stability, which likely contribute significantly to the observed seasonality in the distribution of the wind speed. The distribution of the stability during periods of strong northwesterly and southeasterly winds is also evaluated. Strong northwesterly winds are defined as hourly observations with a meteorological wind direction between 270 degrees and 360 degrees and a speed exceeding the 95th percentile for that month. Strong southeasterly winds are defined as those exceeding the climatological 95th percentile with meteorological wind directions between 45 and 135 degrees.

3.5.2 Results

The wind roses of observed winds indicate that the July surface winds are primarily northwesterly (following the topography) or northerly to easterly (from the water towards the land), suggesting that topographically or sea breeze generated winds are the most frequent and that the wind rarely blows from the land to the water (Figure 3.6a). The relatively high frequency of flow from the cold water to the warm land brings stable air over the land and is consistent with the lower wind speeds observed in July compared to August or September. In August, the distribution of the surface winds exhibit bimodality in the northwesterly and southeasterly directions (Figure 3.6b), but with most of the extreme winds (speeds exceeding 95th percentile or 10m s^{-1}) from the northwest. The wind direction in September (Figure 3.6c) is also bimodal, but with a higher frequency of large easterly winds. The wind roses indicate a preference for large winds parallel to the topography in either direction while the box plots (Figure 3.4)

indicate that the entire distribution is shifted only for northwesterly winds. This suggests while topography is important for the generation of northwesterly surface winds, a different physical mechanism might be associated with strong easterly or southeasterly winds. To link the observed distribution of wind speeds to the topography, the observed surface wind is related to the overlying geostrophic wind and the stability of the atmospheric column.

The geostrophic wind rose for July (Figure 3.6d) indicates that the distribution of the 925mb geostrophic wind is similar to the observed surface wind with a majority of the large geostrophic winds coming from the west. In August (Figure 3.6e), the distribution of the geostrophic winds is bimodal but with a much higher frequency of northwesterly winds, especially those exceeding 10m s^{-1}. The September geostrophic winds are also bimodal but with more large southeasterly winds than in August, similar to the distribution of the observed winds at the surface. The agreement between the surface and 925mb geostrophic wind roses, especially in August and September, is consistent with momentum mixing. To directly compare the wind direction, the 2-dimensional histograms of the observed and geostrophic wind directions are used to identify the mechanism.

In all three months, the histograms indicate that the non-zero probabilities tend to fall along the line indicating that the geostrophic wind and the surface wind are in the same direction (Figure 3.7 a, b and c). In July and September, the histograms suggest that the most frequently observed flow is easterly 925hPa geostrophic (90 – 150 degrees) and surface (60 – 90 degrees) winds with a lower frequency of northwesterly winds. The flow is significantly different in August with the histogram indicating a much higher probability that the surface winds and the 925hPa geostrophic winds are both northwesterly.

The 2-dimensional histograms of the joint distribution of observed and geostrophic wind speeds in July, August and September (Figure 3.7d, e and f) also indicate that the non-zero probabilities tend to fall along the line where the surface wind speed and the geostrophic wind speed are of similar magnitude. The correlation between the 925hPa wind speed and the surface wind speed is 0.333, 0.439 and 0.409 for July,

August and September respectively and is statistically significant ($p<0.99$) for each month. The positive correlation between the speed of the geostrophic wind and the surface wind is consistent with the suggestion that momentum mixing is a significant factor in producing the observed distribution of the wind speed and direction. The high frequency of strong northwesterly surface winds can be explained by a pressure gradient that produces northwesterly geostrophic winds aloft that are frequently mixed to the surface. For momentum mixing to be the dominant mechanism, neutral or unstable conditions are also required.

The CDF plot of θ_z indicates that the stability of the atmosphere is quite different in July, August and September (Figure 3.8 a). The CDFs are shifted such that in July the atmosphere is less likely to have negative (unstable) or extremely small (neutral) values than in August which in turn is less likely to be unstable or neutral than September. Box plots of the 975hPa stability during periods of strong northwesterly winds are shifted towards smaller values in all three months (Figure 3.8 b, c, d). The distribution is also much narrower, indicating that most periods of strong northwesterly winds at the surface tend to occur when the atmosphere is unstably or neutrally stratified. During periods of strong easterly to southeasterly winds, the distribution of the stability is shifted towards higher values and a larger spread. The strong easterly winds are not exclusively associated with unstable to neutral conditions, often occurring during periods of highly stable stratification. This is consistent with the suggestion that different physical mechanisms favor strong northwesterly and strong southeasterly surface winds at Tuktoyaktuk.

The wind roses (Figure 3.6) demonstrated that while the distribution of 925hPa geostrophic winds is very similar in July and September, the surface winds are very different. In both July and September, westerly winds at the surface tend to occur with westerly geostrophic winds aloft. The higher stability in July is unfavorable for the mixing of northwesterly geostrophic momentum to the surface and explains why fewer large northwesterly winds are observed at the surface in July than in September. The situation is quite different in August when the atmosphere is on average more stable than in September. Large surface winds in August are more likely to be northwesterly than in

September not because of differences in stability, but because the geostrophic winds are much more likely to be northwesterly during August than September.

The sea level pressure (SLP) and 975mb temperature (T_{975}) anomalies during periods with low stability and extreme northwesterly surface wind at Tuktoyaktuk are shown in Figure 3.9. The NARR data are used because the 32 km horizontal resolution better represents mesoscale features in the anomaly fields. Hours with observed surface westerlies exceeding the climatological 95th percentile were identified from the station data at Tuktoyaktuk. Any-three hour period in the NARR data (1979 to 2006) during which at least one hour of extreme northwesterly winds are observed at Tuktoyaktuk and a θ_z less than 5 K km^{-1} was included in the calculation of the SLP and T_{975} anomalies. This criterion identified 55 such events in July, 144 in August and 128 in September between 1979 and 2006 that are used to create composites for each month. The long-term mean (1979 to 2006) was subtracted from SLP and T_{975} and maps of the anomalies constructed to demonstrate the importance of cold air and high surface pressure parallel to the mountains on strong northwesterly winds at Tuktoyaktuk.

The SLP anomalies (Figure 3.9 a, b and c) indicate anomalously low pressure to the north and east of Tuktoyaktuk and anomalously high pressure to the west. The low-pressure anomaly is largest in September while the high-pressure anomaly along the coast west of Tuktoyaktuk is strongest in August. The U-shaped stretching of the SLP anomaly contours parallel to the topography indicates that high pressure anomalies form to the north of the mountains and strengthen the pressure gradient favorable for northwesterly geostrophic winds at Tuktoyaktuk. This pattern of SLP anomalies resembles the SLP contours typically observed during cold air damming events in the Appalachians (Bell and Bosart, 1988).

Maps of 975 hPa temperature anomalies (T_{975}) confirm the role of cold temperatures in producing the observed sea level pressure anomalies (Figure 3.9 d, e and f). Negative temperature anomalies are observed over most of the Beaufort Sea and adjacent land areas, with the coldest air observed north of the Brooks Range to the west of Tuktoyaktuk. The coldest anomalies are observed where the Brooks Range meets the coast with the edge of the coldest anomalies tending to follow the topography. The

strongest negative anomalies are observed in August, consistent with the larger high-pressure anomalies that extend farther to the east. The build up of cold air to the north of the mountains causes the pressure and overlying geopotential heights to rise producing a pressure gradient that is conducive for down gradient flow parallel to the coastal topography. The pattern of low-level flow associated with the observed temperature and pressure are investigated by creating a composite of the 10m wind from the NARR averaged over the same set of hours.

The map of the composite mean wind in Figure 3.10 zooms in along the region of the Beaufort Sea where Brooks Range approaches the coast. Here, the composite mean of the wind vectors and the wind speed are shown and not the anomalies because the long-term mean of the wind is approximately zero over much of the domain (not shown). The 10m wind speed (shaded) indicate that the upstream winds over the coastal region of the Beaufort Sea are also much larger during the identified periods of extreme winds at Tuktoyaktuk and are significantly larger in August and September than in July. The wind vectors indicate that the 10m winds are also northwesterly and directed parallel to the coastal mountains over the entire domain upstream of Tuktoyaktuk, especially in August and September, consistent with the observed pressure gradient directed along the topography. The near shore 10m winds are enhanced and oriented parallel to the topography for several hundred kilometers upstream of Tuktoyaktuk. The composites in Figures 3.9 and 3.10 demonstrate that the coastal topography creates conditions favorable for the generation of strong northwesterly winds over open water upstream from Tuktoyaktuk.

3.5.3 Discussion

In this study, the climatology of late summer (July through September) surface winds at Tuktoyaktuk was developed. We have clearly documented that the distribution of the wind speed is linked to the meteorological wind direction, with the distribution of westerly to northwesterly winds significantly shifted towards higher wind speeds compared to winds in other directions. The relationship between the geostrophic winds at 925hPa and the winds at the surface is investigated to determine why the distribution of wind speed at Tuktoyaktuk during the late summer so strongly favors strong

northwesterly winds. The results indicate that momentum mixing is the most likely explanation for the observed distribution of wind speed and direction. Westerly to northwesterly surface winds at Tuktoyaktuk tends to occur when the overlying geostrophic wind is from the same direction. A statistically significant positive correlation also exists between the surface and 925hPa geostrophic wind speeds, consistent with the suggestion that momentum is frequently mixed to the surface. For momentum to be effectively mixed by turbulent eddies, neutral to unstable stratification is required. Our results demonstrate that northwesterly winds exceeding the 95th percentile occur during periods of low atmospheric stability, strongly suggesting that momentum mixing is a significant factor in the observed distribution of wind speed and direction at Tuktoyaktuk.

Composites were also created to examine the sea level pressure, 950hPa temperature and 10m winds during periods of strong northwesterly wind at Tuktoyaktuk. In all three months, high pressure over the Barents Sea with low pressure to the east, consistent with a northwesterly geostrophic wind, is observed in the composite. In August and September, the months with higher frequencies of strong northwesterly winds, a U-shaped ridge is also observed along the Brooks Range. The ridge in the pressure field produces anomalous northwesterly flow parallel to the topography, consistent with previous findings suggesting that barrier jets commonly occur north of the Brooks Range.

The role of sea ice, topography and sea surface temperatures on the development of the storms themselves has not been addressed in this study. Furthermore, we have not addressed the strong seasonal differences in stability characteristics. Our results demonstrate that seasonal contrasts in stability are an important factor in understanding why the risk for storm surge events increases later in the season. Kahl et al. (1999) investigated stability in the eastern Arctic and demonstrated the importance of rapid seasonal changes in cloud cover, sea ice and radiation, all of which are possibly important for the coastal wind regime. A detailed study of the physical mechanisms that produce the observed stability distribution shown in Figure 3.8 has not been performed and is beyond the scope of the current study.

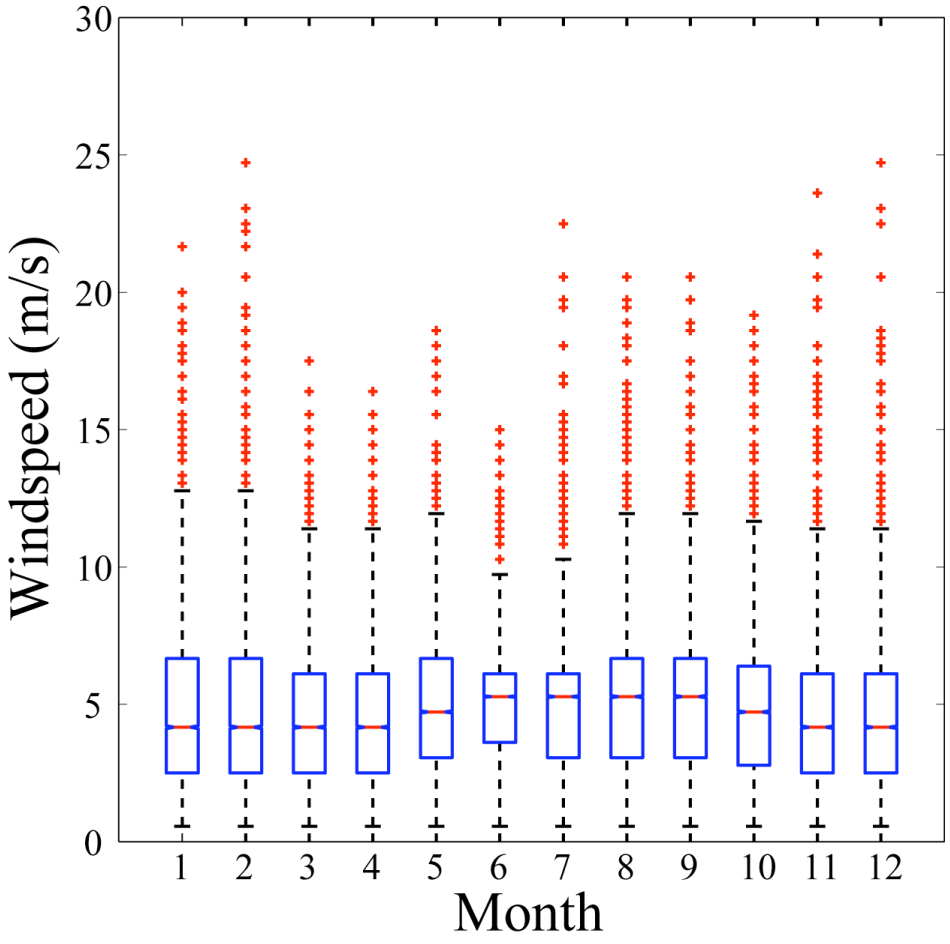

Figure 3.1. Box plots of the hourly wind speed distribution by month. The top and bottom of the box indicates the 75th and 25th percentile wind speeds respectively. The line inside the box indicates the median wind speed. The length of the dashed lines (whiskers) is 1.5 times the width of the box (the inter-quartile range). All observations outside the whiskers (crosses) are considered to be outliers. The wind speed has units of m s^{-1}. On the x-axis, month 1 corresponds to January, month 2 to February, month 3 to March, month 4 to April, month 5 to May, month 6 to June, month 7 to July, month 8 to August, month 9 to September, month 10 to October, month 11 to November and month 12 to December.

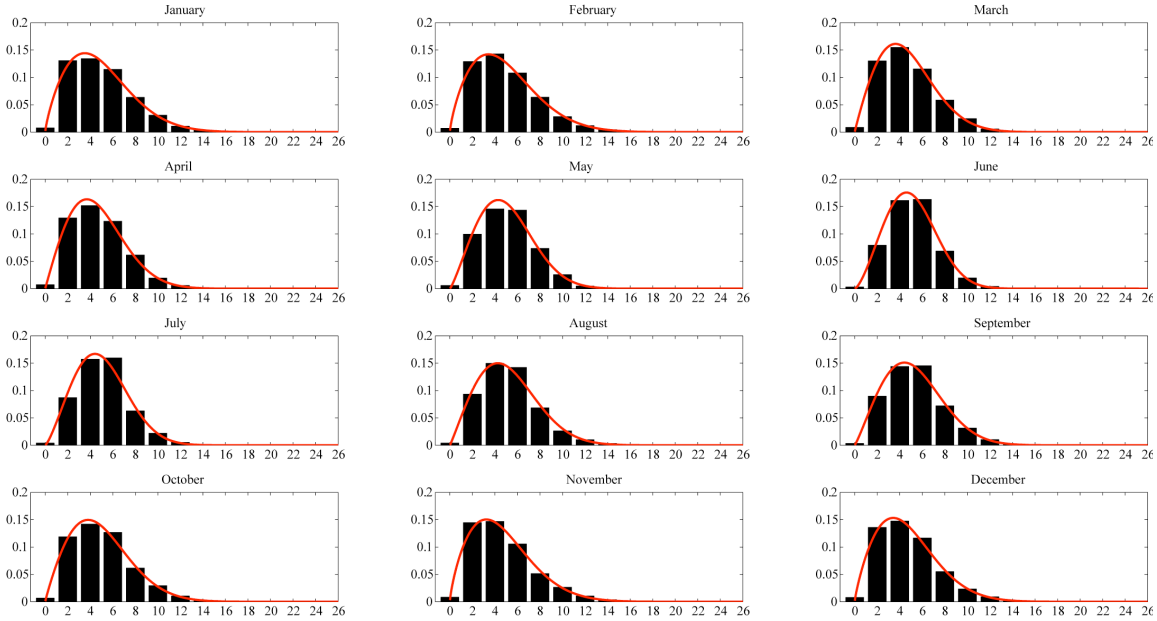

Figure 3.2. The probability distribution (PDF) of the observed hourly winds at Tuktoyaktuk for each month. The heights of the black bars represent the empirical PDF estimated directly from the data and normalized such that the area (probability) under the histogram is equal to one. The red line is the histogram of the Weibull distribution with parameters determined from the observed hourly winds using maximum likelihood estimators.

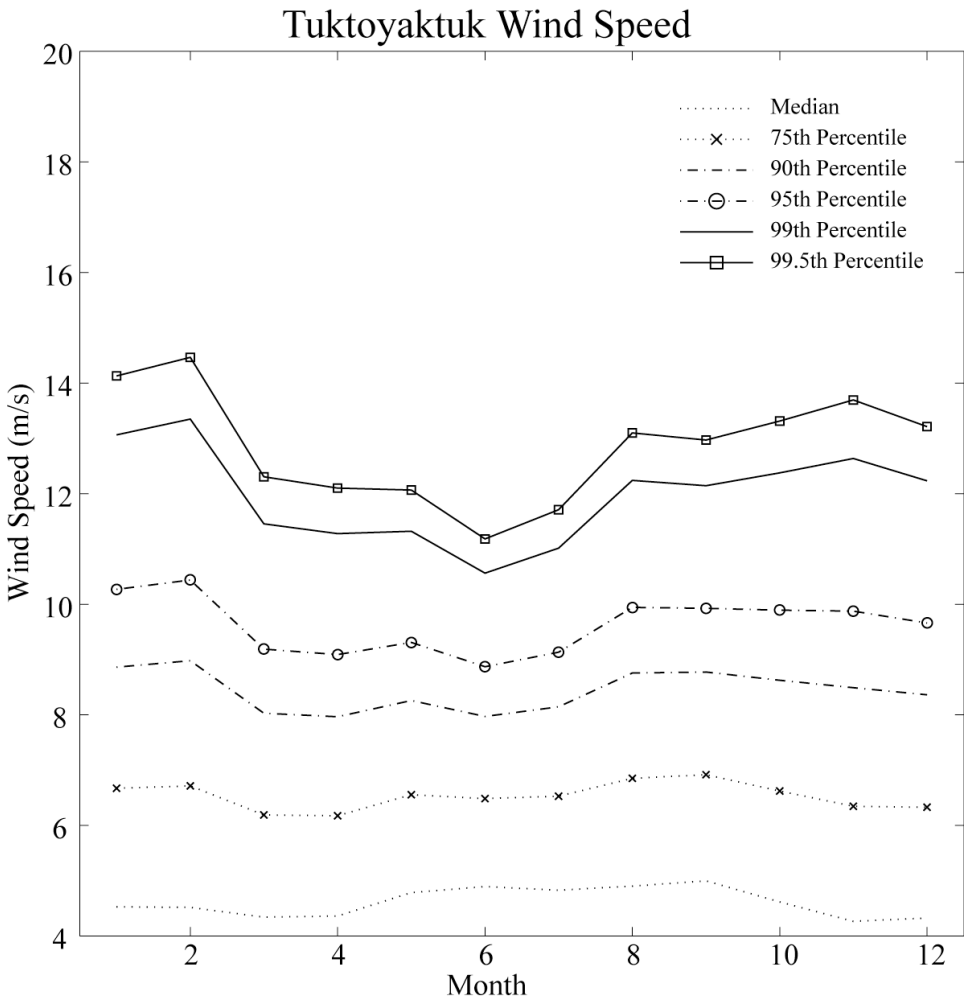

Figure 3.3. The seasonal variation in critical values of the hourly wind speed at Tuktoyaktuk. The median, 75th, 90th, 95th, 99th and 99.5th percentile hourly wind speeds for each month are taken from the Weibull distribution with parameters estimated from the observed data using maximum likelihood estimators.

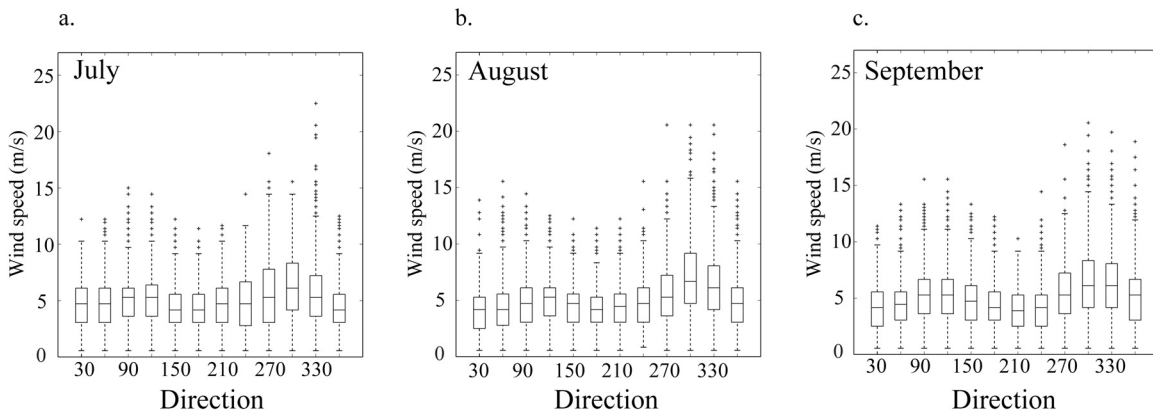

Figure 3.4. Box plots of the observed wind speed at Tuktoyaktuk by direction for the months of July (a), August (b) and September (c). The wind speed is sorted by meteorological wind direction into bins of 30 degrees and a box plot created for each bin. The top and bottom of the box indicates the 75th and 25th percentile wind speeds respectively. The line inside the box indicates the median wind speed. The length of the dashed lines (whiskers) is 1.5 times the width of the box (the inter-quartile range). All observations outside the whiskers (red crosses) are considered to be outliers. The wind speed is in units of m s^{-1}.

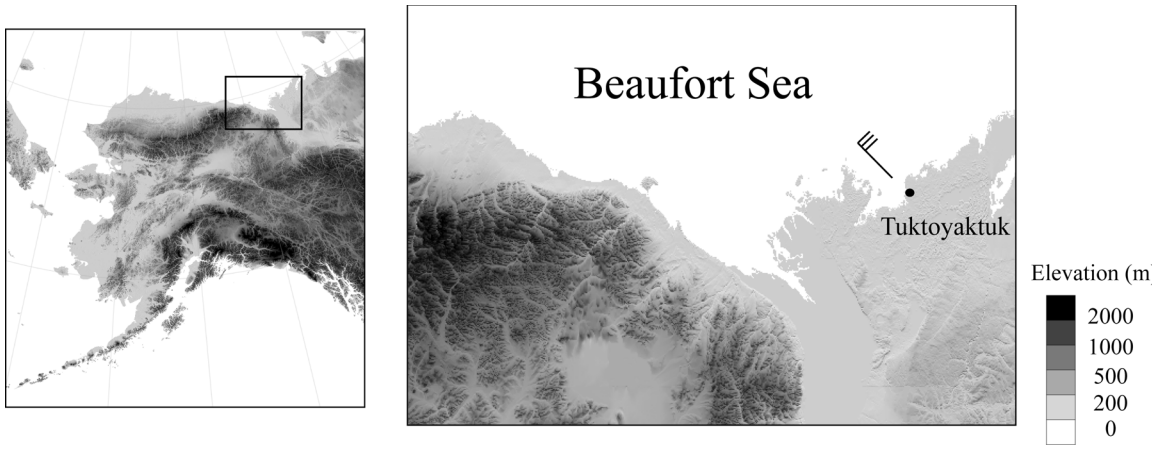

Figure 3.5. Map of the Beaufort Coast showing the location of the Tuktoyaktuk station and the surface elevations of the local topography. A wind barb with an arbitrary wind speed and 270° meteorological wind direction (northwesterly) is inserted for reference.

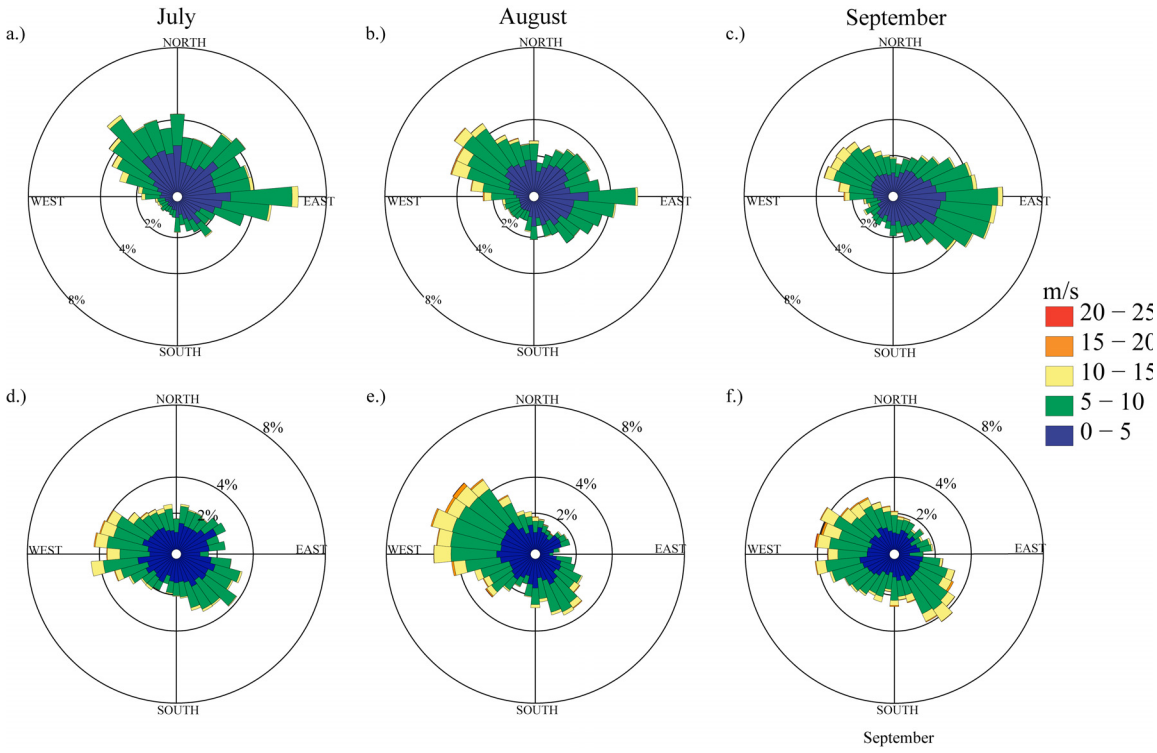

Figure 3.6. Wind roses of observed (a,b,c) and 925mb geostrophic (d,e,f) winds at Tuktoyaktuk (m s^{-1}) for July, August and September.

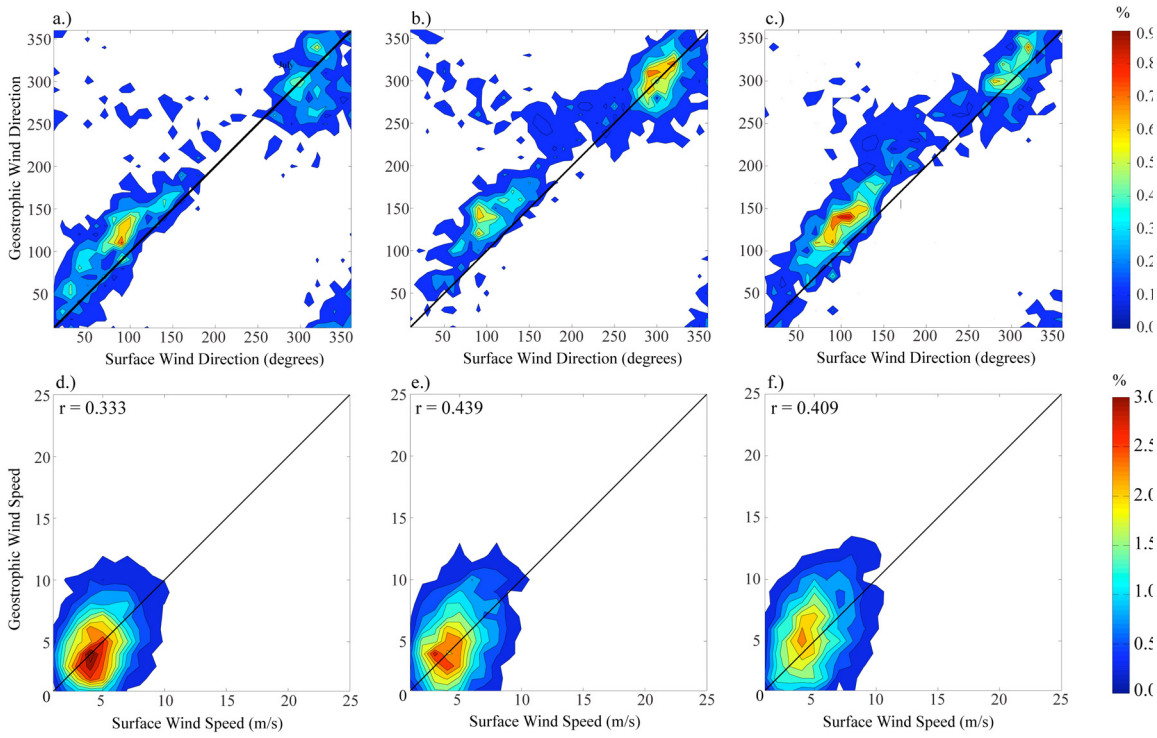

Figure 3.7. The empirical 2-dimensional histogram of the joint probability distribution of the July, August and September 925mb geostrophic and observed wind directions (a., b., c.) and wind speed (d., e. and f.) at the same observation time. The black line indicates where the 925mb geostrophic and surface winds are in the same direction or have the same wind speed. The histogram is normalized so that the units are the percentage of total observations. Note that the histograms of the wind direction and wind speed are on different scales.

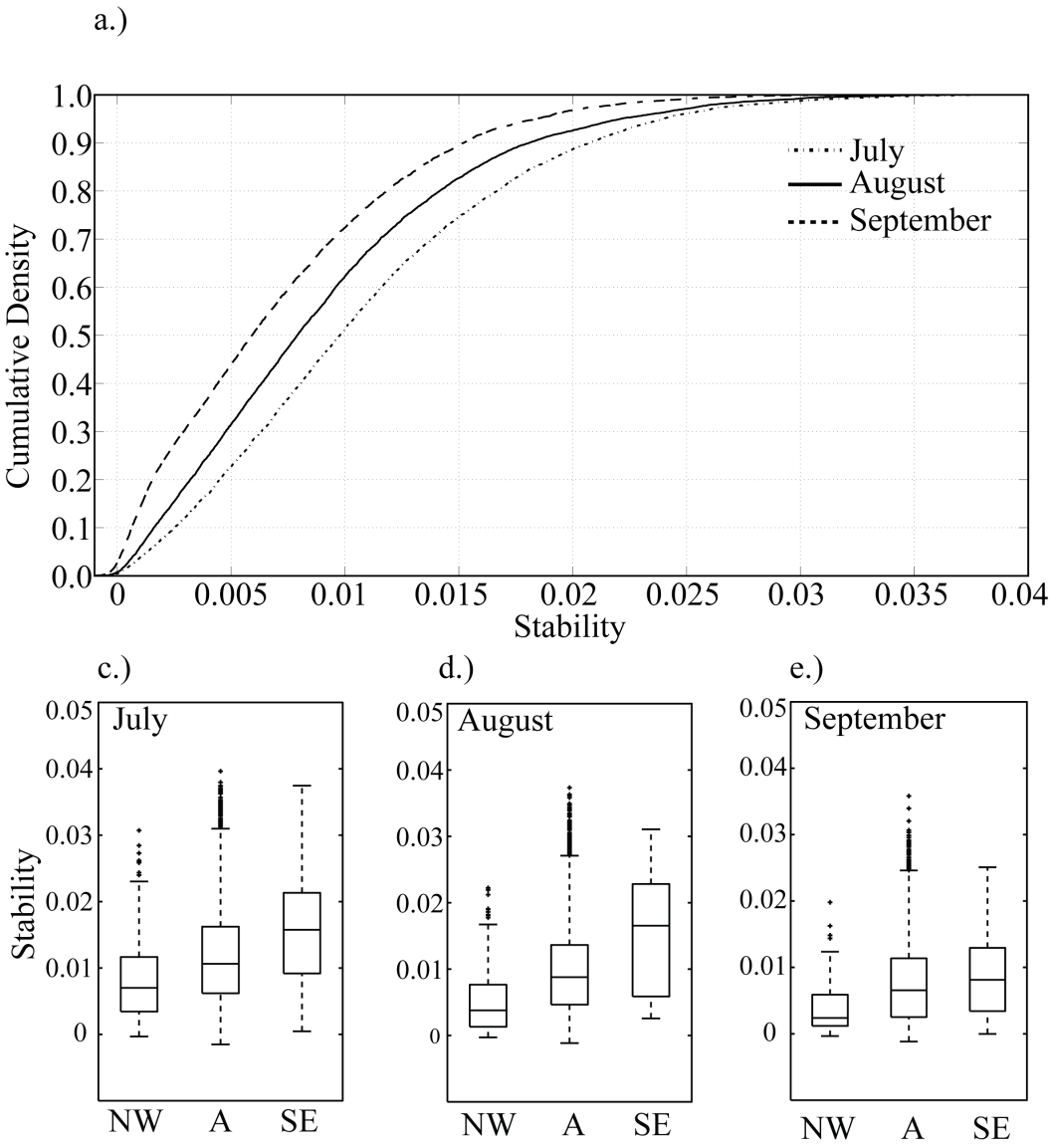

Figure 3.8. The empirical cumulative distribution function of the 975mb stability (θ_z) for the months of July, August and September (a). The box plots show the distribution of the stability index for cases of extreme northwesterly winds (NW; 270°-360°), extreme southeasterly winds (SE; 45°-135°) and for all hourly observations (A) during the months of July (c), August (d) and September (e). The stability has units of K m^{-1}.

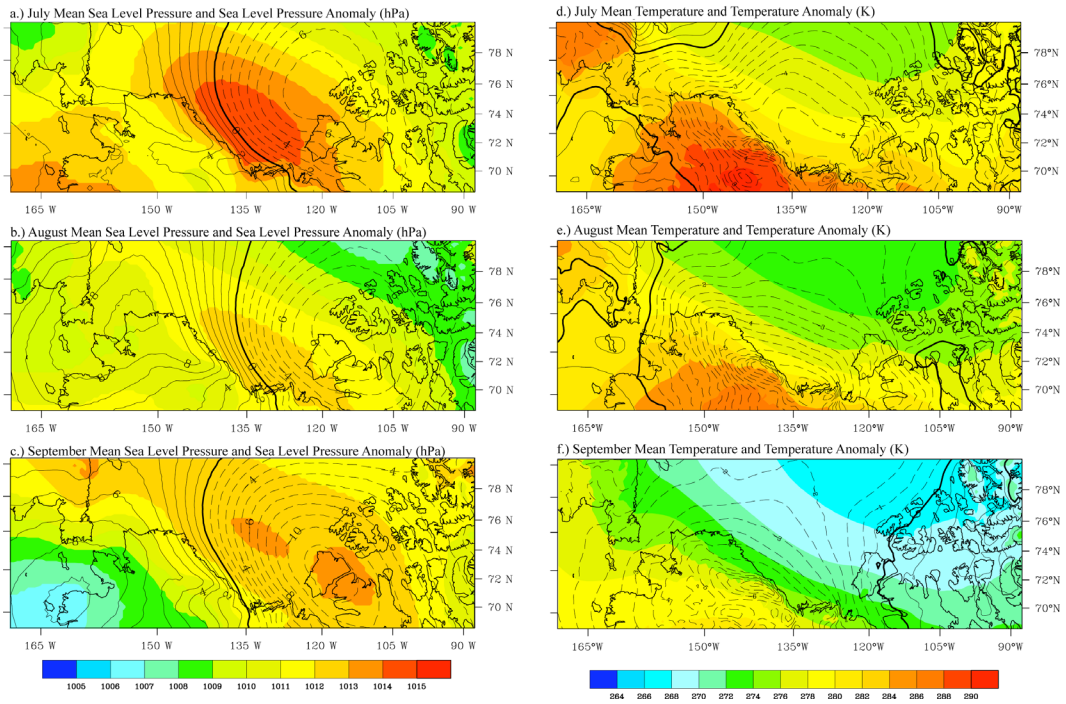

Figure 3.9. The mean sea level pressure and sea level anomalies (a, b, c) and mean 975mb temperature and anomalies (d,e,f). The anomalies are the deviation from the long-term mean during those 3-hour periods with extreme northwesterly winds and a neutral to unstably stratified atmospheric column at Tuktoyaktuk. Negative anomalies are shown with dashed contours and positive anomalies, solid contours and the zero contour in bold. The contour interval is 1 hPa for sea level pressure and 0.5 K for the temperature anomalies. The long-term mean (1979 – 2006) of the sea level pressure and temperature used to create the anomalies for each month are shaded.

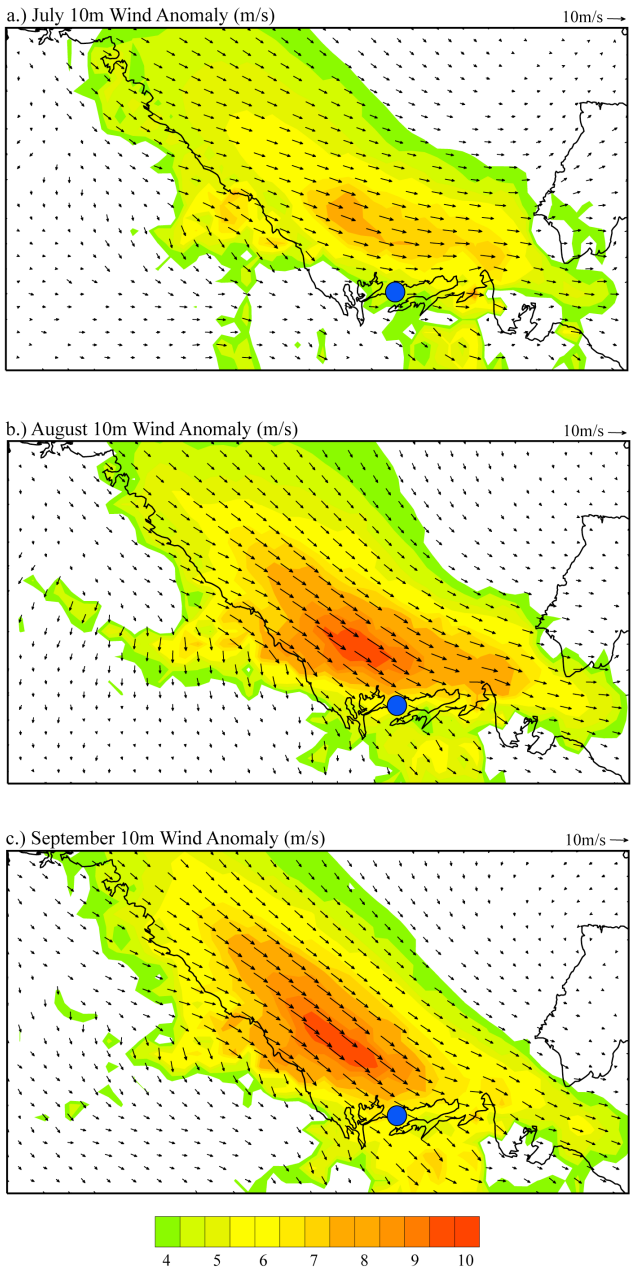

Figure 3.10. The mean 10m wind composite averaged over the 3-hour periods with extreme northwesterly winds and a neutral to unstably stratified atmospheric column at Tuktoyaktuk. The wind speed is shaded to highlight the location of the strongest winds. Only wind speed anomalies greater than 4 m/s are shaded. The location of Tuktoyaktuk is marked with a filled blue circle.

Chapter 4

Meteorological Conditions Conducive for the Devastating September 1999 Extreme Wind Event at Tuktoyaktuk

4.1 Introduction

Between September 24 and 28 September 1999, the hamlet of Tuktoyaktuk, a community along the Beaufort coast of Canada, experienced significant storm surge damage during a period of unusually persistent northwesterly winds (Solomon, personal communication). The event is notable not only because of the strength of the cyclone that passed along the Beaufort coast or the persistence of the northwesterly winds observed over Tuktoyaktuk, but also because of the unusual sequence of meteorological events that preceded them.

Ideally, tidal gage data would be used to identify the beginning and end of a storm surge event. Unfortunately, tidal gage data are not available for the period of this damaging storm surge event. The hourly wind speed, wind direction, sea level pressure and temperature data for the station at Tuktoyaktuk used to identify the period of extreme winds are from the Environment Canada hourly surface data archive. Timeseries of the observed hourly wind speed (knots), meteorological wind direction (degrees from north), sea level pressure (hPa) and temperature (degrees Celsius) at the Tuktoyaktuk station are shown in Figure 4.1. The timeseries includes observations from 0000UTC on September 14 to 2300UTC on September 30 and is complete except for missing values between 0500UTC and 1100UTC when the airport is closed each day. For this discussion, an intense northwesterly wind is defined as a wind observation with a meteorological wind direction between 270° and 360° degrees and a wind speed exceeding the climatological 95^{th} percentile value of approximately 20 knots (10 m s^{-1}) for September.

The timeseries in Figure 4.1 indicates that the winds turned northwesterly and intensified around 1800UTC on September 23, when the wind speed abruptly increased from approximately 10 knots to over 20 knots and the wind direction changed from

approximately 90 degrees (easterly) to 270 degrees (westerly). An extremely large drop in the sea level pressure preceded the shift in the wind speed and direction, with the observed sea level pressure at Tuktoyaktuk falling from a high of approximately 1007hPa at 0000UTC on September 22 to a minimum of 969hPa between 1200UTC and 1900UTC on September 23. The shift in the wind direction from southeasterly to northwesterly began after the sea level pressure at Tuktoyaktuk began to increase, suggesting that a deep surface low passed to the south of Tuktoyaktuk late on September 22 causing the sea level pressure to fall and the winds to turn westerly.

The observed winds at Tuktoyaktuk remained intense and westerly to northwesterly until about 0600UTC on September 26, after which time they began to weaken and turn southerly (meteorological wind direction of approximately 180 degrees), eventually reaching a minimum wind speed of approximately 7 knots by 0000UTC on September 27. Intense northwesterly winds were again observed intermittently at Tuktoyaktuk between 0000UTC and 1800UTC on September 28. This second period of intense northwesterly winds occurred as the temperatures steadily fell and the pressure rose to nearly 1040hPa. The wind speed continued to weaken as the sea level pressure rose, though the direction remained northwesterly until late on September 30. The timeseries of the wind observations suggest that the strong westerly winds occurred in two distinct phases, possibly with different physical mechanisms underlying each.

The evolution of the synoptic conditions preceding the storm surge event is summarized in a series of NOAA-14 satellite images (Figure 4.2). At 1402UTC on September 22 (Figure 4.2a), the satellite shows that a very deep cyclone was present in the Gulf of Alaska. At this time, the well-developed comma shape cloud associated with this system can be seen approaching the southern coast of Alaska. Four hours later, at 1800UTC (not shown), the central pressure in this storm reached a minimum of 949hPa according to the ERA40 Reanalysis. Like most cyclones having reached such a low central pressure, this storm had undergone explosive or bomb cyclogenesis (Sanders and Gyakum, 1980) with the central pressure dropping by approximately 32hPa in the preceding 24 hours.

By 1441UTC on September 23, two separate storms are clearly visible in the satellite image (Figure 4.2b). In addition to the parent cyclone in the Gulf of Alaska, the image shows that a secondary cyclone has developed along the Beaufort coast in the lee of the Rocky Mountains southwest of Tuktoyaktuk. The ERA SLP field indicates that the central pressure in the two storms was approximately the same (971hPa) at 1200UTC. By 1351UTC on September 24 (Figure 4.2c), the secondary cyclone has moved east along the Beaufort coast and the original cyclone in the Gulf of Alaska has substantially weakened. The satellite image from 1351UTC on the 24th also shows another interesting meteorological feature of this meteorological wind event. A cloud streak is clearly visible extending from the Alaska coast north across the Beaufort Sea, suggesting the presence of a strong front.

The satellite images demonstrate that a deep cyclone in the Gulf of Mexico approached the southern coast of Alaska, redeveloped along the Beaufort coast in the Canadian Arctic and moved off to the east of Tuktoyaktuk. The goal of this part of the study is to identify the physical processes that helped to create the conditions favorable for rapid cyclogenesis and the subsequent redevelopment along the Beaufort coast and how they contributed to the damaging wind event at Tuktoyaktuk.

A detailed case study is performed to identify the synoptic scale precursors and physical processes that created conditions favorable for persistent NW winds at Tuktoyaktuk during late September 1999. Several objectives are directly addressed in this study:

- Identify the important physical processes that led to bomb cyclogenesis event in the Gulf of Alaska and the subsequent redevelopment of the surface cyclone along the Beaufort Coast.
- Identify the meteorological conditions that created conditions favorable for the strong NW winds to persist near Tuktoyaktuk for a period of several days.
- Discuss the role of the Brooks Range, if any, in the generation of the persistent NW winds at Tuktoyaktuk.

4.2 Background Information

4.2.1 Bomb Cyclogenesis

Rapidly intensifying extratropical cyclones have been extensively studied over the past several decades because of their potential for causing extensive damage to ships and land based infrastructure and because the difficulty that early forecast models had in forecasting them (Wang and Rogers, 2001). The first study to document the climatology of explosive deepening or "bomb" cyclogenesis was Sanders and Gyakum (1980), who defined bomb cyclones as low-pressure systems whose sea level pressure falls at a rate of at least 1 Bergeron (BER). The authors named the unit of explosive deepening after Tor Bergeron, who characterized rapidly deepening extra-tropical cyclones as those in which the central sea level pressure falls at a rate of at least 1 hPa hr^{-1} for 24 hours. Sanders and Gyakum defined the unit Bergeron to be the geostrophically equivalent deepening rate of 24 hPa in 24 hours at arbitrary latitude, ϕ, relative to 60°N where Bergeron made his observations,

$$BER = 24\frac{\sin(\phi)}{\sin(60^\circ)} \tag{4.1}$$

Explosive cyclogenesis is a cold-season phenomenon that is primarily observed over maritime regions (Sanders and Gyakum, 1980), though they have also been observed over the continents (Gyakum and Barker, 1988; Hakim et al., 1995; Bosart et al., 1996). Several recent climatologies (Sanders and Gyakum, 1980; Gyakum et al., 1989; Roebber, 1984; Chen et al., 1992) have identified the northwestern Pacific and northwestern Atlantic as the primary regions for explosive cyclogenesis, although it is also frequently observed in the eastern Pacific and Gulf of Alaska (Murty et al., 1983) and eastern Atlantic (Wang and Rogers, 2001). The western regions of the ocean basins typically have the warmest sea surface temperatures at any latitude, suggesting that diabatic processes including latent heat release are an important factor in explosive development (Davis and Emanuel, 1988). These regions also exist along the primary storm tracks where the strongest baroclinicity is observed, indicating that dynamic forcing and baroclinic processes are also important. The combination of unstable

maritime air, baroclinicity and upper level dynamic forcing in these regions is thought to be conducive for explosive deepening (Wang and Rogers, 2001).

Many studies have suggested that bombs, like the majority of cyclones, arise from baroclinic instability (Wang and Rogers, 2001) while other studies have questioned whether the development of explosive events is significantly different from the majority of cyclones. Roebber (1984) used a statistical approach to argue that the mechanism of explosive development is a combination of baroclinic processes and other processes, possibly including dynamic and thermodynamic processes that modify the conditions favorable for baroclinic instability. It has also been suggested that physical processes of lesser consequence under normal conditions contribute to the rapid development (Davis and Emmanuel, 1988; Nuss and Anthes, 1987).

Explosive development has been linked to the presence of a mobile short wave trough (Sanders and Gyakum, 1980). Two of the most severe and widely studied explosive events, the QEII storm (Gyakum, 1983ab., 1991; Uccellini, 1986) and the President's day cyclone (Bosart, 1981) both underwent explosive deepening during periods when the surface cyclone was located underneath a region of strong 500mb vorticity advection. Other studies have identified the presence of a mobile upper level jet streak (Uccellini et al, 1985) or the intrusion of high PV air from the stratosphere during tropopause folding events (Bosart and Lin, 1984; Uccellini et al., 1985) as important dynamic factors in explosive events. It has also been suggested that the surface response to upper level vorticity anomalies depends on the antecedent surface vorticity with periods of rapid deepening often being preceded by pre-existing surface developments (Gyakum et al., 1992).

Low-level baroclinicity is another well-know contributor to the deepening of surface systems. Many studies have identified the importance of latent heat release (Gyakum, 1983b; Reed et al., 1988), surface energy and moisture fluxes (Davis and Emanuel, 1988; Nuss and Anthes, 1987; Gyakum and Danielson, 2000) and low-level stability (Nuss and Anthes, 1987) on the explosive deepening process.

4.2.2 Lee-Side Cyclogenesis

It has long been known that the lee side of the Rockies and Alps are among the preferred cyclogenesis regions of the globe. Petterssen and Smebye (1971) described a type of cyclone formation frequently observed in the lee of mountain ranges in the mid latitudes where an upper level trough moves ahead of the cold front that has been blocked by the topography. The resulting cyclonic vorticity advection over a shallow, barotropic lee trough often results in rapid development of surface cyclones. A conceptual model to explain the development and movement of cyclones and troughs to the lee of the Rocky Mountains was suggested by Palmen and Newton (1969). They suggested that the formation of the lee cyclone is often preceded by the landfall of a cyclone from the Pacific. As the cyclone approaches the coast, the wind in the lower troposphere increases and a lee trough forms to the east of the topography where the air is warmed by down slope flow. The lee trough broadens as warm air advection east of the topography increases. The approach of an upper level trough or strong jet streak with cyclonic vorticity promotes the development of a surface cyclone within the trough. The development continues until a cold front shuts off the warm advection and causes the cyclone to move east, although other studies suggested that a cold front is not required for the cyclone to break away from the topography and move to the east (Locatelli et al., 1989).

Other mechanisms are also important in lee cyclone development. Lee cyclones often form when mid- to upper-level differential vorticity advection produces ascent over top of low-level descent, stretching the atmospheric column and producing cyclonic vorticity (Steenburgh and Mass, 1994; Schultz and Doswell, 2000; McGinley, 1982). Hovanec and Horn (1975) stressed the importance of weak static stability in the 800-300mb layer and the presence of a 300mb jet streak normal to the topography in developing lee side cyclones. Achter and Horn (1986) also found that most Colorado lee cyclones develop in the left front quadrant of upper level jet streaks where the upper level divergence is largest due to cyclonic vorticity advection and the influence of indirect ageostrophic circulation induced by the jet streak. Hu and Reiter (1987) showed the importance of modifications to the low-level baroclinicity by intense low-level frontogenesis in the lee of the Rockies in explosive lee-side cyclogenesis.

Several recent studies have discussed the importance of lee-side cyclogenesis for precipitation in the Mackenzie River basin of the Canadian arctic (Lackmann et al., 1998; Spence and Rausch, 2005; Asuma et al., 1998). Few studies, however, have addressed the dynamics of the lee-side cyclogenesis in this region. Chung and Reinelt (1973) identified four features that were common to cyclones redeveloping in the lee of the northern Canadian Rockies. They suggested that a lee cyclone initially forms under a diffluent upper level flow with a strong jet stream perpendicular to the Rocky Mountains, and intensifies with the approach of an upstream upper cold trough that contributes upper level vorticity advection. The authors observed that a southwesterly diffluent flow pattern is particularly favorable for the appearance of a lee-side redevelopment downstream and suggest that the diffluent cross-barrier flow is due to vertical stretching and low-level convergence as the flow moves down slope after crossing the topography.

4.3 Data

Atmospheric fields used in this study are from the European Centre for Medium Range Weather Forecasting (ECMWF) ERA40 Reanalysis dataset (Uppala et al., 2005) on a N80 reduced Gaussian grid (approximately 1.125° grid squares) and from the North American Regional Reanalysis (NARR) dataset on a Lambert conformal projection with approximately 32 km spacing (Mesinger et al., 2006). ERA40 dynamic tropopause, pressure level and vertically integrated moisture flux and flux divergence fields are used to diagnose the synoptic scale processes that favored the development of persistent northwesterly winds at Tuktoyaktuk. The dynamic tropopause is defined as the 2PVU (potential vorticity unit) surface. The NARR seal level pressure (SLP), 10m wind and 950hPa temperature are used to examine the finer scale structures in the evolution of the extreme wind event.

4.4 Meteorological Precursors to the Extreme Wind Event

4.4.1 Methodology

Potential vorticity (PV) and moisture diagnostics are used to identify the physical processes that led to the explosive deepening of a cyclone in the Gulf of Alaska and subsequent redevelopment along the Beaufort coast. The use of potential vorticity and

dynamic tropopause maps has increased since Hoskins et al. (1985) demonstrated the advantages of their use.

The potential vorticity in isentropic coordinates (P) is defined by Equation 4.2, where g is the gravitational constant (9.81 m s^{-1}), f is the Coriolis parameter (s^{-1}), ζ_θ is the isentropic potential vorticity (s^{-1}) and θ is the potential temperature (K),

$$P = -g\left(f + \zeta_\theta\right)\frac{\partial\theta}{\partial p} \tag{4.2}$$

The units of P are $m^2\ s^{-1}\ K\ kg^{-1}$, which is often expressed in terms of PVUs (potential vorticity units) where $1PVU = 1x10^{-6}\ m^2\ s^{-1}\ K\ kg^{-1}$.

Morgan and Nielsen-Gammon (1998) discuss the merits of two different types of PV plots: PV on isentropic surfaces (IPV) and potential temperature on constant PV surfaces. In the latter, the potential temperature and wind are often viewed on the dynamic tropopause, which is defined as the 2PVU surface. On the dynamic tropopause, a warm potential temperature anomaly is equivalent to an area of low PV on an IPV map and represents an upper level ridge. Similarly, a cold potential temperature anomaly on the dynamic tropopause indicates an area of high PV and an upper level trough. Because potential temperature on a constant PV surface is conserved in the absence of friction and diabatic processes, non-conservation (i.e. large increases) of potential temperature on the tropopause indicate diabatic heating. Dynamic tropopause maps also allow the flow regime throughout the troposphere to be visualized by combining the tropopause analysis with a surface analysis. This is often called the "Eady view," and is very useful when studying the interaction between shallow warm core systems and an upper level trough or downstream development of ridges and troughs. Dynamic tropopause fields are also insensitive to orography and are therefore useful in studying the development of systems in the presence of mountain ranges.

The ERA40 Reanalysis products are used in the following diagnostics. The vertically integrated moisture flux and moisture flux divergence are plotted along with the 850hPa geopotential height over the north Pacific to demonstrate the importance of the low-level circulation and moisture transport on the bomb cyclogenesis and

subsequent downstream development. Maps of the 925hPa relative vorticity contoured on top of the wind and potential temperature on the dynamic tropopause are constructed to investigate the interaction between shallow warm core cyclonic vorticity anomalies developing over the north Pacific and the potentially cold upper level trough along the northern edge of the jet stream. Maps of sea level pressure, 1000-500hPa thickness and 500hPa vorticity are also used to track the central pressure of the developing system and to highlight the role that the deep warm tropical air mass plays during different stages of the development process.

4.4.2 Bomb Cyclogenesis

The discussion of the meteorological precursors to the explosive deepening begins at 1200UTC September 19. At this time, the moisture flux and moisture flux divergence are both strong across the central extratropical Pacific (Figure 4.3a). The source of the moisture appears to be the western subtropical Pacific south of Japan, where the southerly moisture flux is greatly enhanced in the region between super typhoon Bart to the west and a strong subtropical high to the east. The 850hPa geopotential height anomalies indicate a strong baroclinic zone north of the subtropical high stretching across the central Pacific into the Gulf of Alaska that is favorable for strong winds to carry warm moist air from the tropics over the north Pacific. A cyclone over the Aleutian Islands is also favorable for enhanced moisture transport into the Gulf of Alaska. The environment over the North Pacific is highly conducive for cyclogenesis, with large heat (not shown) and moisture fluxes from the subtropical Pacific and a strong baroclinic zone across the North Pacific separating very cold polar air and a deep warm tropical air mass.

The location of the disturbance that explosively deepened in the Gulf of Alaska is identified in the sea level pressure (Figure 4.3b) and 925hPa relative vorticity (Figure 4.3c) fields. A small vortex is observed in the 925hPa relative vorticity between 40°N and 45°N between 150°E and 180°. This system is embedded within a deep layer of warm air as demonstrated by its proximity to the 5760 meter thickness contour and the overlying tropopause potential temperature of approximately 370K. The large thickness, potentially warm tropopause (anticyclonic vorticity) and anticyclonic shear in the layer between 925Pa and the tropopause (not shown) indicate that this is a warm core system.

It should be noted that another 925hPa cyclonic vorticity maximum and closed low is near 165°W. This system developed into a cyclone that reached the coast of Alaska well before the explosive deepening occurred.

Over the following twenty-four hours, by 1200UTC September 20, the 925hPa vorticity of the system increased while remaining underneath the upper level ridge, in the warm thickness (5700m) and on the anticyclonic shear side of a 130 knot upper level jet streak (Figure 4.4). A secondary shallow warm core low-level vorticity anomaly has also appeared ahead of the initial system on the warm side of the jet. This second system will also continue to develop and move into the Gulf of Alaska ahead of the primary (initial) disturbance. Twenty-four hours later, at 1200UTC September 21, both of the shallow warm core systems have moved into the Gulf of Alaska, south of the Aleutian Islands (Figure 4.5). The central pressure of the primary system has continued to deepen, with the central pressure reaching 994hPa, as the 925hPa vorticity anomaly increased in strength and moved closer to the upper level trough. The secondary low-level vorticity anomaly has moved under the upper level trough and 500hPa absolute vorticity maximum and has deepened to a minimum pressure of 991hPa.

The explosive deepening began at approximately 1800UTC September 21 (Figure 4.6) as the system moved into the Gulf of Alaska. At this time, the primary low-level vorticity maximum has moved into the colder air (5560m). After moving towards the upper level trough, the low central pressure dropped by approximately 8hPa to 986hPa. The moisture flux convergence also increased over the Gulf of Alaska as the system started to deepen.

By 0000UTC September 22, the minimum sea level pressure dropped to 977hPa (Figure 4.7) as the primary system continued to move into the cold thickness and towards the upper level trough. With the moisture flux convergence over the Gulf of Alaska increasing and moving closer to the Alaska coast, a weak ridge is now observed in the 850hPa geopotential height and tropopause potential temperature fields downstream over British Columbia. At 0600UTC September 22, the cyclone has a single closed contour in the sea level pressure field, although the two 925hPa vorticity maxima are still separate (Figure 4.7). The minimum sea level pressure dropped to 966hPa and the system has

become a cold core cyclone underneath the potentially cold air of the upper level trough. As the moisture flux convergence approaches the Alaska coast ahead of the deepening cyclone over the next 12 hours, the signature of the diabatic heating in the tropopause potential temperature also increases, amplifying the downstream ridge.

Between 0600UTC (Figure 4.7) and 1200UTC (Figure 4.8) September 22, the central pressure dropped another 11hPa to 955hPa and the system continued to move towards the Alaska coast. The moisture flux convergence also increased and moved towards the southern coast of Alaska ahead of the deepening cyclone. The downstream ridge in the 850hPa height and tropopause potential temperature fields amplified dramatically and began to move towards the interior of Alaska and the Yukon territories as the diabatic heating increased. Small patches of very high tropopause potential temperature are observed near the coast, suggesting that latent heat release ahead of the deepening cyclone is helping to amplify the strong downstream ridge.

The explosively deepening system reached the minimum sea level pressure of approximately 949hPa at 1800UTC September 22 (Figure 4.8). As the amplification of the ridge in the 850hPa geopotential height and tropopause continued, a small 925hPa cyclonic vorticity maximum developed downstream in the lee of the orography, just to the west of Great Slave Lake. This small 925hPa cyclonic vorticity maximum eventually developed into a deep cyclone as the upper level trough currently over the Gulf of Alaska began to rapidly move towards the Beaufort coast.

During the 24-hour period beginning at 1800UTC September 21, the minimum pressure of the system dropped from 984hPa to 949hPa, a deepening rate of approximately 1.6 Bergerons, exceeding the criterion for the deepening rate of a bomb cyclone of 1 Bergeron (Sanders and Gyakum, 1980). After 1800UTC September 22, the central pressure of the cyclone began to increase as the system made landfall along the southern coast of Alaska.

4.4.3 Secondary Development Along the Beaufort Coast

The signature of strong diabatic heating over the interior of Alaska is observed in the tropopause potential field at 0000UTC September 23 (Figure 4.9). The 925hPa

cyclonic vorticity anomaly in the lee of the topography increased in magnitude as diabatic heating just to the south continued to strengthen. The diabatic heating has also continued to amplify the downstream ridge, increasing the cross barrier flow and mid-level vorticity advection perpendicular to the topography. By 0600UTC, the diabatic heating has continued to increase with the downstream ridge amplifying and moving off to the east (Figure 4.9). The upper level trough on the tropopause that was previously located over the Gulf of Alaska has rapidly moved to the north and approached the Beaufort coast. A trough is also observed in the sea level pressure and 850hPa height contours south of the Beaufort coast near the low-level vorticity anomaly, indicating that surface development has already started to occur to the southwest of Tuktoyaktuk.

At 1200UTC September 23, a closed low is apparent in the sea level pressure and 850hPa geopotential height fields in the lee of the topography to the southwest of Tuktoyaktuk (Figure 4.10). The secondary development of the surface cyclone increased after the upper level trough on the tropopause approached the 925hPa cyclonic vorticity anomaly that had developed in the lee of the topography. By this time, the 925hPa cyclonic vorticity anomalies have increased substantially along the coast and to the southeast in the lee of the topography as the diabatic heating continued to increase and amplify the downstream ridge. At 1800UTC, the surface cyclone has deepened and moved to east as the diabatic heating has continued to amplify the ridge (Figure 4.10).

The moisture flux divergence, 850hPa geopotential height and tropopause potential temperature fields demonstrate the importance of moisture transport over the north Pacific and the subsequent convergence along the Alaska coast on the diabatic amplification of the downstream ridge. The modification of the downstream air mass over the Mackenzie River basin and Beaufort Sea contributed to the secondary development of a cyclone in the lee of the topography. Observed soundings from Inuvik, Northwest Territories, show the evolution of the atmospheric conditions associated with the nearby surface development between September 22nd and September 24th.

At 1200UTC September 22, the winds throughout the column are relatively weak with southerly winds below 700hPa and southwesterly winds at middle and upper levels (Figure 4.11). The temperature profile indicates an inversion from the surface up to

approximately 950hPa that remained intact until 0000UTC September 24, the approximate time that the extreme wind event began at Tuktoyaktuk.

Twelve hours later (0000UTC September 23), the wind speed has increased with southeasterly winds extending from the surface up to about 500hPa and southwesterly winds up to 100hPa. The height of the tropopause and the veering of the winds increased significantly between 1200UTC September 22 and 0000UTC September 23, indicating the passage of the upper level ridge and an increase in warm air advection. During this 12-hour period, the temperature increased throughout the atmospheric column, but with a much larger warming (as much as 10 degrees Celsius) observed in the middle to upper troposphere above 500hPa.

By 1200UTC September 23, the winds have reversed directions, with southwesterly winds observed at lower levels and southeasterly winds near the tropopause. The backing of the winds indicates that cold air advection is beginning. By 0000UTC September 24, the height of the tropopause dropped by approximately 1.5 km, indicating the passage of the upper level trough. The lower level winds have also turned westerly up to 700hPa and increased in magnitude. The stability has also weakened below 700mb and the low level temperature inversion observed in the previous soundings is no longer present, indicating that stability conditions favorable for momentum mixing are now present. The soundings demonstrate that low to mid-level warm air advection extending well beyond the top of the topography and dynamic forcing associated with the upper level trough are the most important factors in the period leading up to the strong northwesterly wind event.

4.5 Meteorological Conditions During the First Extreme Wind Event

The hourly station data indicated that the winds at Tuktoyaktuk turned northwesterly at approximately 1800UTC September 23 (Figure 4.2) after the cyclone that developed to the southwest during the previous 12 hours moved off to the east. The speed of the observed northwesterly winds varied significantly over the next several hours until consistently exceeding 20 knots after 0000UTC September 24. In addition to maps of the 925hPa relative vorticity contoured on top of the wind and potential temperature on the dynamic tropopause, sea level pressure, 10m wind and 950hPa

potential temperature from the NARR are used to identify the physical processes important for the generating the persistent northwesterly winds at Tuktoyaktuk. The NARR fields are plotted on their native projection to avoid distortion of the finer scale features of the circulation along the Beaufort coast.

At 0000UTC September 24, the ridge downstream of the Gulf of Alaska has moved to the east and weakened as the latent heating has stopped (Figure 4.12) though potentially warm air is still observed on the tropopause over the Beaufort Sea. A deep and persistent cyclone is observed off the Arctic coast of Siberia. A front is observed over the Beaufort Sea in the region between the potentially cold air on the tropopause associated with the Siberian cyclone and the potentially warm air that was transported into the area by the diabatically-generated ridge. The line of cyclonic vorticity at 925hPa indicates the location of the front that was clearly visible as a cloud streak in the satellite photo over the Beaufort taken at 1315UTC (Figure 4.1).

An anticyclone is observed along the Beaufort coast of western Alaska that along with the cyclone east of Tuktoyaktuk forms part of a deformation zone over the Beaufort Sea. The anticyclone is situated ahead of ridge on the tropopause over Siberia that provides a source of anticyclonic vorticity advection favorable for the continued development of the surface feature. Strong northerly winds at 10m and 950hPa are observed in the confluence zone between the cyclone-anticyclone pair, though it is too far to the west to directly affect Tuktoyaktuk at the current time. The SLP contours along the Alaska coast north of the Brooks Range display the characteristic U-shaped ridge that is commonly observed during cold air damming events in the Appalachians (Bell and Bosart, 1988). The 950hPa potential temperature field also indicates that significant cold air advection along the Alaskan coast at this time is starting to build a pool of potentially cold air near the surface to the north of the mountains. The U-shaped ridge in the SLP field is favorable for turning the northerly winds to the west along the direction of the Brooks Range.

At 1200UTC September 24 (Figure 4.13) the tropopause analysis indicates that the upstream ridge over the Barents Sea and Siberia has strengthened and moved to the east where it continues to provide a source of anticyclonic vorticity advection in support

of the strengthening surface anticyclone along the Chukchi coast of western Alaska. The northerly 10m winds have also strengthened in the frontal zone between the anticyclone to the west and the cyclone to the east of Tuktoyaktuk. The pressure contours along the Brooks Range still display the characteristic U-shaped ridge characteristic of cold air damming. The pattern of 950hP and 10m winds are similar, with strong northerly winds impinging upon the coastal topography and advecting cold air from the north. The pattern of cold air closely follows the shape of the Brooks Range, indicating that the pool of cold air is continuing to develop along the northern edge of the topography. The combination of the northwesterly flow along the trailing edge of the cyclone to the east, strong northerly flow along the front over the Beaufort Sea and the cyclonic turning of the winds parallel to the topography has created a confluence zone for NW winds just upstream from Tuktoyaktuk. Similar conditions are observed at 1800UTC (not shown), with the cyclone continuing to slowly move to the southeast of Tuktoyaktuk and the anticyclone over the Chukchi Sea strengthening and moving to the east as the upper level ridge continued to provide anticyclonic vorticity advection.

At 0000UTC September 25, a surface cyclone is beginning to develop along the eastern coast of Siberia (Figure 4.14), just to the west of the ridge and anticyclone in the Chukchi Sea. This small cyclone continues to develop over the next 12 hours as an upper level trough moves into the Chukchi Sea. By 1200UTC September 25, the upper level ridge and anticyclone over the Barents Sea (Figure 4.15) have started to weaken as the upper level trough and surface cyclone over eastern Siberia have moved into the Barents Sea. The cyclone east of Tuktoyaktuk is also continuing to weaken and move to the east, causing the pressure gradient and confluent flow in the deformation zone over the Beaufort Sea to also weaken and move to the east. Strong northerly winds and northwesterly flow parallel to the coast are still observed upstream from Tuktoyaktuk. As the upper level ridge weakens over the next 12 hours, the surface cyclone and upper level trough in eastern Siberia are able to approach the western coast of Alaska.

By 0000UTC September 26, the surface cyclone in eastern Siberia has deepened as the upper level trough amplifies and pushes the upper level ridge to the east, with the subsequent reduction in the anticyclonic vorticity advection continuing to weaken the

surface anticyclone (Figure 4.16). With the anticyclone weakening significantly, and the cyclone moving farther to the north and east of Tuktoyaktuk, the pressure gradient over the Beaufort Sea has weakened, though weaker northerly flow over the Beaufort Sea and northwesterly flow parallel to the topography are still observed at 10m and 950hPa.

The hourly surface data (Figure 4.2) indicated that the winds at Tuktoyaktuk weakened to less than 10 knots and turned southerly around 0600UTC. At this time (Figure 4.17), the upper level trough and surface low in the Chukchi Sea have reached the western coast of Alaska, further weakening the upper level support for the coastal anticyclone crucial in the production of the northwesterly winds at Tuktoyaktuk. As the cyclone east of Tuktoyaktuk moved farther to the north and east and weakens, the strong pressure gradient over the Beaufort Sea also continued to weaken and move to the east. The strongest northwesterly winds at 10m are now observed well to the east of Tuktoyaktuk, although the upstream 950hPa winds parallel to the coast still exceed 20 knots. The barrier jet along the windward edge of the mountains is no longer present. The surface wind speed at Tuktoyaktuk continued to weaken before once again turning to the northwest and increasing to 20knots on 0000UTC September 28.

4.6 Meteorological Conditions During the Second Extreme Wind Event

By 0000UTC September 27, super typhoon Bart has undergone extratropical transition, moved into the north Pacific south of Siberia and helped to create a surface ridge downstream over Siberia (Figure 4.18). Downstream from an upper level ridge, a surface anticyclone has formed over the Barents Sea along the east coast of Siberia just to west of the surface cyclone along the Beaufort coast near Barrow. The 10m and 950hPa winds show that the flow around the anticyclone is favorable for the advection of cold air north of the Brooks Range. With the Coriolis force also tending to turn the westerly flow upslope where it can be cooled adiabatically, the flow pattern is favorable for falling temperatures north of Brooks Range ahead of the cyclone. The lack of warm air advection to the east of the cyclone is not favorable for continued development of the upper level support for the cyclone, which rapidly dissipates over the following 12 hours.

By 1200UTC, as the atmosphere north of the topography continued to cool, the sea level pressure began to increase north of the Brooks Range as seen in the U-shaped

pressure contours that have once again appeared along the coast (Figure 4.19). At 0000UTC September 28, with the continued upper level support from the persistent ridge to the west (Figure 4.20), the surface anticyclone in the Chukchi Sea has continued to develop and push cold air against the Brooks Range. The rapidly decreasing temperatures to the north of the mountains lead to an increase in the U-shaped ridge of high pressure along the topography.

The timeseries of hourly winds at Tuktoyaktuk (Figure 4.1) indicated that strong northwesterly winds were observed from 0000UTC to 1800UTC September 28. During this second period of intense northwesterly winds, the anticyclone over the Chukchi Sea has substantially increased and moved to the east, with the northerly winds increasing the cold air advection and up slope flow and causing the 950hPa potential temperature north of the Brooks Range to drop (Figure 4.21). The U-shaped ridge north of the topography has become more prominent and the strong northerly winds over the Beaufort Sea along the leading edge of the anticyclone turn cyclonically towards Tuktoyaktuk. This continued until 0000UTC September 29 when the upstream ridge and surface anticyclone moved well to the east. After the anticyclone weakened and moved to the east and the upper level trough visible in Figure 4.21 moved to east along the Beaufort coast, the pressure gradient was no longer favorable for northwesterly winds over Tuktoyaktuk.

As was the case during the earlier period of northwesterly winds, the advection of cold air from over the Beaufort Sea help to create a pool of cold air north of the Brooks Range. The resulting U-shaped ridge in the pressure field indicates that cyclonic turning of the northerly winds along the windward edge of the topography that produced strong northwesterly winds over Tuktoyaktuk.

4.7 Discussion

A detailed case study was performed to identify the meteorological conditions favorable for the persistent northwesterly winds along the Beaufort coast that caused a damaging storm surge event at Tuktoyaktuk. Although the persistent northwesterly winds favorable for the storm surge along the Beaufort coast began at approximately 00UTC on September 24th, 1999, the precursors that led to the development of the strong winds began as early as 12Z on September 19th over the Northwestern Pacific. As super

typhoon Bart approached the southern islands of Japan, warm and moist tropical air was transported into the north Pacific. A series of shallow, warm core systems formed in the enhanced baroclinic zone ahead of the tropical cyclone, two of which eventually moved into the Gulf of Alaska and underwent explosive development after interacting with an upper level trough. The resulting rate of deepening was approximately 1.6 Bergerons in the 24 hours after 18Z on September 21st, exceeding the criterion proposed by Sanders and Gyakum (1980) for an explosively deepening system.

The strong moisture flux convergence ahead of the explosively deepening cyclone led to significant latent heat release along the southern coast of Alaska that diabatically amplified a downstream ridge that carried warm air over the continent and into the Arctic. The subsequent modification of the air mass along the Beaufort Coast downstream of the latent heating created conditions favorable for secondary development in the lee of the topography. The combination of strong moisture transport, upper level dynamic forcing and low-level baroclinicity conducive for the bomb cyclogenesis also contributed to the formation of a rapidly deepening lee-side cyclone along the Beaufort coast.

Anticyclonic vorticity advection from a persistent upstream ridge over the Barents Sea also helped to create an anticyclone over the Chukchi Sea. A strong front formed over the Beaufort Sea that produced very strong northerly winds over the Beaufort Sea. The resulting flow of cold air perpendicular to the Brooks Range resulted in an increase in the pressure along the topography and a cyclonic turning of the northerly winds parallel to the coast. The combination of a northwesterly barrier jet and northwesterly winds along the trailing edge of the cyclone east of Tuktoyaktuk both contributed to the strong northwesterly wind event that caused extensive storm surge damage. The persistence of the upstream ridge and anticyclone contributed significantly to the persistence of the extreme wind event.

A second period of strong northwesterly winds was observed after the initial cyclone moved off to the east and began to decay. Another upper level ridge moved over Siberia and produced an anticyclone over the Chukchi Sea. The anticyclone along the north shore of Alaska produced northerly flow perpendicular to the Brooks Range. The

resulting cold air advection and upsloping flow along the north side of the topography led to a second cold air damming event that produced a pressure gradient favorable for strong northwesterly winds at Tuktoyaktuk. This second anticyclone, much stronger than the first, produced a second period of persistent and extreme northwesterly winds at Tuktoyaktuk in the absence of a strong cyclone to the east. The cyclone previously observed to the east of Tuktoyaktuk had long since moved to the northeast and occluded.

The results of this study demonstrate that an upper level ridge over the Barents and downstream surface anticyclone over the Chukchi Sea is conducive for strong winds at Tuktoyaktuk. The presence of a deep cyclone was certainly an important factor in the generation of strong northwesterly winds during the first part of the event, although the winds would likely not have been as strong or as persistently from the northwest without the presence of an anticyclone to the west. An anticyclone alone appears to have triggered the second period of strong northwesterly winds in the absence of a downstream cyclone. In both cases, the upstream topography was demonstrated to have played an important role in the severity and persistence of the wind event.

Previous studies have demonstrated that the presence of a ridge and surface anticyclone over the Barents and Chukchi Seas is a frequent occurrence. The results from this case study are consistent with the composites of SLP anomalies for strong NW winds presented in Figure 3.9, and suggest that the high frequency of upper level ridges and surface anticyclones observed over the Barents and Chukchi Seas is likely to be an important factor in the generation of extreme NW winds at Tuktoyaktuk.

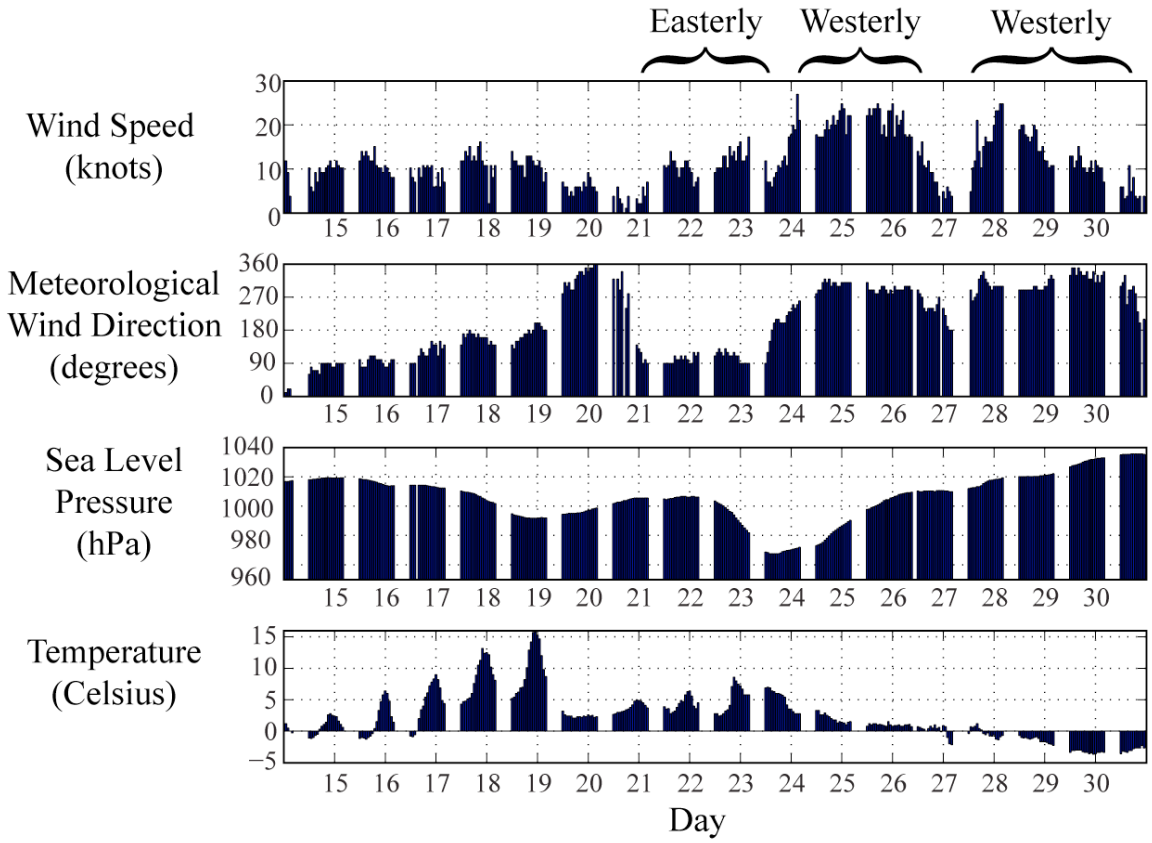

Figure 4.1. Timeseries of the hourly observations from Tuktoyaktuk from 0000UTC September 15 to 2300UTC September 30. The wind speed is in knots, the wind direction in degrees from north, the sea level pressure in hPa and the temperature in degrees Celsius. Missing observations are left blank.

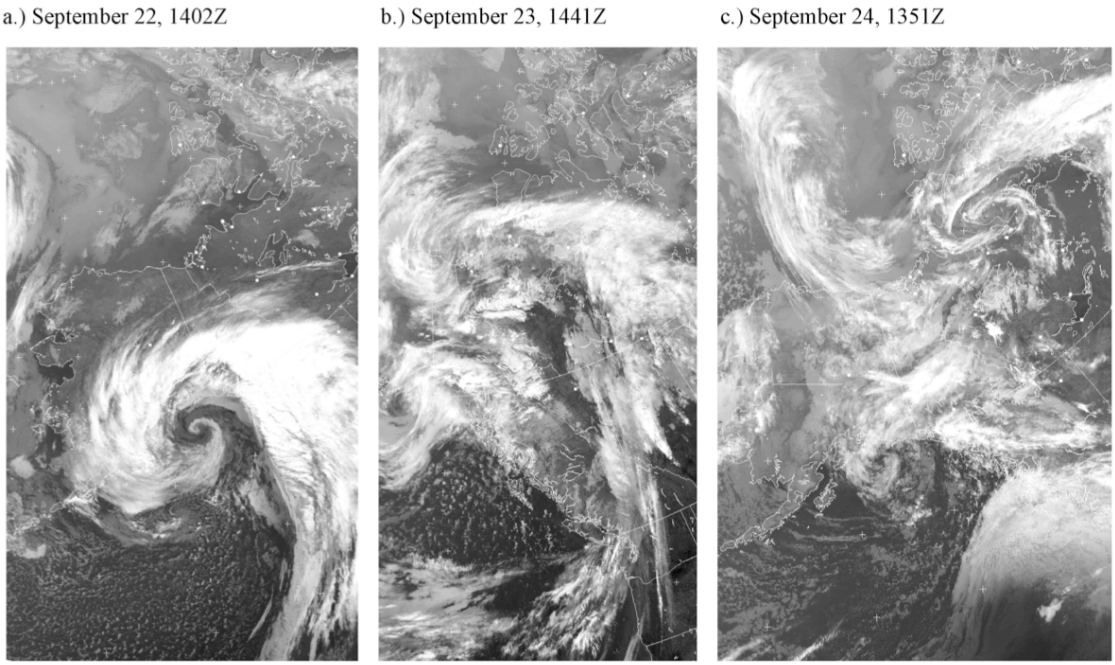

Figure 4.2 The NOAA-14 satellite image of the cyclone in the Gulf of Alaska on a.) 1402UTC September 22, b.) 1441UTC September 23 and c.) 1351UTC September 24.

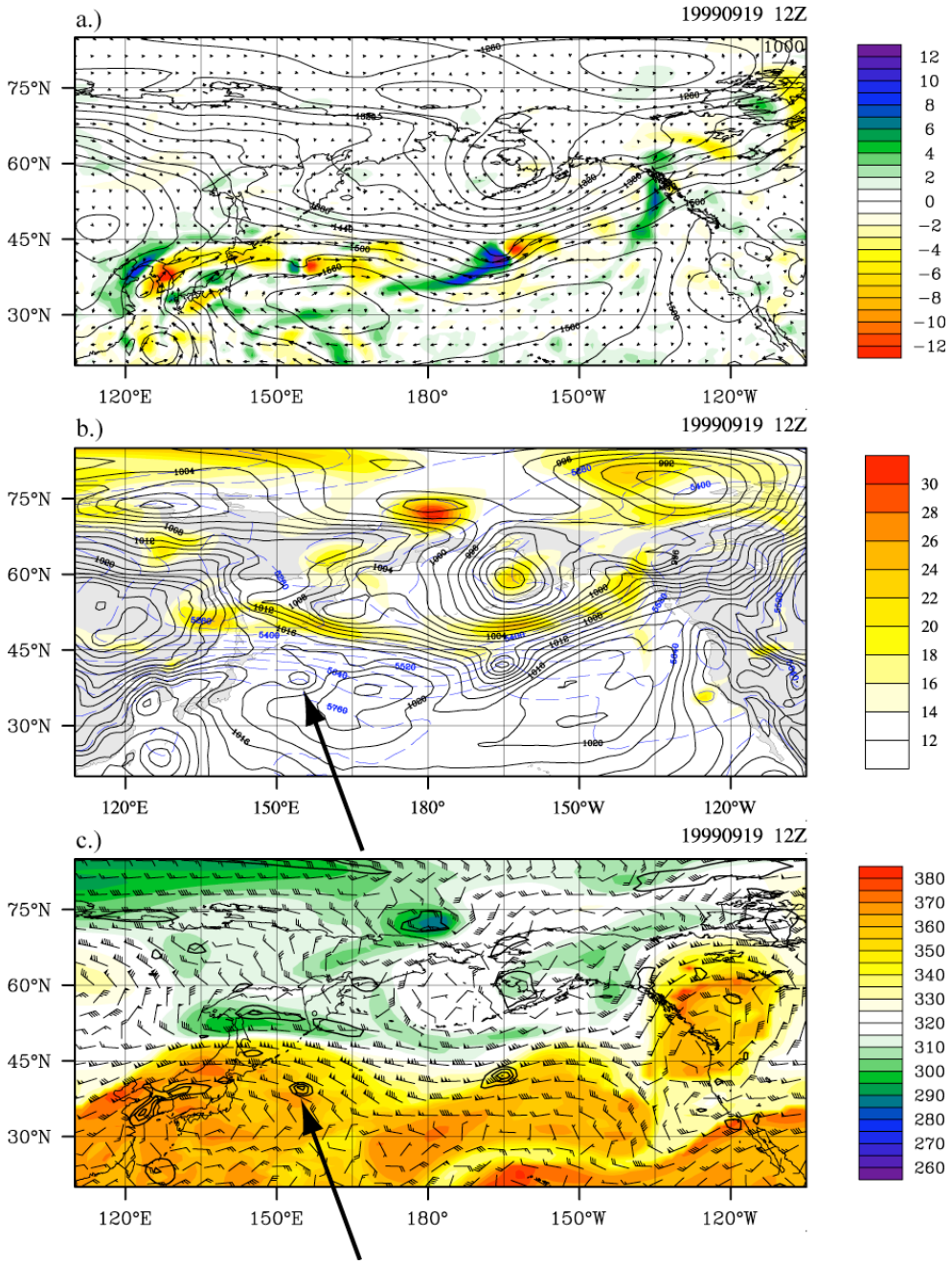

Figure 4.3. ERA40 surface and upper level dynamic fields over the north Pacific for19990919 12Z. a.) The moisture flux (kg $m^{-1}s^{-1}$), moisture flux convergence (color, 10^{-4} kg $m^{-2}s^{-1}$) and 850hPa geopotential height. b.) The sea level pressure (dark 10^{-5} s^{-1}), 1000-500 hPa thickness (blue dashed contours, 60m interval) and 500mb absolute vorticity (10^{-5} s^{-1}). c.) Potential temperature (K; shaded) and wind (knots) on the dynamic tropopause with the 850 hPa relative vorticity (contoured every 5 x 10^{-5} s^{-1} beginning at 5 x 10^{-5} s^{-1}). The black arrows mark the initial location of the disturbance.

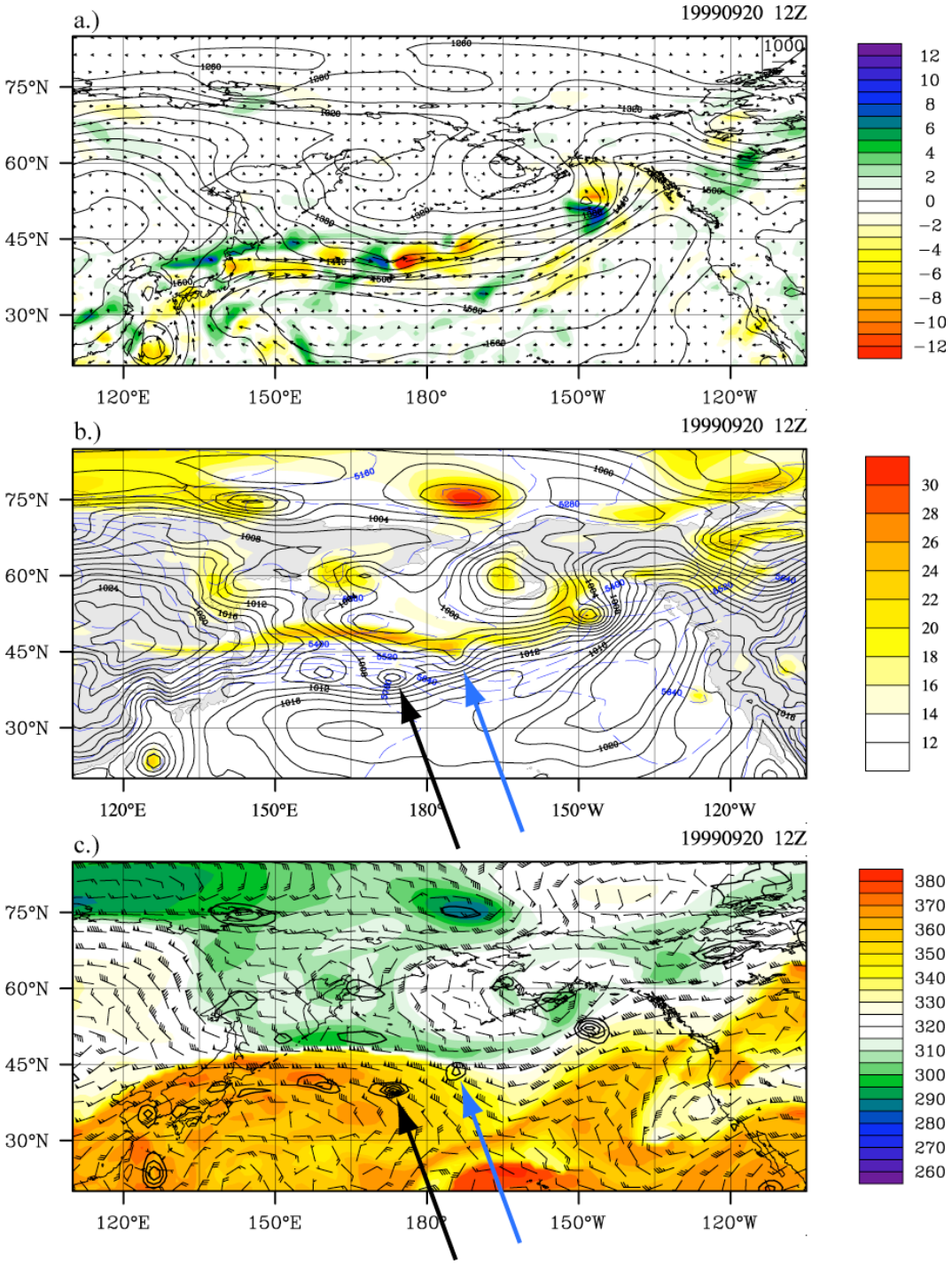

Figure 4.4. Same as Figure 4.3 for 1200UTC September 20. The blue arrow marks the location of the secondary development.

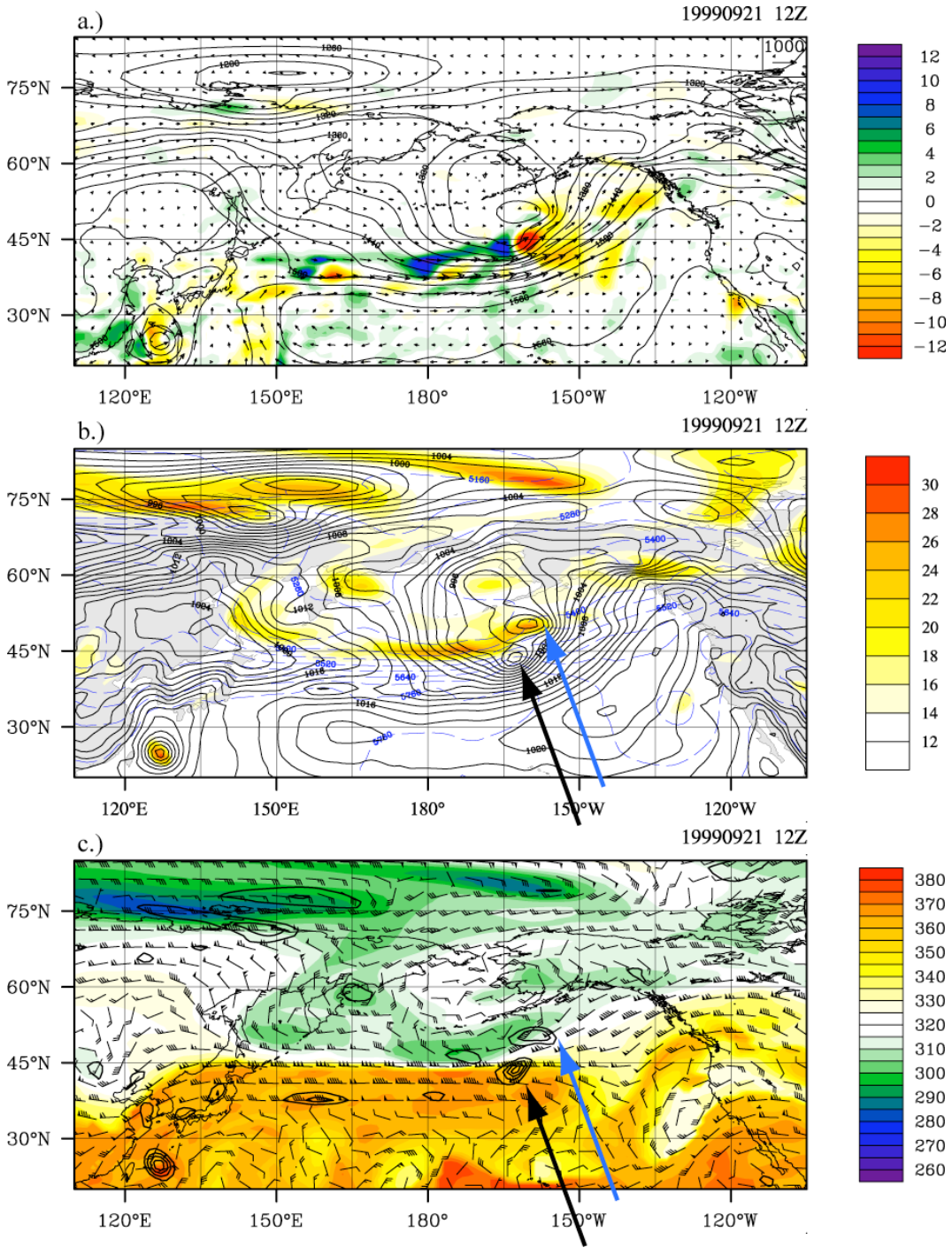

Figure 4.5. Same as Figure 4.3 for 1200UTC September 21.

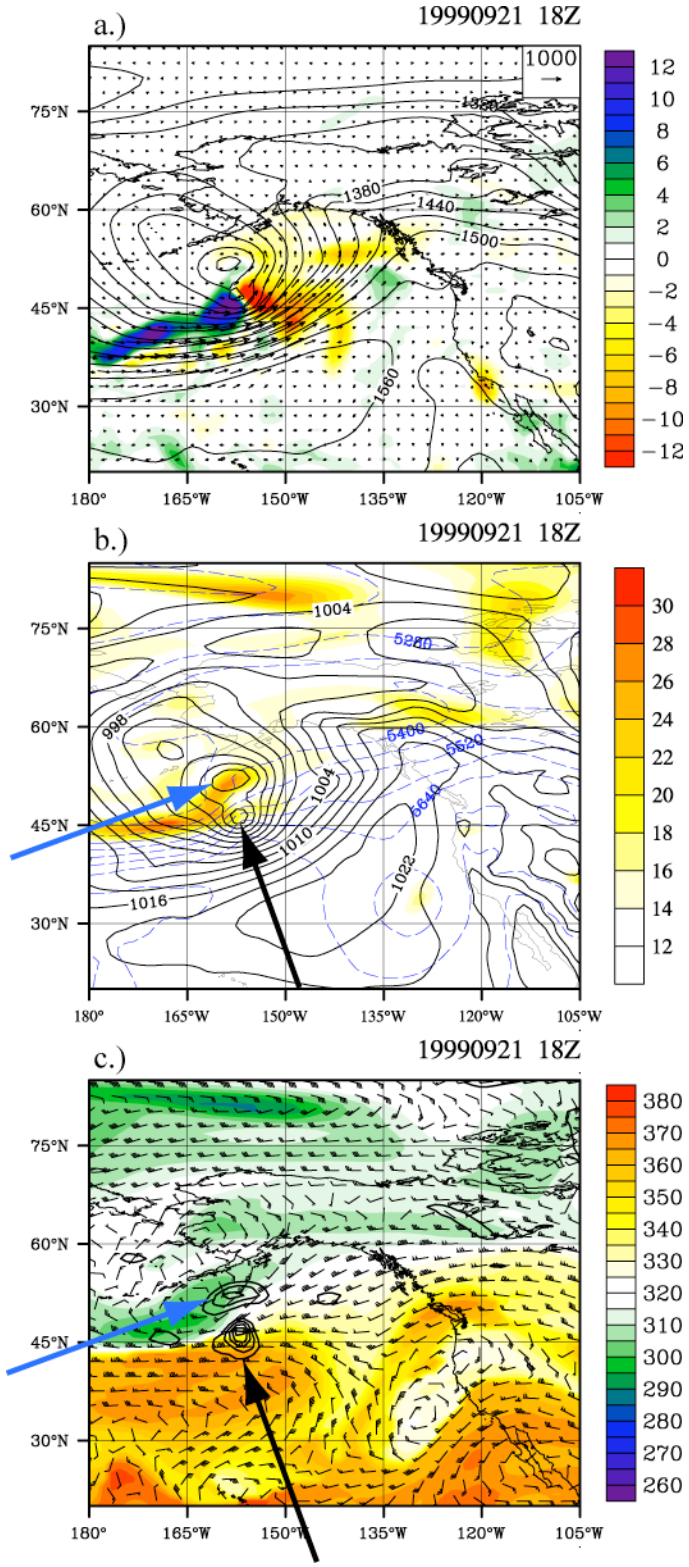

Figure 4.6. Same as Figure 4.4 for 1800UTC September 21.

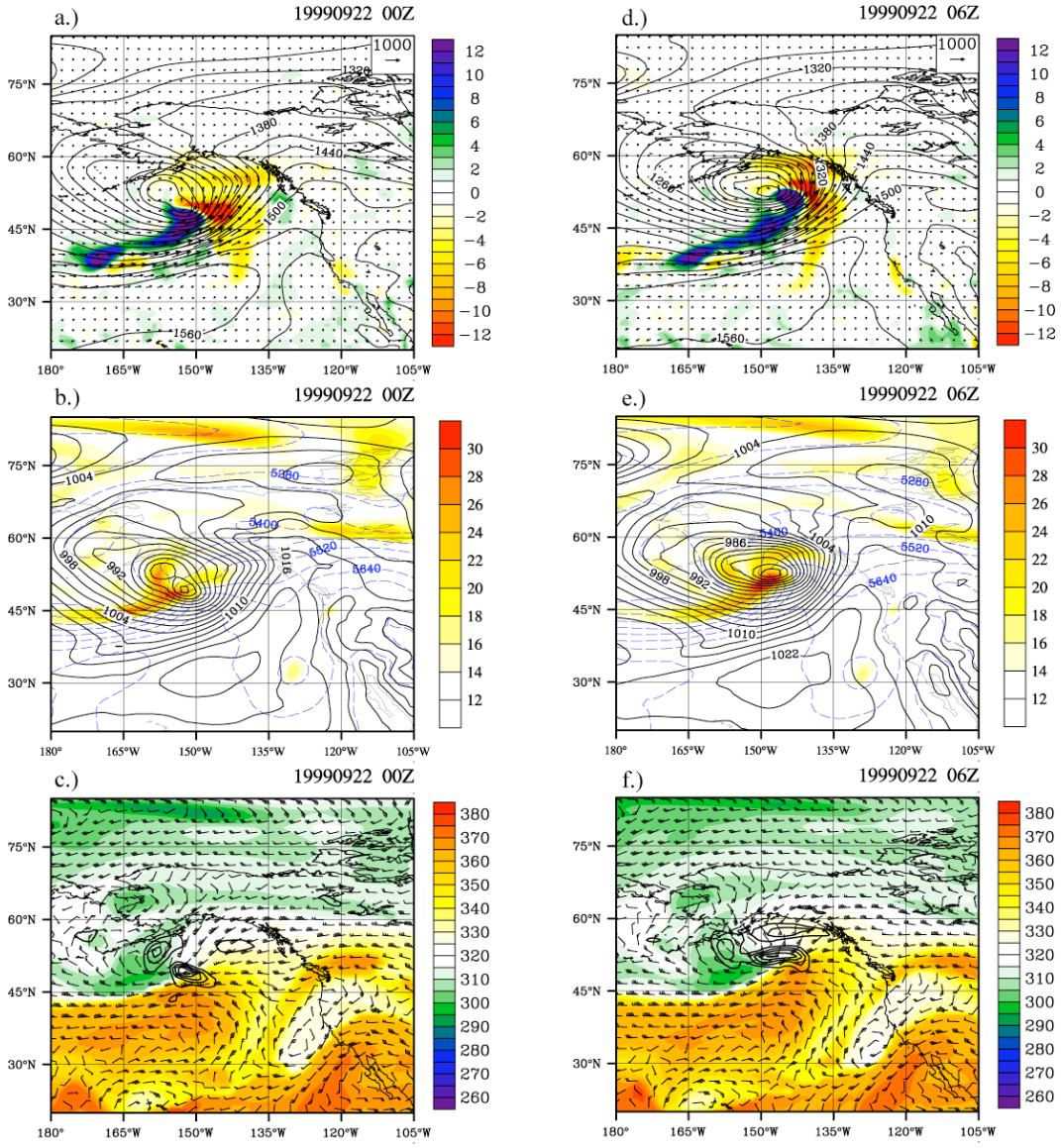

Figure 4.7. Same as Figure 4.3 for 0000UTC and 0006UTC September 22.

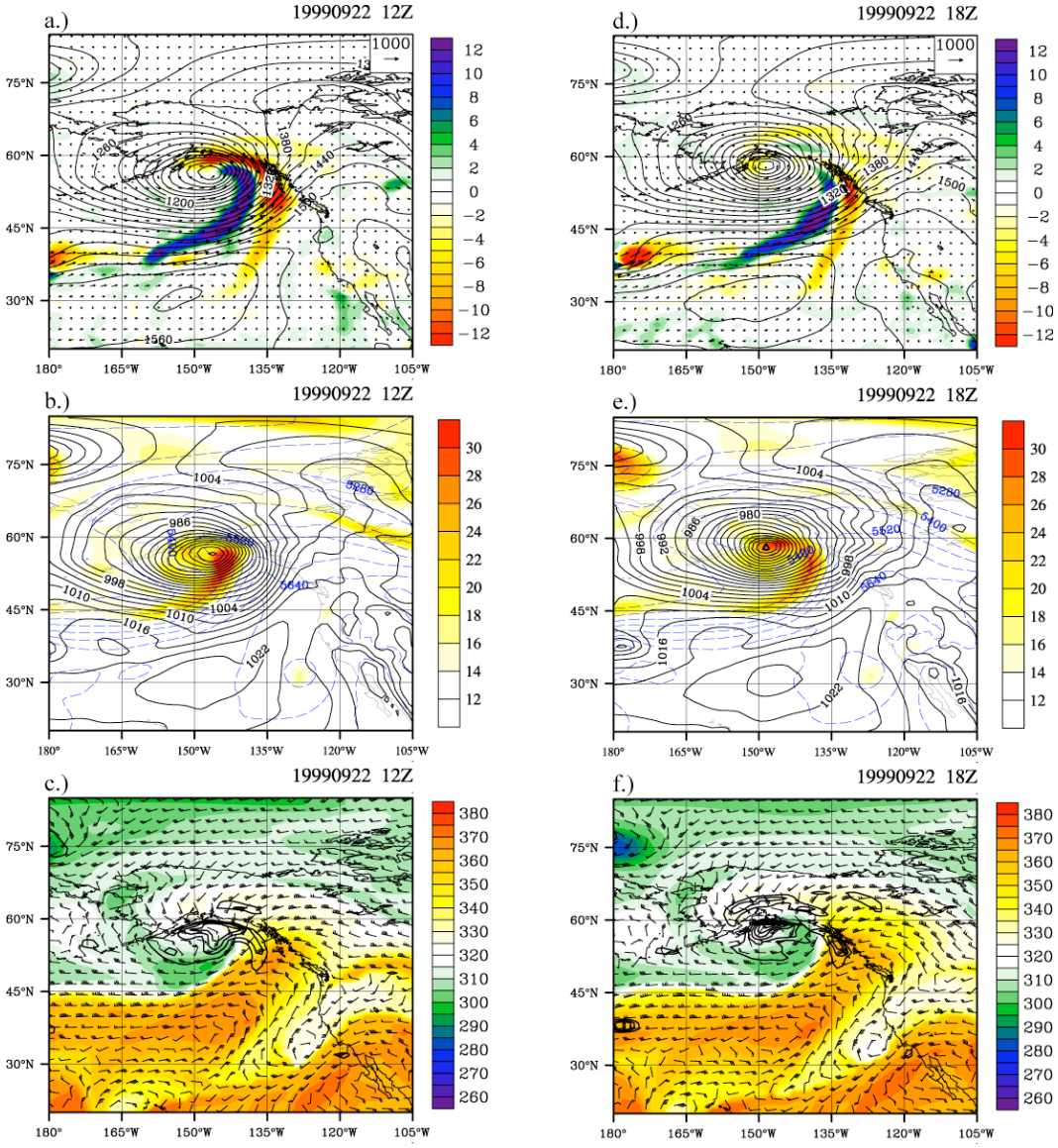

Figure 4.8. Same as Figure 4.3 for 1200UTC and 1800UTC September 22.

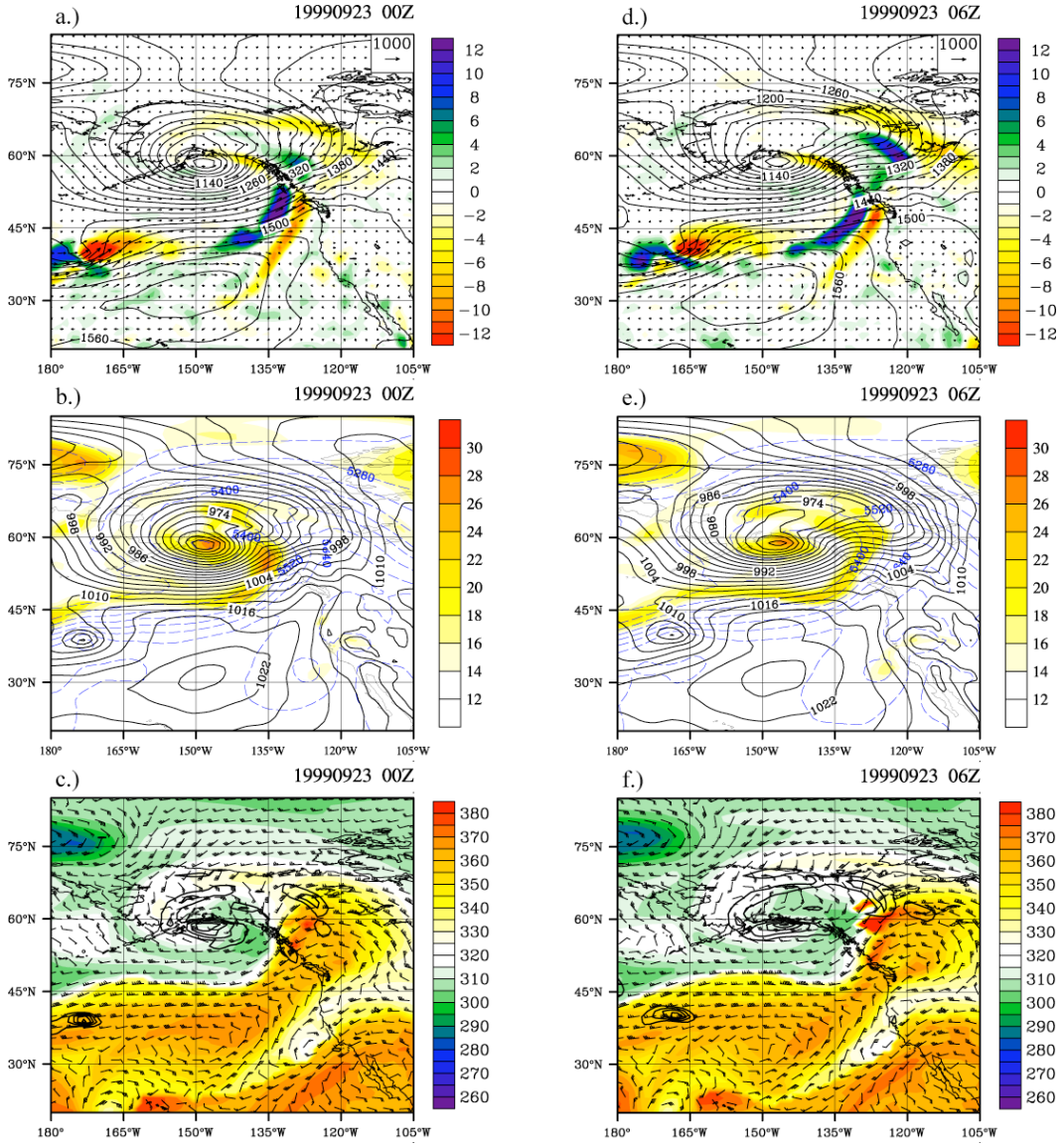

Figure 4.9. Same as Figure 4.3 for 0000UTC and 0006UTC September 23.

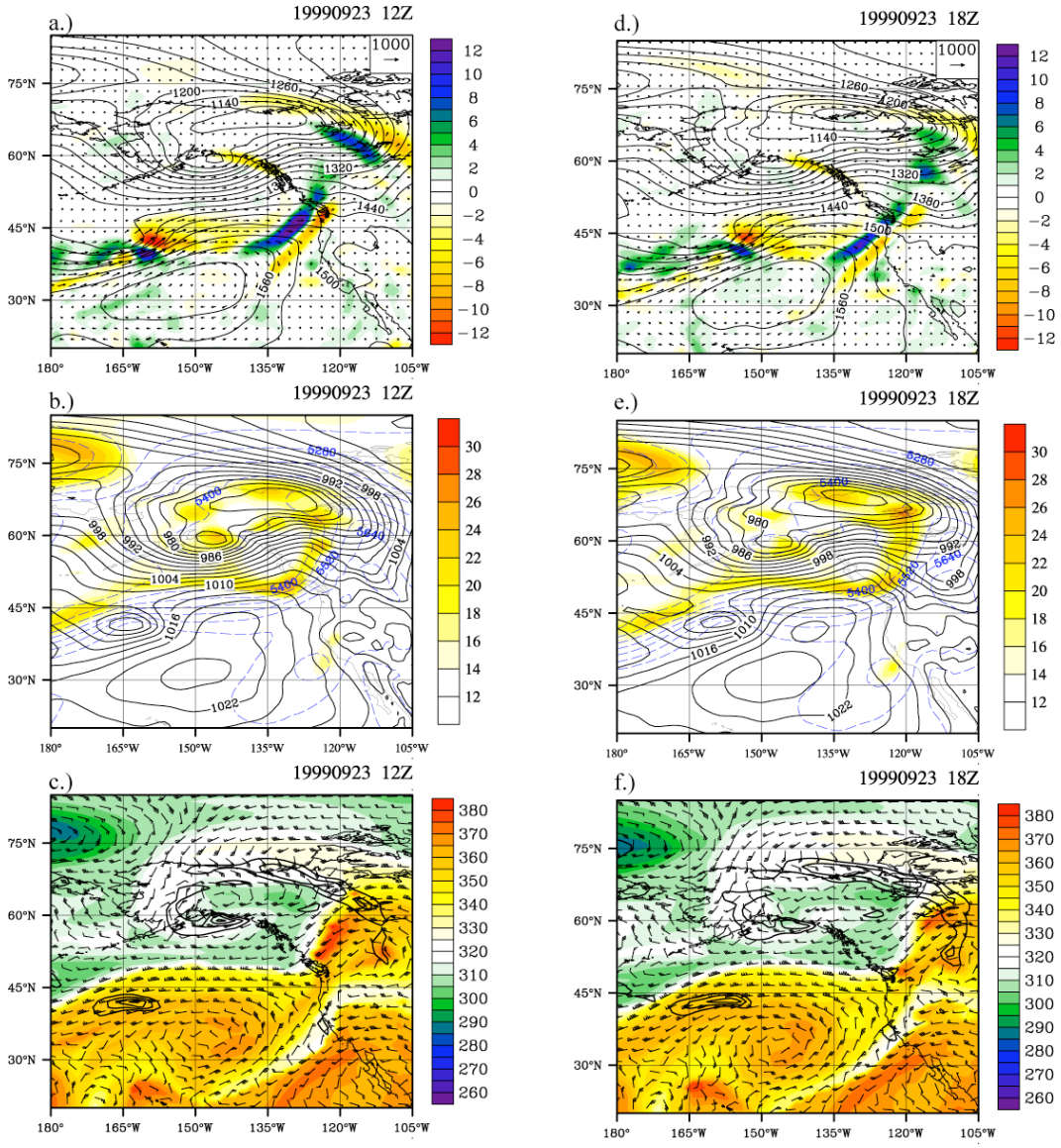

Figure 4.10. Same as Figure 4.3 for 19990923 12Z and 19990923 18Z.

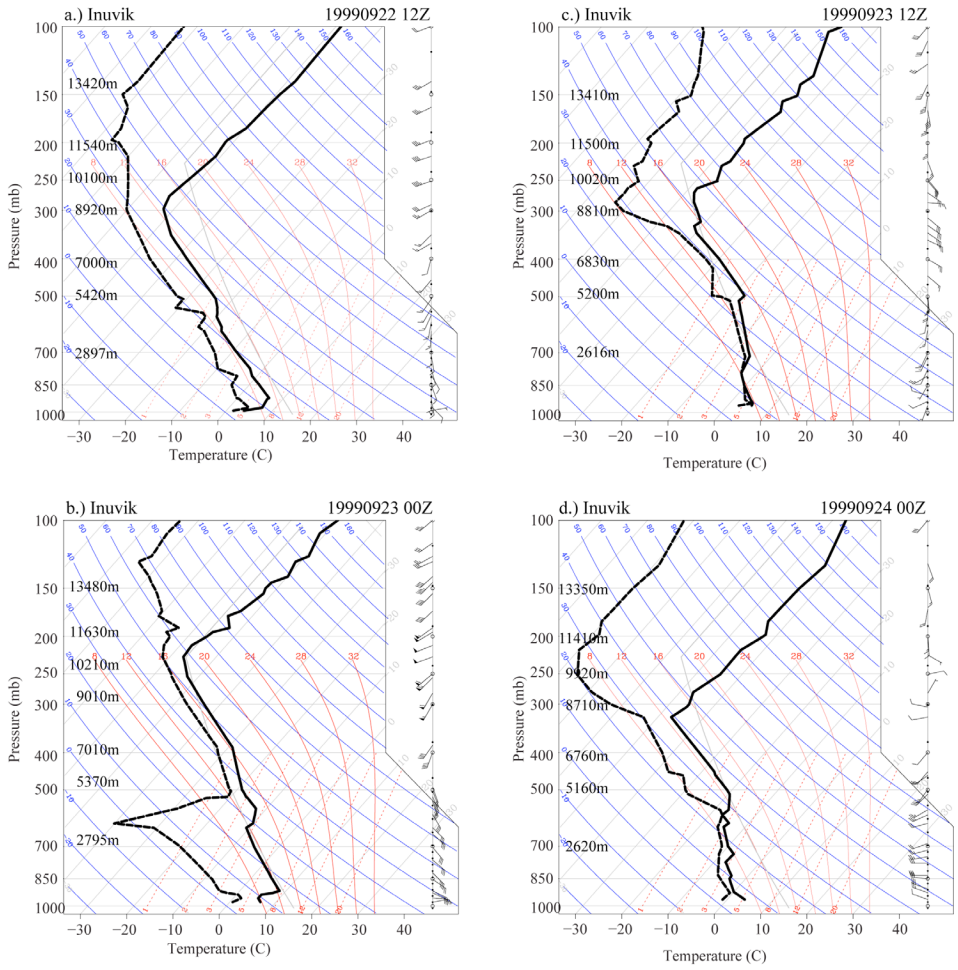

Figure 4.11. Observed soundings for the station at, Northwest Territories on a.) 1200UTC September 22, b.) 0000UTC September 23, c.) 1200UTC September 23 and d.) 0000UTC September 24. The solid line is temperature and the dashed line is the dew point temperature. The winds are in knots.

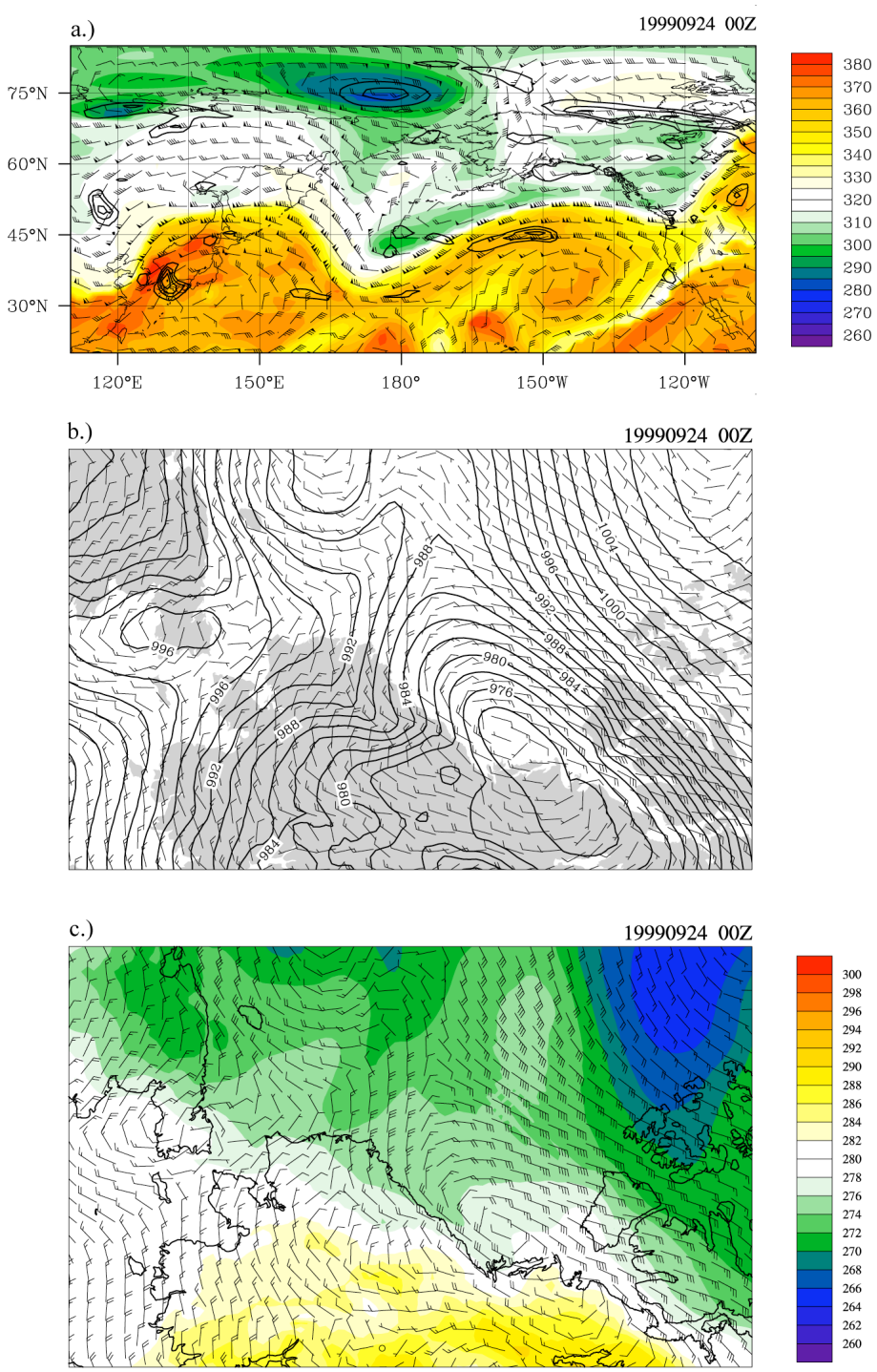

Figure 4.12. a.) Tropopause potential temperature, wind and 925hPa absolute vorticity as in Figure 4.3. b.) The NARR 10m wind (m/s) and SLP (hPa; 2hPa contour interval). c.) NARR 950 hPa potential temperature (K) for 0000UTC September 24.

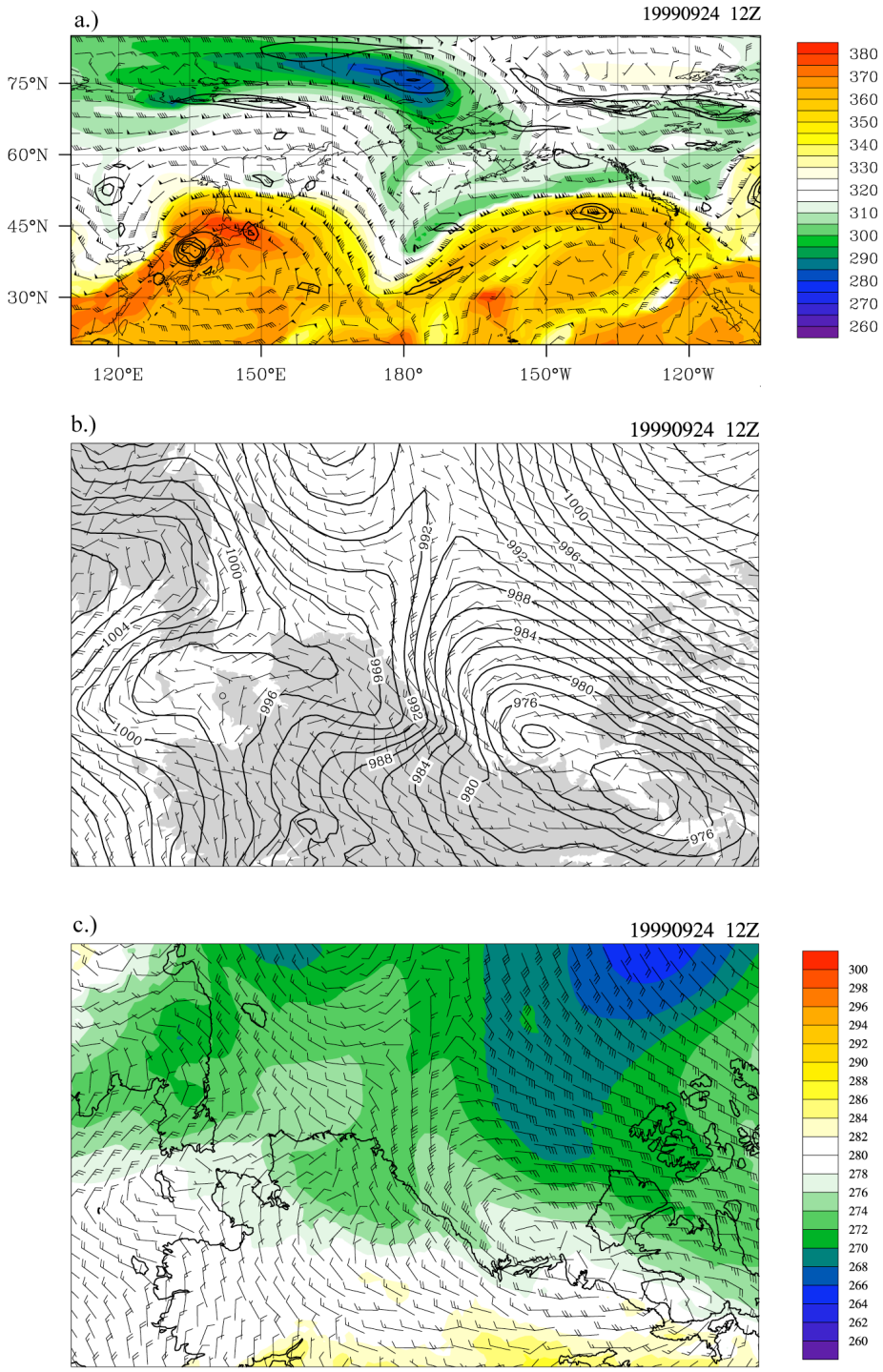

Figure 4.13. As in Figure 4.12 but for 1200UTC September 24.

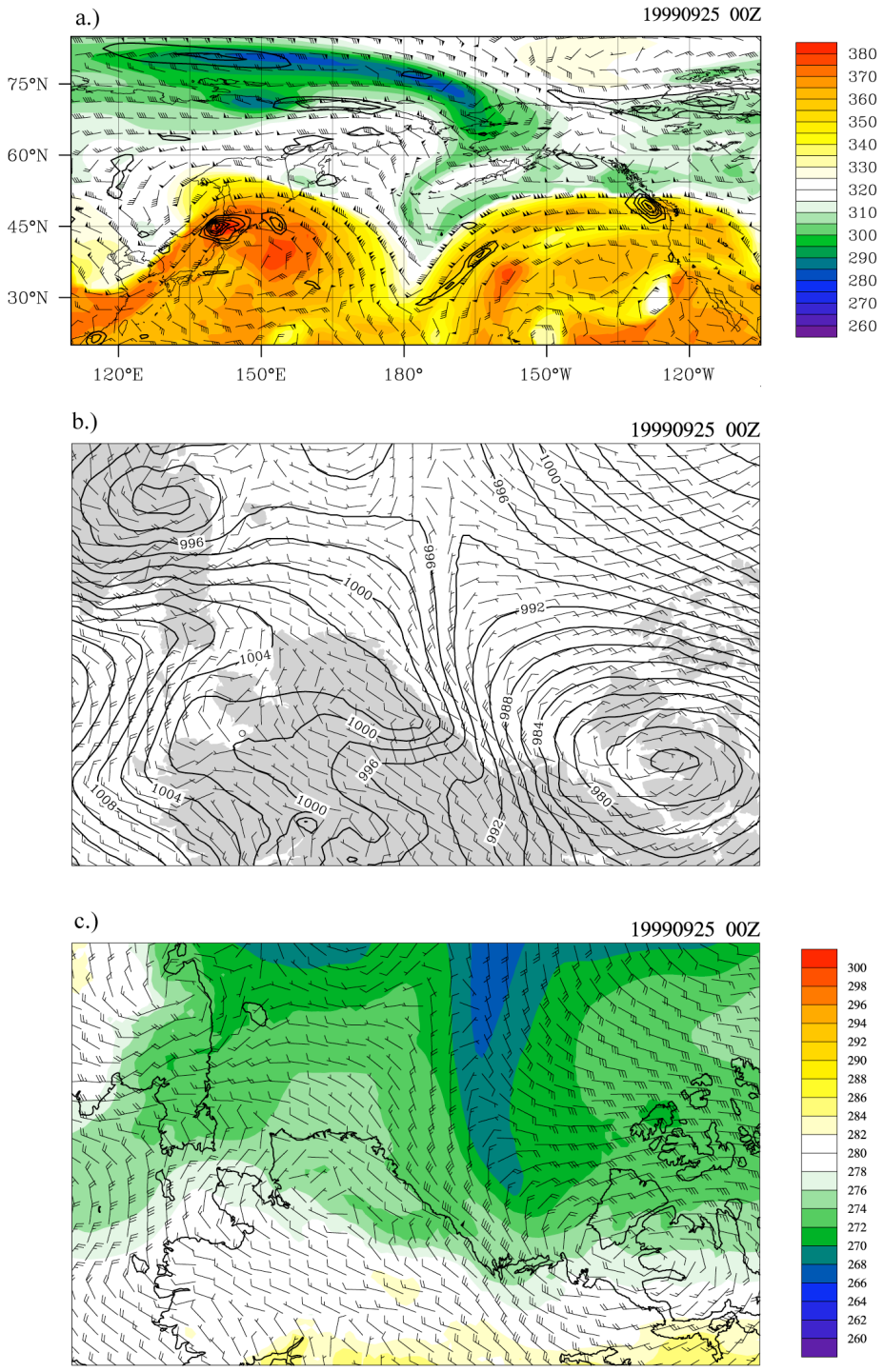

Figure 4.14. As in Figure 4.12 but for 0000UTC September 25.

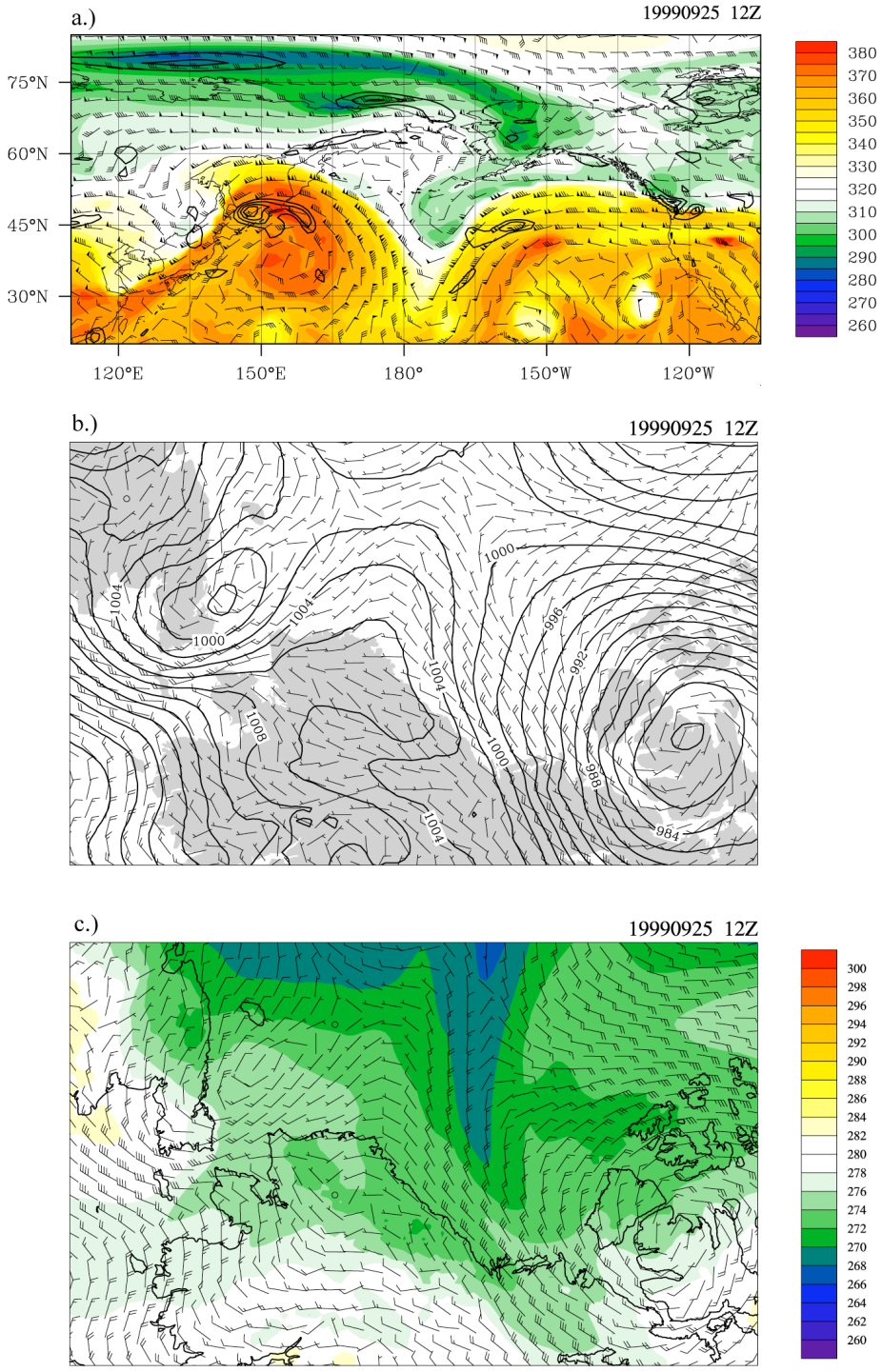

Figure 4.15. As in Figure 4.12 but for 1200UTC September 25.

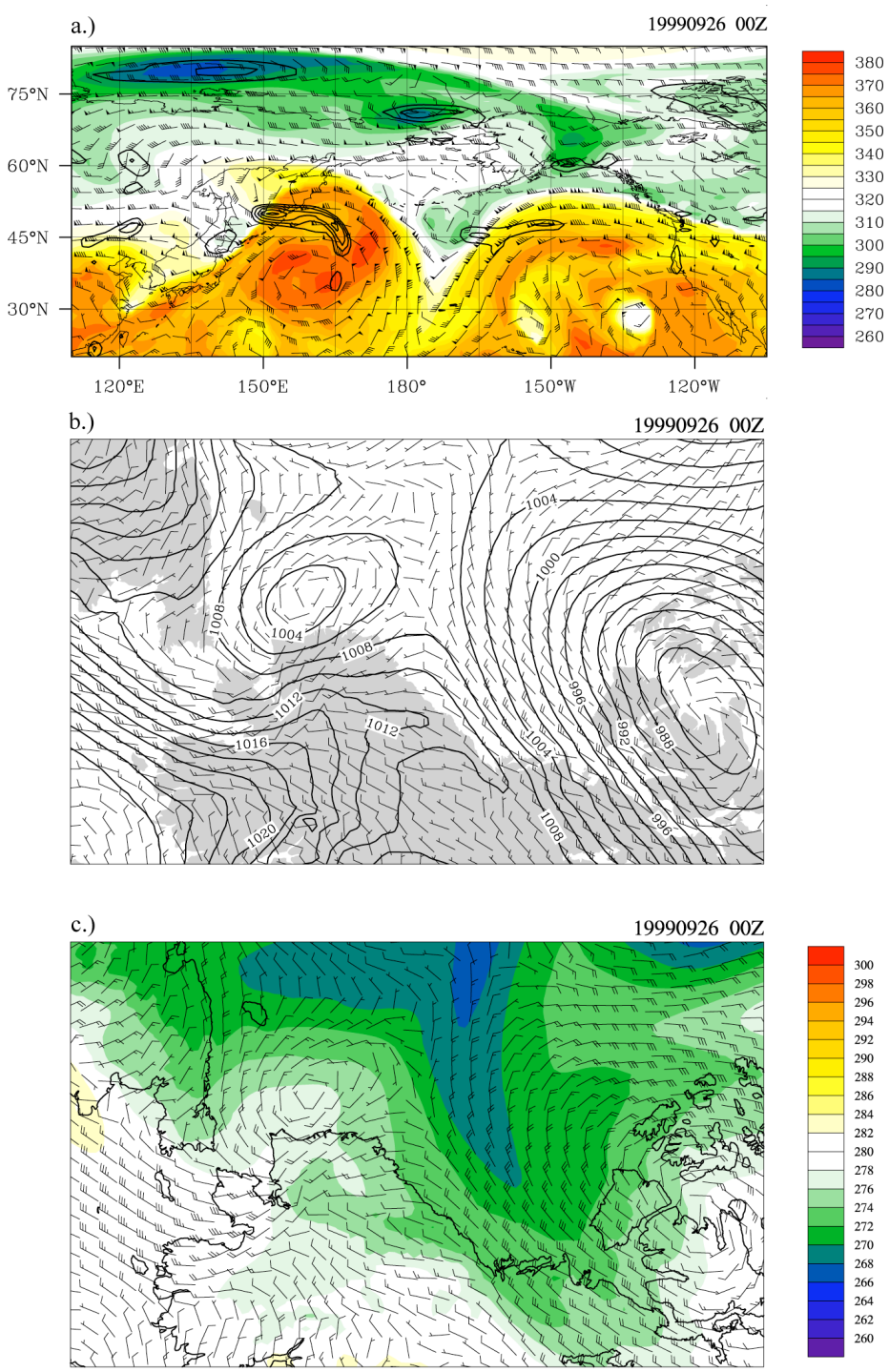

Figure 4.16. As in Figure 4.12 but for 0000UTC September 26.

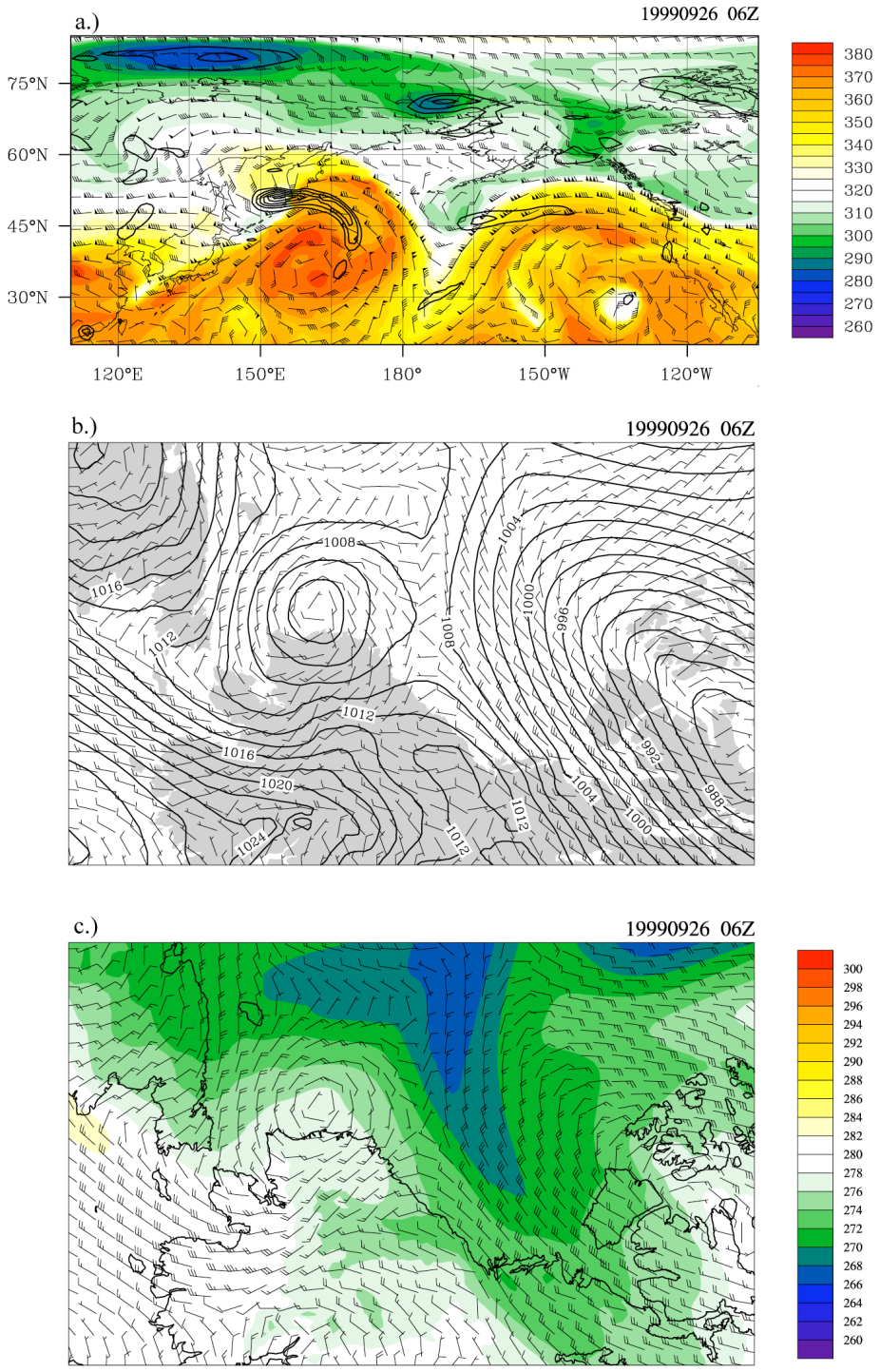

Figure 4.17. As in Figure 4.12 but for 1200UTC September 26.

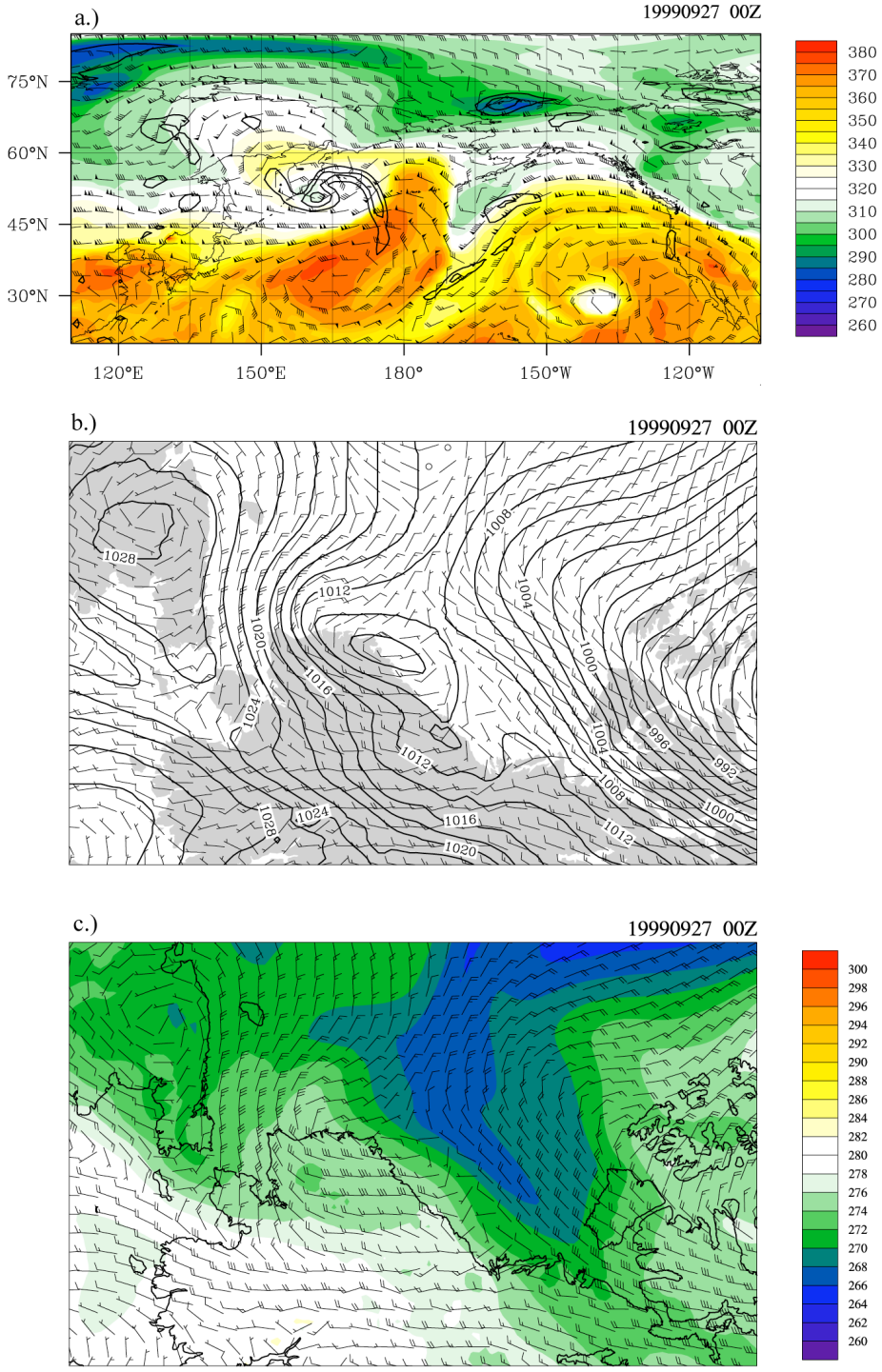

Figure 4.18. As in Figure 4.12 but for 0000UTC September 27.

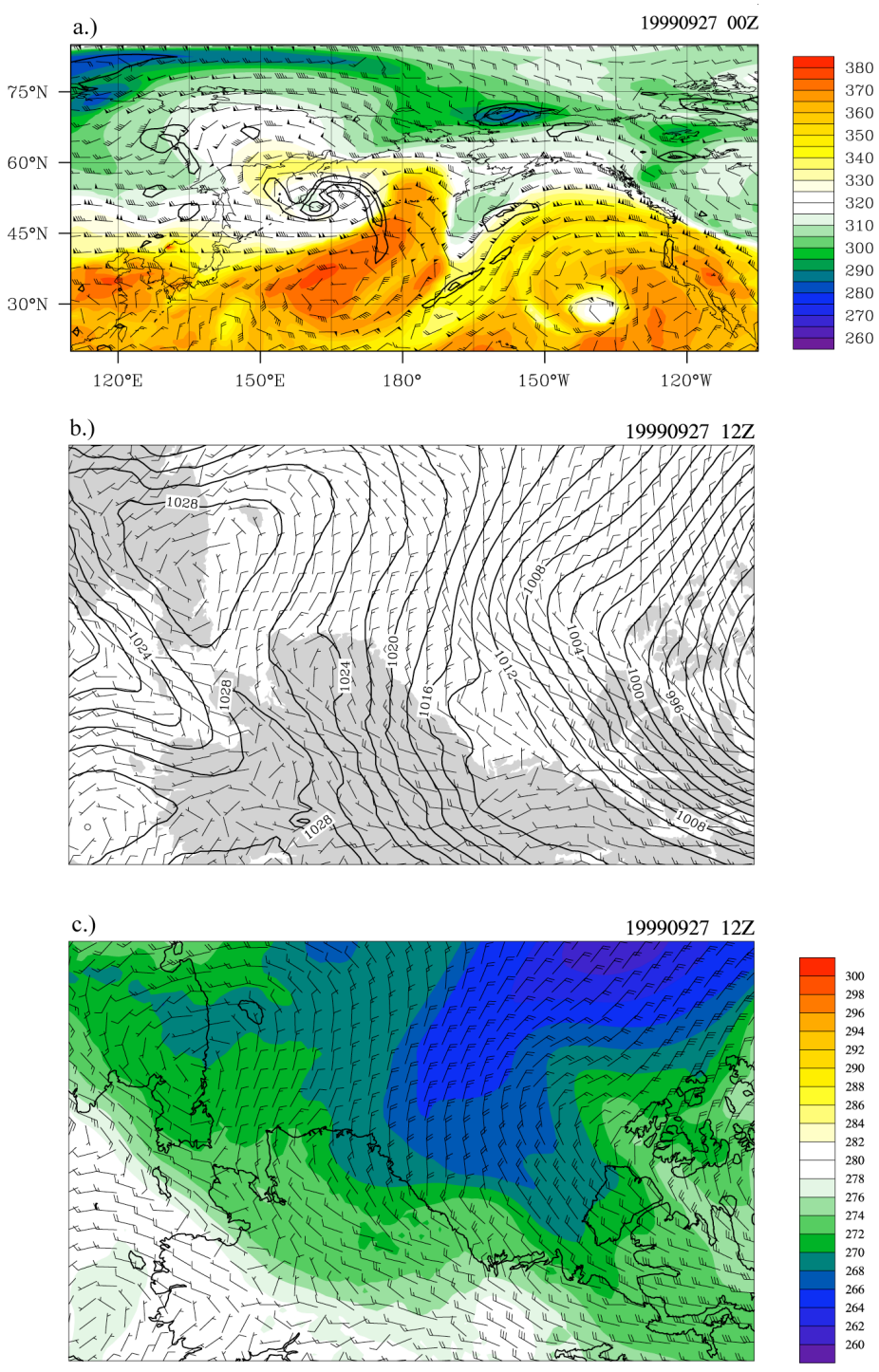

Figure 4.19. As in Figure 4.12 but for 1200UTC September 27.

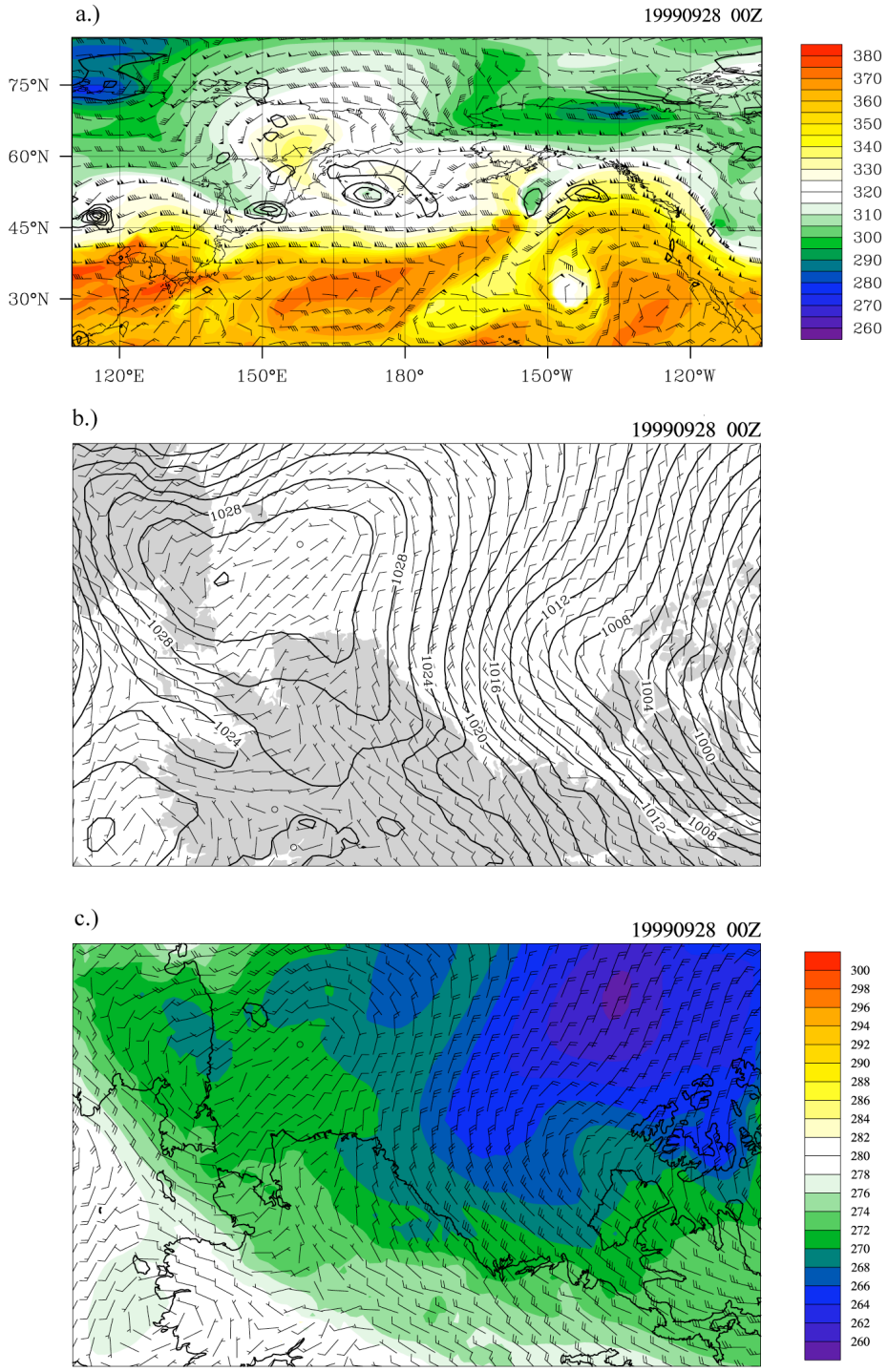

Figure 4.20. As in Figure 4.12 but for 0000UTC September 28.

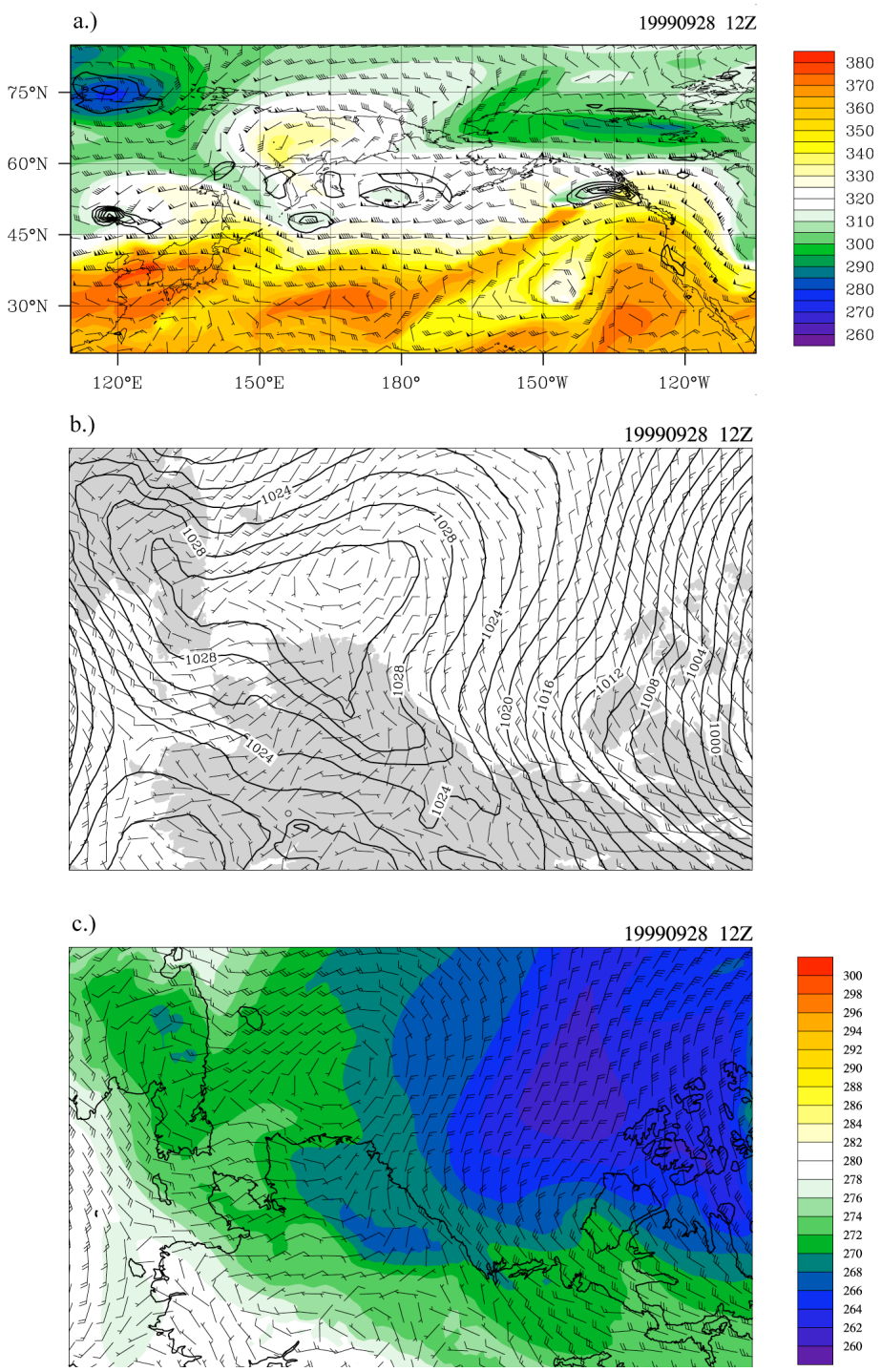

Figure 4.21. As in Figure 4.12 but for 1200UTC September 28.

Chapter 5

Summary and Conclusions

This study has examined the wind regime at Tuktoyaktuk, a community along the Beaufort coast in the Canadian Arctic. Identifying the physical processes that shape the distribution of the winds here is critical because this is the region of the Arctic where temperature has risen (Comiso, 2003) and sea ice coverage has declined (Barber and Hanesiak, 2004) the fastest of anywhere on earth. The increase in open water and degradation of the permafrost (Jorgenson et al., 2006) from the rapid warming have led to large increases in the rate of coastal erosion in many regions of the Arctic, including the Beaufort coast, where the rates are already among the highest the world (Jones et al., 2009; Solomon, 2005).

The coastal community of Tuktoyaktuk along the Beaufort coast in the Canadian Arctic is especially vulnerable to coastal erosion during frequent periods of persistent northwesterly winds observed along the Beaufort coast in August and September (Manson and Solomon, 2007; Danard et al., 2003; Solomon, 2005). Previous studies have found that the wind regime along the Beaufort coast is bi-modal during the late summer with high frequencies of northwesterly and southeasterly winds (Solomon et al., 2005; Manson and Solomon, 2007; Atkinson, 2005; Hudak and Young, 2002). The prevalence of northwesterly winds along the Beaufort coast has often been linked to the passage of powerful storms (Manson and Solomon, 2007; Hudak and Young, 2002). By constructing a climatology of late summer (July through September) winds and performing a detailed case study of an extreme northwesterly wind, this study has demonstrated the importance of anticyclones and upstream topography in shaping the northwesterly wind regime.

The results of the July through September wind climatology demonstrate that the entire distribution of the hourly wind speed at Tuktoyaktuk is preferentially shifted towards higher values for westerly and northwesterly winds only. Because small and median wind speeds are also enhanced, and not just the extremes, the passage of powerful

storms cannot alone explain the high frequency of northwesterly winds. By comparing the direction (and speed) of the observed winds at Tuktoyaktuk to the overlying geostrophic wind, this study linked the high frequency of northwesterly winds at the surface to momentum mixing. Periods of NW surface winds exceeding the climatological 95th percentile were shown to occur when the atmospheric column is neutrally stratified, allowing momentum to be mixed to the surface from above.

Composites of the temperature and sea level pressure anomalies during periods of extreme northwesterly winds suggest that anomalous high pressure over the Chukchi Sea and low pressure east of Tuktoyaktuk are conducive for extreme northwesterly winds at Tuktoyaktuk. The composites also indicated that strong northwesterly winds at Tuktoyaktuk occur with anomalously low potential temperatures over the Beaufort Sea, with the potentially coldest anomalies observed along the windward edge of the Brooks Range. The cold air trapped by the mountains is consistent with an anomalous U-shaped ridge along the Brooks Range also observed in the composite sea level pressure anomalies. The cold air and U-shaped ridge in the sea level pressure is consistent with previous studies documenting the formation of northwesterly barrier jets north of the topography.

The importance of a surface anticyclone over the Chukchi Sea in producing extreme northwesterly winds at Tuktoyaktuk was demonstrated with a case study. During the storm surge event occurring during late September of 1999, two periods of persistent northwesterly winds exceeding the climatological 95th percentile were observed. Both periods of strong northwesterly winds occurred when an upstream ridge on the tropopause over Siberia maintained an anticyclone at the surface over the Chukchi Sea. In both cases, the resulting anticyclonic flow over the Beaufort Sea was conducive for cold air advection and upslope flow to build a pool of cold air at low levels along the windward edge of the Brooks Range. The northerly flow of cold, stable air caused the pressure to rise along the topography, creating a pressure gradient favorable for a northwesterly barrier jet to form.

In the first case, a strong cyclone formed to the southwest of Tuktoyaktuk and moved off to the east. The combination of the northwesterly flow along the trailing edge

of the cyclone to the east, strong northerly flow along the front over the Beaufort Sea and the cyclonic turning of the winds parallel to the topography created a confluence zone for NW winds just upstream from Tuktoyaktuk. The presence of a deep cyclone was certainly an important factor in the generation of strong northwesterly winds, although the winds would likely not have been as strong or as persistently from the northwest without the presence of an anticyclone to the west. An anticyclone alone appears to have triggered the second period of strong northwesterly winds in the absence of a strong cyclone to the east. In both cases, the upstream topography was demonstrated to have played an important role in the severity and persistence of the wind event.

The sea level pressure and potential temperature anomalies observed in the climatology of strong NW wind events (Figure 3.9) are consistent with the results of the case study. The presence of an upstream ridge and surface anticyclone, an important climatological feature of the circulation over the Chukchi and Beaufort Seas, is conducive for northerly flow perpendicular to the Brooks Range. When cold stable air along the leading edge of the anticyclone encounters the Brooks Range, cold air damming produces a SLP anomaly along the topography that produces a pressure gradient favorable for NW geostrophic winds over Tuktoyaktuk. During periods of extreme NW winds, such as those described in the case study, the results indicate that the cold air damming north of the Brooks Range is conducive for a northwesterly barrier jet along the coast that contributes to strong northwesterly winds observed downstream at Tuktoyaktuk.

Bibliography

Achtor, T. H., and L. H. Horn, 1986: Spring season Colorado cyclones. Part I: Use of composites to relate upper and lower tropospheric wind fields. Journal of Climate and Applied Meteorology, 25, 732–743.

Arfeuille, G., L.A. Mysak, and L.B. Tremblay, 2000: Simulation of the interannual variability of the wind-driven Arctic sea ice cover during 1958-1998. Climate Dynamics, 16, 107-121.

Asuma, Y., S. Iwata, K. Kikuchi, G.W.K. Moore, R. Kimura, and K. Tsuboki, 1998: Precipitation Features Observed by Doppler Radar at Tuktoyaktuk, Northwest Territories, Canada, during the Beaufort and Arctic Storms Experiment. Monthly Weather Review, 126, 2384–2405.

Atkinson, D. E., 2005: Observed storminess patterns and trends in the circum-Arctic coastal regime. Geo-Marine Letters, 25, 98–109.

Barber, D. G., and J. M. Hanesiak, 2004: Meteorological forcing of sea ice concentrations in the southern Beaufort Sea over the period 1979 to 2000. Journal of Geophysical Research, 109, C06014, doi:10.1029/2003JC002027.

Barry, R.G., 2008: Mountain Weather and Climate. Cambridge University Press.

Bell, G.D., and L.F. Bosart, 1988: Appalachian Cold-Air Damming. Monthly Weather Review, 116, 137–161.

Bluestein, H., 1992: Synoptic-Dynamic Meteorology in Midlatitudes Volume I: Principles of Kinematics and Dynamics. Oxford University Press.

Bosart, L. F., 1981: The Presidents' Day snowstorm of 18–19 February 1979: A subsynoptic-scale event. Monthly Weather Review, 109, 1542–1566.

Bosart, L. F. and S. C. Lin, 1984: A diagnostic analysis of the Presidents' Day storm of February 1979. Monthly Weather Review, 112, 2148–2177.

Bosart, L.F., G.J. Hakim, K.R. Tyle, M.A. Bedrick, W.E. Bracken, M.J. Dickinson, and D.M. Schultz, 1996: Large-Scale Antecedent Conditions Associated with the 12–14 March 1993 Cyclone ("Superstorm '93") over Eastern North America. Monthly Weather Review, 124, 1865–1891.

Brümmer B., S. Thiemann, and A. Kirchgäbner, 2000: A cyclone statistics for the Arctic based on European Centre re-analysis data. Meteorology and Atmospheric Physics, 75, 233–250.

Cassano, E.N., A.H. Lynch, J.J. Cassano, and M.R. Koslow, 2006: Classification of synoptic patterns in the western Arctic associated with extreme events at Barrow, Alaska, USA. Climate Research, 30, 83-97.

Cavalieri D. J., C. L. Parkinson, and K. Y. Vinnikov, 2003: 30-year satellite record reveals contrasting Arctic and Antarctic decadal sea ice variability. Geophysical Research Letters, 30, 1970, doi:10.1029/2003GL018031.

Chen, S.-J., Y.-H. Kuo, P.-Z. Zhang, and Q.-F. Bai, 1992: Climatology of explosive cyclones off the east Asian coast. Monthly Weather Review, 120, 3029–3035.

Christensen, J., et al., 2007: Regional climate projections. Climate Change 2007: The Physical Science Basis. Contribution of Working Group I to the Fourth Assessment Report of the Intergovernmental Panel on Climate Change, S. Solomon, D. Qin, M. Manning, Z. Chen, M. Marquis, K. Averyt, M. Tignor, and H. Miller, Eds., Cambridge University Press, Cambridge, United Kingdom and New York, NY, USA.

Chung, Y. and E.R. Reinelt, 1973: On cyclogenesis in the lee of the Canadian Rocky Mountains. Arch. Meteorol. Geoph. Bioklim., Series A 22:205-226.

Colle, B. A., and C. F. Mass, 1995: The structure and evolution of cold surges east of the Rocky Mountains. Monthly Weather Review, 123, 2577–2610.

Colle, B.A., K.A. Loescher, G.S. Young, and N.S. Winstead, 2006: Climatology of Barrier Jets along the Alaskan Coast. Part II: Large-Scale and Sounding Composites. Monthly Weather Review, 134, 454–477.

Colucci, S.J., and J.C. Davenport, 1987: Rapid Surface Anticyclogenesis: Synoptic Climatology and Attendant Large-Scale Circulation Changes. Monthly Weather Review, 115, 822–836.

Comiso, J.C., 2003: Warming Trends in the Arctic from Clear Sky Satellite Observations. Journal of Climate, 16, 3498–3510.

Comiso, J. C., C. L. Parkinson, R. Gersten, and L. Stock, 2008: Accelerated decline in the Arctic sea ice cover. Geophysical Research Letters, 35, L01703, doi:10.1029/2007GL031972.

Cox, D. R., and D. Oakes, 1984: Analysis of Survival Data. Chapman & Hall.

Danard, M., A. Munro, and T. Murty, 2003: Storm surge hazard in Canada. Natural Hazards 28, 2–3, 407–431.

Davis, C. A., and K. A. Emanuel, 1988: Observational evidence for the influence of surface heat fluxes on rapid maritime cyclogenesis. Monthly Weather Review, 116, 2649–2659.

Dickey, W., 1961: A Study of a Topographic Effect on Wind in the Arctic. Journal of the Atmospheric Sciences, 18, 790–803.

Doyle, J. D., 1997: The influence of mesoscale orography on a coastal jet and rainband. Monthly Weather Review, 125, 1465–1488.

Drobot, S. D., and J. A. Maslanik, 2003: Interannual variability in summer Beaufort Sea ice conditions: Relationship to winter and summer surface and atmospheric variability. Journal of Geophysical Research, 108(C7), 3233, doi:10.1029/2002JC001537.

Gross, G., and F. Wippermann, 1987: Channeling and Countercurrent in the Upper Rhine Valley: Numerical Simulations. Journal of Applied Meteorology, 26, 1293–1304.

Gyakum, J. R., 1983a: On the evolution of the QE II storm. Part I: Synoptic aspects. Monthly Weather Review, 111, 1137–1155.

Gyakum, J. R., 1983b: On the evolution of the QE II storm. Part II: Dynamic and thermodynamic structure. Monthly Weather Review, 111, 1156–1173.

Gyakum, J.R., and E.S. Barker, 1988: A Case Study of Explosive Subsynoptic-Scale Cyclogenesis. Monthly Weather Review, 116, 2225–2253.

Gyakum, J. R., J. R. Anderson, R. H. Grumm, and E. L. Gruner, 1989: North Pacific cold-season surface cyclone activity: 1975–1983. Monthly Weather Review, 117, 1141–1155.

Gyakum, J. R., 1991: Meteorological precursors to the explosive intensification of the QE II storm. Monthly Weather Review, 119, 1105–1131.

Gyakum, J. R., P. J. Roebber, and T. A. Bullock, 1992: The role of antecedent surface vorticity development as a conditioning process in explosive cyclone intensification. Monthly Weather Review, 120, 1465–1489.

Gyakum, J.R., and R.E. Danielson, 2000: Analysis of Meteorological Precursors to Ordinary and Explosive Cyclogenesis in the Western North Pacific. Monthly Weather Review, 128, 851–863.

Hakim, G.J., L.F. Bosart, and D. Keyser, 1995: The Ohio Valley Wave-Merger Cyclogenesis Event of 25–26 January 1978. Part I: Multiscale Case Study. Monthly Weather Review, 123, 2663–2692.

Hoskins, B., M. McIntyre, and A. Roberston, 1985: On the use and significance of isentropic potential vorticity maps. Quarterly Journal of the Royal Meteorological Society, 111, 877–946.

Hovanec, R. D., and L. H. Horn, 1975: Static stability and the 300 mb isotach field in the Colorado cyclogenetic area. Monthly Weather Review, 103, 628–638.

Hu, Q., and E. R. Reiter, 1987: A Diagnostic Study of Explosive Cyclogenesis in the Lee of the Rocky Mountains. Meteorology and Atmospheric Physics, 36, 161-184.

Hudak, D., and J. Young, 2002: Storm climatology of the southern Beaufort Sea. Atmosphere-Ocean, 40, 2, 145–158.

Jones, P.D., and A. Moberg, 2003: Hemispheric and large-scale surface air temperature variations: An extensive revision and an update to 2001. Journal of Climate 16, 206-223.

Jones, B. M., C. D. Arp, M. T. Jorgenson, K. M. Hinkel, J. A. Schmutz, and P. L. Flint, 2009: Increase in the rate and uniformity of coastline erosion in Arctic Alaska. Geophysical Research Letters, 36, L03503, doi:10.1029/2008GL036205.

Jorgenson, M. T., Y. L. Shur, and E. R. Pullman, 2006: Abrupt increase in permafrost degradation in Arctic Alaska. Geophysical Research Letters, 33, L02503, doi:10.1029/2005GL024960.

Kahl, J.D., N.A. Zaitseva, V. Khattatov, R. Schnell, D.M. Bacon, J. Bacon, V. Radionov, and M. Serreze, 1999: Radiosonde Observations from the Former Soviet "North Pole" Series of Drifting Ice Stations, 1954–90. Bulletin of the American Meteorological Society, 80, 2019–2026.

Kalnay, E., and Coauthors, 1996: The NCEP/NCAR 40-Year Reanalysis Project. Bulletin of the American Meteorological Society, 77, 437–471.

Keegan, T., 1958: Arctic synoptic activity in winter. Journal of the Atmospheric Sciences, 15, 6, 513–521.

Kozo, T. L., 1980: Mountain barrier baroclinity effects on surface winds along the Alaskan arctic coast. Geophysical Research Letters, 7, 5, 377–380.

Kozo, T. L., and R. Q. Robe, 1986: Modeling Winds and Open-Water Buoy Drift Along the Eastern Beaufort Sea Coast, Including the Effects of the Brooks Range. Journal of Geophysical Research, 91(C11), 13,011–13,032.

Lackmann, G.M., J.R. Gyakum, and R. Benoit, 1998: Moisture Transport Diagnosis of a Wintertime Precipitation Event in the Mackenzie River Basin. Monthly Weather Review, 126, 668–692.

Locatelli, J. D., J. M. Sienkiewicz, and P. V. Hobbs, 1989: Organization and structure of clouds and precipitation on the mid-Atlantic coast of the United States. Part I: Synoptic evolution of a frontal system from the Rockies to the Atlantic Coast. Journal of Atmospheric Science, 46, 1327–1348.

Loescher, K.A., G.S. Young, B.A. Colle, and N.S. Winstead, 2006: Climatology of Barrier Jets along the Alaskan Coast. Part I: Spatial and Temporal Distributions. Monthly Weather Review, 134, 437–453.

Lynch, A.H., A.G. Slater, and M. Serreze, 2001: The Alaskan Arctic Frontal Zone: Forcing by Orography, Coastal Contrast, and the Boreal Forest. Journal of Climate, 14, 4351–4362.

Lynch, A., E. Cassano, J. Cassano, and L. Lestak, 2003: Case studies of high wind events in Barrow, Alaska: Climatological context and development processes. Monthly Weather Review, 131, 4, 719–732.

Lynch, A., J. Curry, R. Brunner, and J. Maslanik, 2004: Toward an integrated assessment of the impacts of extreme wind events on Barrow, Alaska. Bulletin of the American Meteorological Society, 85, 2, 209–221.

Manson, G., S. Solomon, D. Forbes, D. Atkinson, and M. Craymer, 2005: Spatial variability of factors influencing coastal change in the Western Canadian Arctic. Geo-Marine Letters, 25, 2, 138–145.

Manson, G., and S. Solomon, 2007: Past and future forcing of Beaufort Sea coastal change. Atmosphere-Ocean, 45, 2, 107–122.

Mass, C.F., and G.K. Ferber, 1990: Surface Pressure Perturbations Produced by an Isolated Mesoscale Topographic Barrier. Part I: General Characteristics and Dynamics. Monthly Weather Review, 118, 2579–2596.

McCabe G. J., M. P. Clark, and M. C. Serreze, 2001: Trends in Northern Hemisphere surface cyclone frequency and intensity. Journal of Climate, 14, 2763–2768.

McGinley J., 1982: A diagnostic study of Alpine lee cyclogenesis. Monthly Weather Review, 110, 1271-1287.

Mesinger, F., and Coauthors, 2006: North American Regional Reanalysis. Bulletin of the American Meteorological Society, 87, 343–360.

Monahan, A.H., 2006: The Probability Distribution of Sea Surface Wind Speeds. Part I: Theory and SeaWinds Observations. Journal of Climate, 19, 497–520.

Morgan, M.C., and J.W. Nielsen-Gammon, 1998: Using Tropopause Maps to Diagnose Midlatitude Weather Systems. Monthly Weather Review, 126, 2555–2579.

Murty, T., G. McBean, and B. McKee, 1983: Explosive Cyclogenesis over the Northeast Pacific Ocean. Monthly Weather Review, 111, 1131–1135.

Nuss, W.A., and R.A. Anthes, 1987: A Numerical Investigation of Low-Level Processes in Rapid Cyclogenesis. Monthly Weather Review, 115, 2728–2743.

Ogi, M., and J. M. Wallace, 2007: Summer minimum Arctic sea ice extent and the associated summer atmospheric circulation. Geophysical Research Letters, 34, L12705, doi:10.1029/2007GL029897.

Ogi, M., I. G. Rigor, M. G. McPhee, and J. M. Wallace, 2008: Summer retreat of Arctic sea ice: Role of summer winds. Geophysical Research Letters, 35, L24701, doi:10.1029/2008GL035672.

Overland, J., and M. Wang, 2005: The Arctic climate paradox: The recent decrease of the Arctic Oscillation. Geophysical Research Letters, 32, 6.

Palmén, E., and C. W. Newton, 1969: Atmospheric Circulation Systems. Academic Press.

Petterssen S, and S. J. Smebye, 1971: On the development of extratropical cyclones. Quarterly Journal the Royal Meteorological Society, 97, 457–482.

Reed, R., and B. Kunkel, 1960: The Arctic circulation in summer. Journal of the Atmospheric Sciences, 17, 5, 489–506.

Reed, R. J., A. J. Simmons, M. D. Albright, and P. Undén, 1988: The role of latent heat release in explosive cyclogenesis: Three examples based on ECMWF operational forecasts. Weather and Forecasting, 3, 217–229.

Rigor, I. G., J. M. Wallace, and R. L. Colony, 2002: Response of sea-ice to the Arctic Oscillation. Journal of Climate, 15, 2648–2663.

Rigor, I. G., and J. M. Wallace, 2004: Variations in the age of Arctic sea-ice and summer sea-ice extent. Geophysical Research Letters, 31, L09401, doi:10.1029/2004GL019492.

Roebber, P. J., 1984: Statistical analysis and updated climatology of explosive cyclones. Monthly Weather Review, 112, 1577–1589.

Roebber, P.J., and J.R. Gyakum, 2003: Orographic Influences on the Mesoscale Structure of the 1998 Ice Storm. Monthly Weather Review, 131, 27–50.

Rogers, J.C., 1978: Meteorological Factors Affecting Interannual Variability of Summertime Ice Extent in the Beaufort Sea. Monthly Weather Review, 106, 890–897.

Sanders, F., and J. R. Gyakum, 1980: Synoptic-dynamic climatology of the "bomb." Monthly Weather Review, 108, 1589–1606.

Schultz, D.M., and C.A. Doswell, 2000: Analyzing and Forecasting Rocky Mountain Lee Cyclogenesis Often Associated with Strong Winds. Weather and Forecasting, 15, 152–173.

Schwerdtfeger, W., 1974: Mountain barrier effect on the flow of stable air north of the Brooks Range. Proc. 24th Alaskan Science Conf., Fairbanks, AK, Geophysical Institute, University of Alaska Fairbanks, 204–208.

Serreze, M., J. Box, R. Barry, and J. Walsh, 1993: Characteristics of Arctic synoptic activity, 1952–1989. Meteorology and Atmospheric Physics, 51, 3, 147–164.

Serreze, M. C., 1995: Climatological aspects of cyclone development and decay in the Arctic. Atmosphere–Ocean, 33, 1–23.

Serreze, M., A. Lynch, and M. Clark, 2001: The Arctic frontal zone as seen in the NCEP– NCAR reanalysis. Journal of Climate, 14, 7, 1550–1567.

Serreze, M. C., J. A. Maslanik, T. A. Scambos, F. Fetterer, J. Stroeve, K. Knowles, C. Fowler, S. Drobot, R. G. Barry, and T. M. Haran, 2003: A record minimum arctic sea ice extent and area in 2002. Geophysical Research Letters, 30, 3, 1110, doi:10.1029/2002GL016406.

Serreze, M., and R. Barry, 2005: The Arctic Climate System. Cambridge University Press.

Serreze, M., and J. Francis, 2006: The Arctic amplification debate. Climatic Change, 76, 3, 241–264.

Serreze, M., M. Holland, and J. Stroeve, 2007: Perspectives on the Arctic's shrinking sea-ice cover. Science, 315, 5818, 1533.

Serreze, M., and A. Barrett, 2008: The Summer Cyclone Maximum over the Central Arctic Ocean. Journal of Climate, 21, 5, 1048–1065.

Simmonds, I., C. Burke, and K. Keay, 2008: Arctic Climate Change as Manifest in Cyclone Behavior. Journal of Climate, 21, 5777–5796.

Solomon, S., and B. Covil, 1995: Impacts of the September, 1993 Storm on the Coastline at Four Sites Along the Canadian Beaufort Sea Coast. Proceedings of the Canadian Coastal Conference, 779-795.

Solomon, S. M., 2005: Spatial and temporal variability of shoreline change in the Beaufort-Mackenzie region, Northwest Territories, Canada. Geo-Marine Letters, 25, 127–137.

Spence C, and J. Rausch, 2005: Autumn synoptic conditions and rainfall in the subarctic Canadian Shield of the Northwest Territories, Canada. International Journal of Climatology 25, 1493 – 5106.

Steele, M., W. Ermold, and J. Zhang, 2008: Arctic Ocean surface warming trends over the past 100 years. Geophysical Research Letters, 35, L02614, doi:10.1029/2007GL031651.

Steenburgh, W.J., and C.F. Mass, 1994: The Structure and Evolution of a Simulated Rocky Mountain Lee Trough. Monthly Weather Review, 122, 2740–2761.

Stroeve, J. C., M. M. Holland, W. Meier, T. Scambos, and M. Serreze, 2007: Arctic sea ice decline: Faster than forecast. Geophysical Research Letters, 34, L09501, doi:10.1029/2007GL029703.

Thompson, D., and J. Wallace, 1998: The Arctic Oscillation signature in the wintertime geopotential height and temperature fields. Geophysical Research Letters, 25, 9, 1297– 1300.

Tremblay L. B, and L.A. Mysak, 1998: On the origin and evolution of sea-ice anomalies in the Beaufort-Chukchi Sea. Climate Dynamics, 14, 451-460.

Uccellini, L.W., D. Keyser, K. F. Brill, and C. H. Wash, 1985: The Presidents' Day cyclone of 18–19 February 1979: Influence of upstream trough amplification and associated tropopause folding on rapid cyclogenesis. Monthly Weather Review, 113, 962–988.

Uccellini, L.W., 1986: The Possible Influence of Upstream Upper-Level Baroclinic Processes on the Development of the QE II Storm. Monthly Weather Review, 114, 1019–1027.

Uppala S. M., and Coauthors, 2005: The ERA-40 Re-Analysis. Quarterly Journal of the Royal Meteorological Society, 131, 2961–3012.

Wang, C.C., and J.C. Rogers, 2001: A Composite Study of Explosive Cyclogenesis in Different Sectors of the North Atlantic. Part I: Cyclone Structure and Evolution. Monthly Weather Review, 129, 1481–1499.

Weibull, W., 1951: A statistical distribution function of wide applicability. Journal of Applied Mechanics-Transactions ASME 18, 3, 293-297.

Whiteman, C.D., and J.C. Doran, 1993: The Relationship between Overlying Synoptic-Scale Flows and Winds within a Valley. Journal of Applied Meteorology, 32, 1669–1682.

Zhang, X., J. E. Walsh, J. Zhang, U. Bhatt, and M. Ikeda, 2004: Climatology and interannual variability of Arctic cyclone activity, 1948–2002. Journal of Climate, 17, 2300–2317.

Zhang J., 2005: Warming of the Arctic ice-ocean system is faster than the global average since the 1960s. Geophysical Research Letters, 32, L19602, doi:10.1029/2005GL024216.

Zhang, X., A. Sorteberg, J. Zhang, R. Gerdes, and J. C. Comiso, 2008a: Recent radical shifts of atmospheric circulations and rapid changes in Arctic climate system. Geophysical Research Letters, 35, L22701, doi:10.1029/2008GL035607.

Zhang, J., R. Lindsay, M. Steele, and A. Schweiger, 2008b: What drove the dramatic retreat of arctic sea ice during summer 2007. Geophysical Research Letters, 35, L11505, doi:10.1029/2008GL034005.